Stony Brook University

Adsorbed polymer nanolayers on solids: mechanism, structure and applications

A Dissertation Presented

by

Mani Kuntal Sen

to

The Graduate School

in Partial Fulfillment of the

Requirements

for the Degree of

Doctor of Philosophy

in

Materials Science and Engineering

Stony Brook University

May 2017

Stony Brook University

The Graduate School

Mani Kuntal Sen

We, the dissertation committee for the above candidate for the

Doctor of Philosophy degree, hereby recommend

acceptance of this dissertation.

Dr. Tadanori Koga – Dissertation Advisor
Associate Professor, Materials Science and Engineering

Dr. Jonathan Sokolov - Chairperson of Defense
Professor, Materials Science and Engineering

Dr. Chang-Yong Nam
Adjunct Professor, Materials Science and Engineering

Dr. Kevin G. Yager
Group Leader, Electronic Nanomaterials, Center for Functional Nanomaterials, Brookhaven National Laboratory, External Member

This dissertation is accepted by the Graduate School

Charles Taber

Dean of the Graduate School

Abstract of the Dissertation

Adsorbed polymer nanolayers on solids: mechanism, structure and applications.

by

Mani Kuntal Sen

Doctor of Philosophy

in

Materials Science and Engineering

Stony Brook University

2017

In this thesis, by combining various advanced x-ray scattering, spectroscopic and other surface sensitive characterization techniques, I report the equilibrium polymer chain conformations, structures, dynamics and properties of polymeric materials at the solid-polymer melt interfaces. Following the introduction, in chapter 2, I highlight that the backbone chains (constituted of CH and CH_2 groups) of the flattened polystyrene (PS) chains preferentially orient normal to the weakly interactive substrate surface via thermal annealing regardless of the initial chain conformations, while the orientation of the phenyl rings becomes randomized, thereby increasing the number of surface-segmental contacts (i.e., enthalpic gain) which is the driving force for the flattening process of the polymer chains even onto a weakly interactive solid. In chapter 3, I elucidate the flattened structures in block copolymer (BCP) thin films where both blocks lie flat on the substrate, forming a 2D randomly phase-separated structure irrespective of their microdomain structures and interfacial energetics. In chapter 4, I reveal the presence of an irreversibly adsorbed BCP layer which showed suppressed dynamics even at temperatures far above the individual glass transition temperatures of the blocks. Furthermore, this adsorbed BCP layer plays a crucial role in controlling

the microdomain orientation in the entire film. In chapter 5, I report a radically new paradigm of designing a polymeric coating layer of a few nanometers thick ("polymer nanolayer") with anti-biofouling properties.

Table of Contents

List of Figures

Acknowledgments

Firstly, I would like to express my deepest appreciation and gratitude to my PhD thesis advisor, Dr. Tadanori Koga for his mentorship and guidance in helping me to hone and enhance my skills as a PhD student. His tremendous support as my PhD advisor helped make this research and thesis possible. Throughout my research in the lab, he has taught me a great deal about polymer science which I will be sure to carry with me in my future endeavors.

I want to thank my collaborators, Dr. Keiji Tanaka and Dr. Daisuke Kawaguchi.

I also want to thank the staff of NSLS, NSLS II, CFN, NIST and CHESS including a special thanks to Maya K. Endoh for providing experimental support and helpful discussions.

My thanks also to Naisheng Jiang, Peter Gin, Deborah Barkley, Justin Cheung, Zhongjie Hu, Shotaro Nishitsuji and all other lab mates and undergraduates in Professor Koga's lab, who supported and helped me immensely during my time as a PhD student.

I am indebted to the staff of the Materials Sciences and Engineering department at Stony Brook University as well for their support.

I also want to thank my parents for their unconditional support during my graduate studies.

I want to thank Stony Brook University, Research Foundation and NSF for their support.

Finally, I want to thank all my defense committee members for taking the time out of their busy schedule to be a part of my PhD journey.

Vita, Publications and/or Fields of Study

List of publications:

1. **Mani Sen**, Naisheng Jiang, Justin Cheung, Maya K. Endoh, Tadanori Koga, Daisuke Kawaguchi, Keiji Tanaka, "**Flattening process of polymer chains irreversibly adsorbed on a solid**", (**ACS Macro Letters**, 2016, 5, 504-508).

2. Brian Momani; **Mani Sen**; Maya Endoh; Xiaoliang Wang; Tadanori Koga, Henning W. Winter, "**Temperature Dependent Intercalation and Self-Exfoliation of Clay/Polymer Nanocomposite**", (**Polymer**, 93, 204-212, 2016).

3. X. Liang, **Mani Sen**, J. Jee, J. E. Marine, O. Gelman, M. K. Endoh, T. Koga, J. G. Rudick "**Poly(oxanorbornenedicarboximide)s Dendronized with Amphiphilic Poly (alkyl ether) Dendrons"**, (**Journal of Polymer Science, Part A: Polymer Chemistry**, 52, 22, 3221–3239, 2014).

4. N. Jiang, L. Sendogdular, **Mani Sen**, M. K. Endoh, T. Koga, M. Fukuto, B. Akgun, S. K. Satija, C.Y. Nam **"Novel effects of compressed CO_2 molecules on structural ordering and charge transport in conjugated poly(3-hexylthiophene) thin films", (Langmuir, 2016, 32 (42), 10851–10860)**

5. Rana Ashkar, Michihiro Nagao, Paul D. Butler, Andrea C. Woodka, **Mani K. Sen**, Tadanori Koga **"Tuning Membrane Thickness Fluctuations in Model Lipid Bilayers"**, (**Biophysical Journal**, Volume 109, July 2015, 106–112).
6. Naisheng Jiang, Levent Sendogdular, Xiaoyu Di, **Mani Sen**, Peter Gin, Maya K. Endoh, Tadanori Koga, Bulent Akgun, Michael Dimitriou, and Sushil Satija, "**Effect of CO_2 on a**

Mobility Gradient of Polymer Chains near an Impenetrable Solid" (**Macromolecules**, 2015, 48, (6), 1795–1803)

7. M. Pan, L. Yang, J. Wang, G. Zhong, **Mani. K. Sen**, M. K. Endoh, T. Koga, and L. Zhu, "**Composite Poly (vinylidene fluoride)/Polystyrene Latex Particles for Confined Crystallization in 180 nm Nanospheres via Emulsifier-Free Batch Seeded Emulsion Polymerization**", (**Macromolecules** (2014), 46, 2632–2644).

8. Z. Li, T. Miyoshi, **Mani K. Sen**, T. Koga, A. Otsubo, K. Akihiro; A. Kamimura, "**Solid−state NMR Characterizaiton of the Chemical Defects and Physical Disorders in α Form of Isotactic Poly(propylene) Synthesized by Ziegler−Natta Catalysts**", (**Macromolecules** (2013), 46, 6507–6519).

Achievements:

1. Second prize for poster at 14th International Conference on Surface X-ray and Neutron Scattering (SXNS-14).
2. Student award for excellence in research at the 2015 and 2016 NSLS/CFN Users' Meeting at Brookhaven National Laboratory, NY.
3. Selected (total of 30 students nationwide) to attend NIST Center for Neutron Research summer school on neutron spectroscopy and small angle neutron scattering (SANS).

Chapter 1

Introduction

Polymer thin films have numerous technological applications in various industrial and biomedical applications including but not limited to protective and functional coatings[1], electronics[2], optics[3], sensors[4], non-fouling bio surfaces[5], biocompatibility of medical implants, separations[6], advanced membranes[7], microfluidics[8], adhesion[9], lubrication and friction modification[10]. Many of these above-mentioned applications require polymer films to be confined in dimensions comparable to the size of a single polymer chain to meet current technological demands. However, it is well known that many fundamental characteristics of these confined polymeric materials, including structure, chain conformations, dynamics and other physical and mechanical properties, differ substantially from those of the bulks due to the so-called "nanoconfinement" effects, where the polymer chains are confined between a polymer/air and polymer/substrate interface[11, 12]. Roth and co-workers reported that poly 2-vinylpyridine (P2VP) exhibited a very strong increase in glass transition temperature (T_g) with decreasing film thickness below 150 nm on silica substrates due to hindered dynamics at the substrate interface caused by the strong interaction of the nitrogen atom in the P2VP repeat unit with the hydroxyl groups of the native oxide layer on silica substrate. Moreover, ultrathin polystyrene (PS) films supported on silica displayed a strong decrease in T_g with decreasing thickness since there is no mechanism of preferential bonding or attractive interactions with the substrate[11]. Koga and co-workers reported the decrease in viscosity in polymer thin films confined in thickness less than 60nm due to substrate-polymer segment interactions[13]. Furthermore, Zheng and co-workers utilized secondary ion mass spectrometry (SIMS) to measure diffusion rates of deuterium-labeled polymers under nanoconfinement. The authors showed that polymer dynamics together with diffusion rates were

reduced by two orders of magnitude relative to the bulk even at distances up to 10 times the radius of gyration, R_g, of the polymer from the substrate interface[12]. Hence, a fundamental understanding of the behavior of polymeric materials under "nanoconfinement" effect is crucial in the development of new nanotechnologies.

Deposition of a polymer on an inorganic substrate via spin coating process is a popular method to prepare smooth and uniform thin films in both scientific research and industrial applications such as semiconductors. In the spin coating process, a few drops of polymer solution are deposited on a solid substrate which is, or, will be, rotated. A thin homogeneous polymer film forms on the substrate after quick evaporation of the solvent. The film thickness can be precisely controlled from a few nanometers to sub micrometers by controlling the viscosity of the solution via changing concentration and molecular weight. A general problem of this method is that polymer chains take a conformation elongated in the substrate plane due to the torque caused by the spinning process and are quickly frozen in a non-equilibrium stressed state[14, 15]. The memory of the configurations adopted in solution persists in the dry film. Upon solvent evaporation, when the volume fraction of the polymer reaches a critical value, vitrification takes place. Polymer chains are thus trapped in frustrated packing geometries where overlaps between chains are reduced (i.e., lower entanglement density), resulting in a lower viscosity[16, 17], which influences dewetting[18, 19]. Several techniques like thermal annealing at temperatures far above the glass transition temperature (T_g) of the polymer and solvent vapor annealing are used to equilibrate the polymer melts against inorganic substrates through polymer chains relaxation and rearrangement.

There is now growing evidence to suggest that annealing also expedites irreversible adsorption of (unfunctionalized or uncharged) polymer melt chains onto impenetrable planar solids[20-36]. Adsorption of polymer chains on solid surfaces is a fundamental but highly complex

phenomenon in polymer physics. From a thermodynamic point of view, the adsorption process of polymers can be described as a counterbalance between the loss in the conformational entropy of chains during the transition from a randomly coiled state in melt to an adsorbed state, and the enthalpic gain achieved upon increased number of solid/segment points[37]. Depending on the interactive forces that are involved in the adsorption process, two major types of adsorption processes are reported in the literature. The first type: when polymer chains are attached to the substrate due to covalent or chemical bonding forces generated by a chemical reaction between the substrate surface and the chains, is called chemisorption. The second type: when no significant chemical reactions are involved but the chains are adsorbed to the substrate surface via dispersion, dipolar forces or van der Waals interactions, is called physisorption. Although the sticking energy experienced by polymer chains during physisorption is of the same order as kT (where k is the Boltzmann constant and T is the temperature), irreversible physisorption of polymer chains is still largely observed even when the polymer-solid interaction is weak since desorption kinetics is often much slower than the kinetics of adsorption[38-40]. Due to the formation of multiple surface-segment contacts, the energy required to desorb one chain is the sum of all the bonding energies per contact of the adsorbed chain. This thesis will discuss about adsorbed layers from physisorption process, unless otherwise stated. Adsorption of polymer chains on the solid substrate is governed by many factors, such as polymer-solid interactions, chain lengths, chain stiffness, chemical compositions of polymer, surface properties, solvent interaction etc. Jiang and co-workers have shown that the final thickness of the adsorbed layer increases with increasing polymer/substrate interactions whereas the thickness is independent of polymer chain length[41]. Moreover, Linse and co-workers have reported that the adsorbed chains from stiffer polymer chains relax much slower than flexible chains and the chains are packed in a 2D nematic structure in the resulting adsorbed layer[42].

Recently, adsorbed layers at the polymer/substrate interface have been linked to deviations in T_g[17] and viscosity[13] in the entire polymer thin films. However, studies on the structure-property relationship of the adsorbed layer coupled with detailed molecular chain conformations at the substrate interface are sparse in the literature. Therefore, a detailed investigation of the molecular orientations linking it to the structure and thus properties of polymer chains at the substrate interface is important to understand the effect of the polymer/substrate interface on the entire polymer film.

To achieve these goals, I have integrated various surface sensitive techniques including x-ray scattering, spectroscopic techniques, atomic force microscopy, optical microscopy and scanning electron microscopy and aimed to provide detailed experimental descriptions of the structures and properties of the adsorbed polymer layers and equilibrium chain conformations from a melt onto smooth, flat solids to help bridge the theoretical and experimental viewpoints.

The first objective of my dissertation (Chapter 2) is to investigate the local equilibrium polymer chain conformations near the solid polymer melt (SPM) interface using sum frequency generation spectroscopy (SFG). Although, spin coating is a popular film deposition technique on solid substrates as mentioned earlier, it has severe limitations on the shape of surfaces or substrates to be coated. In case of irregular shapes of objects, spin coating is impossible. An alternate method in place of spin coating is dip coating or solvent casting by simply dipping the substrate in a polymer solution and thereafter extracting the substrate with a well-defined withdrawal speed under controlled temperature and atmospheric conditions. Dip-coating is a low cost and waste-free process to prepare thin polymer films from solutions and is easy to scale up and offers a good control on thickness. The thickness of the sample can be controlled by controlling the extraction of the substrate from the solution. Recently, Tanaka and coworkers showed the different

polystyrene (PS) chain configurations on quartz prepared from two different methods: the chains are elongated parallel to the substrate due to the spinning torque in case of spin coated films while they were randomly oriented in case of dip coat/solvent cast film[43]. In addition, our group recently showed that the polymer adsorbed layers formed from the melts are composed of the two different nanoarchitectures[44]: the flattened chains that constitute the inner higher density region of the adsorbed layers and loosely adsorbed polymer chains that form the outer bulk-like density region (Fig. 1-1). The polymer adsorption process from melts is dictated by piecemeal deposition of polymer chains with differential spreading dictated by the still-uncovered surface area, analogous to polymer adsorption from dilute solutions[45]. The early theoretical picture given by Simha and co-workers showed that the equilibrium physisorbed polymer chain on a solid surface consists of three types of segment sequences: trains, loops and tails[46]. Trains comprised of all segments fully adsorbed to the substrate. Loops constituted of unbound segments that connect trains, and tails are the unadsorbed chain ends. Here my aim is to answer the question: how does this initial different chain configurations in films from different processes affect the final equilibrium chain conformation in the flattened layer? The technique used was SFG spectroscopy. The laser pulse sequence of SFG spectroscopy consists of an on-resonance infrared (IR) pulse, followed by a non-resonance visible (VIS) pulse. In the SFG experiment a pulsed tunable infrared (IR) (with frequency= ωIR) laser beam is mixed with a visible (VIS) (with frequency= ωVIS) beam to produce an output at the sum frequency (ωSFG = ωIR + ωVIS). SFG is second-order nonlinear process, which is allowed only in media without inversion symmetry.

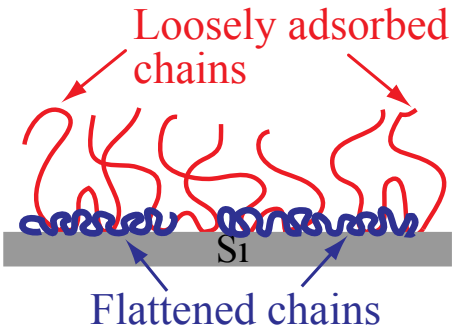

Fig. 1-1: Polymer nanoarchitecture in the adsorbed layer.

At surfaces or interfaces inversion symmetry is necessarily broken, that makes SFG highly surface specific. As the IR wavelength is scanned, active vibrational modes of molecules at the interface give a resonant contribution to SFG signal. The resonant enhancement provides spectral information on surface characteristic vibrational transitions. Different combinations of input and output beam polarizations allow the determination of surface chemistry or molecular orientation. SFG detects vibrational modes, which are rather localized to specific groups of atoms within the molecules. The information about relative orientation of different groups within the same molecule maybe obtained, and, hence, the molecular structure can be deducted. SFG spectroscopy offers intrinsic advantages in studying interfaces, as the output is based on nonlinear optical selection rules that render SFG sensitive only to regions of a material where inversion symmetry is broken. In most materials that are isotropic and homogeneous in the bulk, the technique is ideal for studying surfaces and buried interfaces noninvasively. The resulting output which is an infrared (IR) vibrational spectrum offers molecular information with unparalleled surface sensitivity.

Following the investigation of the local chain conformations in homopolymer flattened layer, I next aim to highlight the flattened chain structures for block copolymers (BCP) in Chapter 3. Block copolymers (BCP) are a class of macromolecules produced by covalently bonding two or more chemically distinct polymer blocks. Due to the thermodynamic incompatibility but covalent bonding of the different constituent blocks in BCP, they self-assemble on nanometer length scales, depending on the relative composition of the blocks, the overall degree of polymerization (N), the polymer–polymer interaction parameter (χ), and the ratio of statistical segment lengths, making them ideal for emerging nanotechnologies. Thus, block copolymers (BCP) offer a simple and effective route to produce highly structured materials with nanoscale regularity, which are potentially useful in nanofabrication applications such as nanoparticle templates[47-49],

nanostructured membranes[50-52], photovoltaic cells[53], low-k dielectrics[54], and high density data storage media[55]. For most of these applications, control over the orientations of microdomain structures is of great importance and the interfacial energetics at the polymer-air and polymer-substrate interfaces play a crucial role in controlling the orientation and ordering of microdomain structures[56, 57]. Recent advances have shown success in switching the orientations (i.e., parallel or perpendicular to a substrate surface) by tuning interactions at the top and bottom surfaces, film thickness[56, 57], external forces such as electric field[58], shear force[59, 60], chemically patterned substrates[61, 62], "neutral" substrates[63-69], thermal annealing above T_g of both blocks [70], and solvent vapor annealing[71-75]. While there is development of advanced surface sensitive experimental tools, several critical questions remain unsolved: what is the self-organization process of BCPs at the buried interface? Can BCP form the same microdomain structures as in the bulk? Are the microdomain structures dependent upon interfacial energetics or film processing? Since the formation of flattened layers on the solid substrate is rather general, such an in-depth study of the flattened BCP layers is fundamental to studies of device design and other applications. I aim to answer the above questions experimentally using atomic force microscopy, scanning electron microscopy, grazing incidence small angle x-ray scattering and x-ray reflectivity.

Chapter 4 of my dissertation elucidates the effect of the adsorbed (consisting of flattened chains and loosely adsorbed chains) BCP layer on the polymer dynamics and thus the microdomain orientations in cylinder forming BCP polymer thin films. Grazing incidence x-ray photon correlation spectroscopy (GI-XPCS) technique was use for this purpose. GI-XPCS technique is the most direct and unambiguous way to study the lateral dynamics of polymer thin films prepared on solid substrates based on the capillary wave fluctuations[76-78]. Photon correlation spectroscopy using laser light is a well-established tool for probing the dynamic properties of matter by

analyzing the temporal correlations among photons scattered by the matter. During the past decade, the development of third-generation synchrotron radiation sources has enabled to extend photon correlation spectroscopy from the optical region into the X-ray domain. The use of the brilliant X-rays enables us to probe the dynamic properties of systems on molecular length scales and use optically dense samples that are not accessible to conventional photon correlation spectroscopy. The technique is based on the generation of a speckle pattern by a scattered coherent light originating from a material where some spatial inhomogeneities are present. If the state of disorder of the scattering system changes with time, the speckle pattern will change accordingly which can thereby be studied with the time dependence of the scattered intensity at a fixed wavevector to probe the dynamics of materials in thermodynamic equilibrium or out of equilibrium. Despite a tremendous amount of work on the phase behavior and static structures of BCPs in thin films, the structural dynamics of BCP in thin films has not been explored yet. The presence of heterogeneous diffusivities and viscosities within the entire film due to the two interfaces (the air/polymer interface and substrate/polymer interface) at different locations within the entire film is expected[79]. The cylinder microdomain structures which orient in the direction normal to the film (upright cylinders) prepared by solvent vapor annealing[80] was used as a model system. I aim to answer the following questions regarding the properties of the adsorbed BCP layer: (i) what is the mobility of the adsorbed chains? (ii) What is the impact of this very thin adsorbed layer on the overall polymer dynamics of BCP thin films? (iii) How far does the effect of this irreversibly adsorbed layer propagate into the film?

Chapter 5 of my dissertation explores the novel antifouling properties of these adsorbed layers against model protein (bovine serum albumin (BSA)) and bacterium *Escherichia coli* (E. Coli). Biofouling or bio-contamination is undesirable in a wide range of applications, such as

surgical equipment and protective apparel in hospitals[81, 82], medical implants[81-84], biosensors[85], textiles[86, 87], food packaging[88] and food storage[89], water purification systems[90], and marine and industrial equipment[90, 91]. Biofouling is the accumulation or attachment of unwanted biological matter on surfaces, with biofilms created by micro-organisms and macro-organisms. Biofouling is generally characterized by the thickness, density, structure, composition, bio-adhesive strength and weight of the attached fouling organisms using a variety of measurement techniques such as optical, transmission electron (TEM), scanning electron (SEM), atomic force and fluorescence microscopy along with other spectroscopic techniques. Biofouling involves attachment of proteins or bacteria on surfaces. Anti-protein fouling is beneficial for in vitro diagnostics, where adsorption of protein molecules can compromise the sensitivity of diagnostic and in vivo applications, such as biomedical implants where protein adsorption can lead to undesirable events that can include thrombus formation or fibrosis and scar tissue formation[92]. Moreover, protein adsorption on the surfaces of biological implants provides a conditioning layer for microbial colonization and subsequent biofilm formation which provides an associated risk of infection[93]. Moreover, biofouling is a common issue with marine vessels where noticeable aquatic growth appears on ships and underwater structures. This increases ship hull drag, corrosion, fuel consumption and engine stress[94]. The most common approach to reduce protein adsorption on a surface is via a coating of poly(ethylene glycol) (PEG)[92]. Chemically or covalently grafted long chain PEGs (PEG polymer brushes) with high grafting density on surfaces showed the highest reductions of adsorption of proteins. However, most of these approaches require extensive chemical modifications and it is often a tedious process. Moreover, long term stability of such coatings is relatively poor, leading to the limited use in marine applications due to rapid oxidation of the coatings in the presence of oxygen and transition ion metals present in seawater[95,96]. In cases where

polymeric brushes display sufficient hydrolytic stability in their main chain, problems may arise at the anchoring point of the brush. This problem is particularly visible for hydrophilic brushes chemically or covalently end tethered on silicon oxide substrates (silicon, glass, and quartz) and anchored to the surface by siloxane bonds (Si−O−Si)[97, 98]. In a hydrophilic environment, the hydrolytic stability of the siloxane bond is compromised because the water is drawn directly to the interface. In the presence of water, a hydrolysis equilibrium between siloxane and silanol (Si−OH) groups is established[99,100]. The equilibrium favors the formation of the siloxane groups, the activation energy for this process can be drastically lowered at acidic and alkaline pH values[100-104]. Also, the generation of strong osmotic pressure at the glass/silane interface is presumed to promote the hydrolytic cleavage of siloxane because of the mechanochemical effect of tensile stress applied to the siloxane bond[98, 100]. Furthermore, hydrophobic coatings are more prone to biofouling due to easier displacement of water molecules on hydrophobic surfaces[105, 106]. Thus, hydrophobic polymers suffer serious fouling problems which limit the practical use of hydrophobic polymers in biomedical applications due to low wettability and nonspecific protein/hydrophobic analyte adsorption and cell/bacterial adhesion. Therefore, there is a present need for the development of novel anti-fouling coatings to resist nonspecific protein adsorption and cell adhesion irrespective of hydrophobicity. In this chapter, I show the novel anti-biofouling property of the polymer adsorbed layers. The emergence of the anti-biofouling property is the structural-based origin, and the preparation of the polymer nanolayers is simple and versatile. In addition, the adsorbed layers are stable against good solvents. The advanced material system will be thus used as a simple, robust, and “green” (i.e., saving materials) coating alternative for a wide range of industrial applications.

Chapter 2

Flattening process of polymer chains irreversibly adsorbed on a solid

2.1: Abstract: We report the structural relaxation process of polymer chains on a weakly attractive solid surface. Polystyrene (PS, M_w = 290 kDa) thin films prepared on curved quartz or planar silicon substrates covered with a very thin silicon oxide layer were used as a model system. Two different film preparation processes (spin coating and dip coating methods) were used to prepare different initial chain conformations; and the resultant thin films were annealed under vacuum at a temperature far above the bulk glass transition temperature up to 300 h. To study the buried polymer-substrate interface, the established approach, which combines the vitrification of the polymer and subsequent solvent washing with a good solvent, was used and the resultant residual layers on the substrates were characterized by using x-ray reflectivity (XR), atomic force microscopy (AFM), and sum-frequency generation spectroscopy (SFG). The SFG results revealed that the backbone chains (constituted of CH and CH_2 groups) of the flattened PS chains preferentially orient normal to the weakly interactive substrate surface via thermal annealing regardless of the initial chain conformations, while the orientation of the phenyl rings becomes randomized. We postulate that increasing the number of surface-segmental contacts (i.e., enthalpic gain) is the driving force for the flattening process of the polymer chains even onto a weakly interactive solid to overcome the conformational entropy loss in the total free energy.

2.2: Introduction:

Thin polymer films on solid substrates are found in a variety of technological fields, such as in both traditional applications (like protective coatings, lubricants, and decorative paints) and newly emerging applications (like photovoltaic cells, semiconductor chips, and biosensors). A spin-coating process is a popular method to prepare smooth and uniform thin polymer films on planar solids. However, polymer chains in as-cast films are trapped in a highly stressed, non-equilibrium state due to the fast solvent evaporation process[107, 108]. A post-thermal annealing process (at temperatures far above the bulk glass transition temperature (T_g)) is thereafter required to remove the residual stress and to facilitate rearrangements of the polymer conformations toward equilibrium[109]. Intriguingly, Thomas and co-workers reported that the recovery of bulk viscosity for a spin-cast polystyrene (PS) film takes more than 100 h (i.e., 5 orders of magnitude longer than the bulk reptation time[110]). Similarly, Chung and co-workers reported that residual stress in a high molecular weight PS spin-cast film exists for more than 100 h of thermal annealing at $T >> T_g$[111]. Different thermal annealing conditions used for bulk thin films would cause different sequences of non-equilibrium chain conformations, resulting in sample history-dependent properties of thin polymer films.

There is growing evidence to suggest that thermal annealing also expedites irreversible adsorption of (unfunctionalized or uncharged) polymer melt chains onto impenetrable planar solids[20-36]. Interestingly, Napolitano and Wübbenhorst showed that extremely long equilibration or relaxation times of thin polymer films are attributed to a sluggish adsorption process of polymer chains on solid surfaces[21]. Taking advantage of Guiselin's approach[112], we recently revealed that adsorbed homopolymer chains consist of two different chain conformations regardless of the magnitude of attractive solid-segment interactions: early arriving chains lie flat on solids

("flattened chains"), while late arriving chains form bridges jointing up nearby empty sites, resulting in "loosely adsorbed polymer chains" (see, the inset of Fig. 2-1b)[25, 32]. This finding suggests that the local rearrangement and deformation of the already adsorbed (flattened) chains evolve with time to promote continued adsorption of additional (late arriving) chain segments[113, 114]. This results in a reduction of free volume[27] and thereby an increase in the density of "matured" flattened chains[25, 32], which is consistent with recent simulation results[42, 114]. It is predicted that the driving force for irreversible chain adsorption is the total enthalpic gain due to an increase in the solid-segment contacts that overcomes a loss in the conformational entropy of the adsorbed polymer chain[115, 116]. However, a critical, but unanswered question is whether polymer chains still favor an increase in contact of the number of segments with a very weakly interactive surface. If that is the case, what are the equilibrium pathways, equilibrium chain conformation, and the time scale of the process at the polymer/solid interface? These questions are still in debate due to the lack of experimental techniques capable of providing the necessary structural information at the buried interface.

To overcome the experimental difficulty and further address these questions, amorphous PS melt chains on a weakly attractive quartz (prism) surface were chosen as a rational model system. The technique used was sum-frequency generation spectroscopy (SFG), which takes advantage of the fact that generation of an SFG photon is forbidden in the centrosymmetric bulk, but is nonzero at interfaces where inversion symmetry is broken[43, 117-120]. In addition, two different film preparation processes, i.e., spin-coating (quick solvent evaporation) and dip-coating processes (slow solvent evaporation), were used to create different initial chain conformations, as previously reported[43]. The SFG results reveal that the backbone chains relax in conjunction with randomization of the side chains (phenyl groups) via the equilibration process irrespective of the

original chain conformations, thereby allowing for an increase of the number of solid-(backbone) segment contacts. This is a unique aspect of thermodynamics at the polymer-solid interface even when the interaction between the polymer and solid is weak.

2.3: Materials and experimental techniques:

PS with an average molecular mass of M_w=290,000 g/mol (M_w/M_n=1.06, Pressure Chemical Co.) was used. The polymer was dissolved in toluene (ACS, 99.5% from Alfa Aesar). Quartz prisms for SFG experiments were cleaned using a hot piranha solution (i.e., a mixture of H_2SO_4 and H_2O_2 [*Caution! A piranha solution is highly corrosive upon contact with skin or eyes and is an explosion hazard when mixed with organic chemicals/materials; extreme care should be taken when handing it.*]) for 30 min, and subsequently rinsed with deionized water thoroughly. Simultaneously, we independently used planar silicon (Si) substrates, which were homogenously covered with a native silicon oxide (SiOx) layer, to mimic the PS-quartz interaction[121] and characterized the structures of the flattened chains on the "SiOx/Si" substrate by X-ray reflectivity (XR) and atomic force microscopy (AFM). We confirmed that the cleaned quartz prism and the SiOx/Si substrate showed very similar contact angle results (Supporting Information), proving that the substrates have no significant effects on the resultant adsorbed layers prepared on the different solids. For XR and AFM experiments (Supporting Information), Si (100) wafers (purchased from University Wafers Inc.) were cleaned using a hot piranha solution for 30 min and subsequently rinsed with deionized water thoroughly. The cleaned Si wafers were thereafter treated by a UV/ozone cleaner (UVOCS Inc.) for 30 min. XR results clarified that the resultant surface of the SiOx/Si was covered with a homogenous 2.3 nm thick oxide layer with a surface roughness of less than 0.5 nm (Supporting Information). PS thin films were also prepared by dipping the cleaned quartz prism or SiOx/Si substrates into a bath of the PS/toluene solution and allowing them to

remain in the solution for 30 minutes, then extracting the prisms/Si substrates and drying the polymer films under ambient conditions. The resultant film thickness was approximately 200 nm, measured by an ellipsometer. In parallel, approximately 200 nm-thick spin coated PS films were prepared from PS/toluene solution onto the cleaned quartz prisms or SiOx/Si substrates. In order to extract the flattened layers from both the spin-coating and dip-coating films, we used the established protocol: the PS thin films were annealed at 150 °C for a long period of time (up to 300 h) in an oil-free vacuum oven (below 10^{-3} Torr) and then solvent-leached with chloroform at room temperature repeatedly until the thickness of the residual layer remained unchanged[32]. On the other hand, the "interfacial sublayers" (composed of the loosely adsorbed chains and flattened chains shown in the inset of Fig. 2-1(b)) were prepared by the same solvent-leaching process but with fresh toluene (a worse solvent than chloroform for PS) at room temperature until no obvious change in thickness was observed (at least a total of 5 times of 30 min leaching)[18]. Such a selective extraction of the two different adsorbed chains is possible due to the large differences in the desorption energy between the outer loosely adsorbed chains and the flattened chains, which is proportional to the number of polymer segment-surface contacts[122]. All the resultant flattened layers and interfacial sublayers were post-annealed at 150 °C under vacuum for 6 h to drive away any excess solvent molecules trapped in them. For the SFG experiments, a PS flattened layer on the quartz prism was pressed together with another PS flattened layer prepared independently on a quartz window to suppress any signals from the polymer/air interface. We confirmed that such a sandwich configuration does not affect the chain conformations at the polymer melt-solid interface (Supporting Information). The details of the SFG set-up have been described elsewhere[43]. In summary, visible (wavelength of 532 nm) and tunable infrared (IR) beams were introduced into the quartz prism with incident angles of 70° and 50°, respectively. The measurements with *ssp*

(SFG/*s*; visible/*s*; and IR/*p*) and *ppp* polarization combinations allow us to detect functional groups oriented only along the normal direction to the interface and along all directions, respectively[43].

2.4: Results and discussion:

Fig. 2-1 shows the time dependence of the growth of the flattened layers extracted from the spin-coated and dip-coated PS films prepared on SiOx/Si. The film thicknesses were measured by XR (Supporting Information). The figure shows the crossover from a power-law growth ($h_f \propto t^{\alpha}$) to a plateau region[32]: α=0.40±0.05 for the flattened layers derived from the spin-coated films and α=0.58±0.05 for the flattened layers derived from the dip-coated films. The crossover time ($t_{cross} \approx$ 6h) is nearly identical between the two flattened layers, while the final thickness of the flattened layer derived from the spin-coated films (1.8 ± 0.2 nm) is slightly larger than that derived from the dip-coated thin films (1.4 ± 0.2 nm)[123]. Similar to a previous report[32], t_{cross} corresponds to the time at which the substrate is fully covered with the flattened chains and the loosely adsorbed chains, while the loosely adsorbed chains further grow at $t > t_{cross}$ via a "reeling-in" process[124] of the

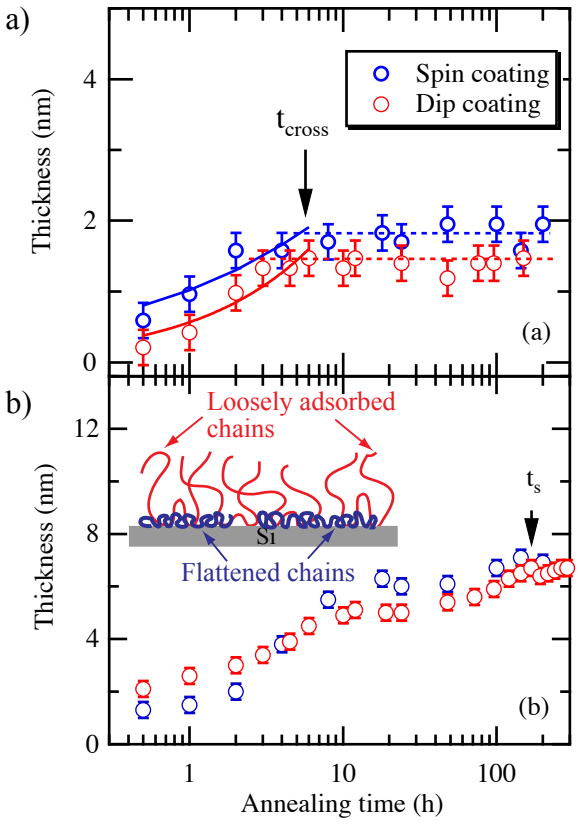

Fig. 2-1 Time evolution of the (a) PS flattened layers and (b) the interfacial sublayer composed of the loosely adsorbed chains and flattened chains derived from the dip-coated and spin-coated PS thin films prepared on SiOx/Si. The inset shows the schematic view of the two different chain conformations.

partially adsorbed (late arriving) chains. As shown in Fig. 2-1(b), we found that the saturation or "quasiequilibrium" adsorption time (t_s)[125] for the interfacial sublayer was 140 h for both the dip-coated and spin-coated films. The final thicknesses of the interfacial sublayers are ~7 nm irrespective of the film preparation processes. It is also interesting to point out that this saturation or "quasiequilibrium" adsorption time is in good agreement with the time (168 h) which takes for the residual stress of a PS (M_w = 654 kDa) spin cast film to completely disappear via thermal annealing at a temperature of 155 °C[111]. The surface morphologies of the flattened layers and interfacial sublayers are summarized in Supporting Information.

Fig. 2-2 shows the SFG spectra from the matured flattened layer extracted from the spin-coated and dip-coated films annealed at 150 °C for 144 h. The multiple peaks located in between 2800-3000 cm^{-1} were assigned to the contributions from the PS backbone chains[126]. The peaks at 2850 and 2906 cm^{-1} were assigned to the symmetric C-H stretching vibration of methylene (CH_2 s) groups[43] and the C-H stretching vibration of methyne (CH) groups, respectively, both of which are included in the backbone and the chain ends[127]. Furthermore, the two peaks (indicated with asterisks) at 2876 and 2960 cm^{-1}, were assigned to the symmetric and antisymmetric methyl groups, respectively. Although PS does not possess methyl groups,

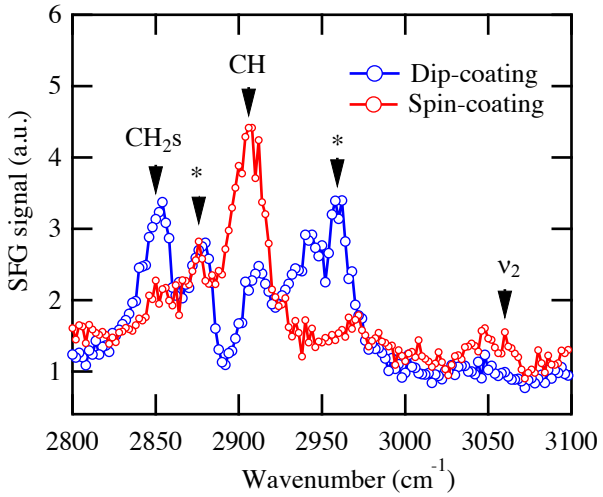

Fig. 2-2 SFG spectra with the *ssp* polarization combination for the flattened layers derived from the spin-coated and dip-coated PS thin films annealed at 150 °C for 144h. The assignments of the multiple peaks are described in the main text. The counterpart SFG spectrum with the *ppp* polarization combination for the flattened layer derived from the dip-coating film is shown in Supporting Information.

they would be present in an initiator fragment, or a chain end portion, as previously indicated by Tanaka and co-workers who used SFG in conjunction with deuterated PS synthesized with two different initiators i.e., *sec*-butyllithium and potassium naphthalenide[43,127]. Hence, the present results reveal evidence of the segregation of the chain ends at the substrate surface, which is consistent with previous experimental[128] and simulation results[129-132]. The peak around 3060 cm^{-1} is attributed to the contribution from the ν_2 vibrational mode of phenyl rings[133]. As shown in Supporting Information, the SFG spectrum from the flattened layer is in good agreement with that of the PS annealed film before extraction of the flattened layer. Moreover, we confirmed that the SFG spectrum from the interfacial sublayer composed of the loosely adsorbed chains and flattened chains is identical to the flattened layer (Supporting Information). Hence, these results clarify that the majority of the SFG signal from the PS thin film results from the flattened chains rather than surface reorganization in glassy polymers which is associated with a surface activated β-relaxation occurring over length scales of a few nanometers[134].

On the other hand, the SFG spectrum using *ssp* polarization from the matured flattened layer derived from the spin-coated film annealed at 150 °C for 144 h is quite different from that previously reported for a spin-coated PS (M_n=56.5kDa) film (~ 100 nm in thickness) on the same quartz prism annealed at 150 °C for 3h[43] (Supporting Information): the ν_2 vibrational mode is clearly seen, suggesting that the phenyl groups of PS are strongly directed toward the quartz substrate[121, 135], while the contributions from the PS backbone chain are insignificant. This preferential interfacial orientation of the phenyl ring is attributed to the polar nature of the silanol groups on the substrate as well as the hydrogen bonding between the π electron cloud of the phenyl ring and a surface hydroxyl (OH) group of the quartz surface[121]. Tanaka and co-workers[43] also reported that, when annealing time is not sufficiently long, the preferential orientation of the

phenyl rings is more significant at the substrate interface of the spin-coated PS film than the solvent-cast PS film (the left part of Fig. 2-3). It is due to the formation of an elongated chain conformation along the lateral direction of a substrate surface due to the shearing force during the spin coating process, as experimentally shown by Kraus and co-workers[136]. Intriguingly, as shown in Figure 2-2, the contributions from the ν_2 vibrational mode of the phenyl group in the matured flattened layer become very weak regardless of the film preparation processes. Hence, the first conclusion from the present SFG results reveals that the initial preferential orientation of the phenyl rings is randomized during the prolonged thermal annealing process at $T >> T_g$, as illustrated in Fig. 2-3.

Fig. 2-2 also reveals that the multiple peaks in between 2800-3000 cm^{-1}, which were assigned to the contributions from the PS backbone chains, were dominant at the substrate interfaces of both the spin-coated films and the dip-coated films in the quasiequilibrium state. This is in contrast to the SFG result from the PS thin film annealed for a much shorter time[43] (Supporting Information). Hence, our results hence indicate that the backbone chains in PS relax in association with the randomization of the phenyl side groups and thereafter attach even with the weakly interactive solid surface (the right illustration of Fig. 2-3) irrespective to the film preparation processes. We postulate that this increase in the number of solid/ (backbone) segment contacts is the driving force for the flattening process to overcome the conformational entropy loss in the total free energy[8, 17] and results in the improvement of the segmental packing of the flattened chains. The local conformations of the flattened chains revealed in this study may

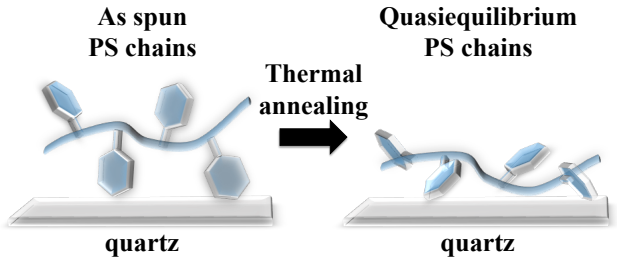

Fig. 2-3 Proposed chain conformational changes on the substrate during the equilibration process.

be consistent with simulation results which describe the tendency of local 2D nematic ordering of "train" parts of adsorbed chains derived from stiff polymers[42, 114].

Tanaka and co-workers[43] also reported that the preferred interfacial orientations of the phenyl ring or backbone chains from the spin coating process disappeared after solvent vapor annealing which facilitates relaxation of non-equilibrium polymer chain conformations even near the substrate[110, 137]. As mentioned earlier, we also used a solvent to extract the flattened layers intensively so that an analogous plasticization effect of the solvent to remove the sample history should take place. Therefore, it is reasonable to suppose that the polymer chains are strongly bound to the solid surface and thereby the solvent effect on the chain relaxation is not critical. Rather, the structural relaxation and re-organization process of the bound polymer chains is inherent in the equilibrium pathway at the polymer melt-solid interface.

In summary, we have investigated the chain relaxation process toward the equilibrium state of PS chains adsorbed onto weakly attractive solids using SFG. Two different kinds of film preparation processes (i.e., dip coating and spin-coating) were used to illuminate the effect of the initial chain conformations. The SFG results reveal that the phenyl side groups, which were initially aligned at the quartz substrate[121, 135], become randomized via the equilibration process regardless of the film preparation processes. Furthermore, the randomization of the phenyl side groups expedites the relaxation of the backbone chains, allowing for an increase of the number of solid/(backbone) polymer segment contacts and thereby overcoming the conformational entropy loss of the bound polymer chains in the total free energy[25, 115, 116].

2.5: Supporting information:

Experimental Section:

Ellipsometry: The thicknesses of the PS spin coating and dip coating films were measured using an AutoEL-II ellipsometer (Rudolph Research) at room temperature. The wavelength of the laser used in the measurements was 633 nm and a literature value of 1.589 as a refractive index for PS[138] was used for the experiments.

X-ray Reflectivity (XR): XR experiments were performed under ambient conditions at the X10B and X20A beamlines of the National Synchrotron Light Source, Brookhaven National Laboratory and the G2 beamline of Cornell High Energy Synchrotron Source (CHESS). The specular reflectivity was measured as a function of the scattering vector (q_z) in the direction perpendicular to the surface, $q_z = 4\pi\sin\theta/\lambda$, where θ is the incident angle and λ is the x-ray wavelength (λ = 0.087 nm at X10B, λ = 0.118 nm at X20A, and λ = 0.110 nm at G2, which are equivalent to the X-ray energies of 14.2 keV, 10.5 keV, and 11.25keV, respectively). The XR data was fit using a standard multilayer fitting routine for a dispersion value (δ in the X-ray refractive index) in conjunction with a Fourier transformation (FT) method, a powerful tool to obtain detailed structures for low X-ray contrast polymer multilayers[139].

Atomic Force Microscopy (AFM) measurements: Surface morphologies of the interfacial sublayers and flattened layers were studied using atomic force microscopy (AFM) (Veeco Multimode V) at Center for Functional Nanomaterials (CFN) at BNL. Standard tapping mode experiments were conducted in air using cantilevers with spring constants of about 40 N/m (for a tapping mode). The scan rate was 0.5 to 1.0 Hz with a scanning density of 512 lines per frame.

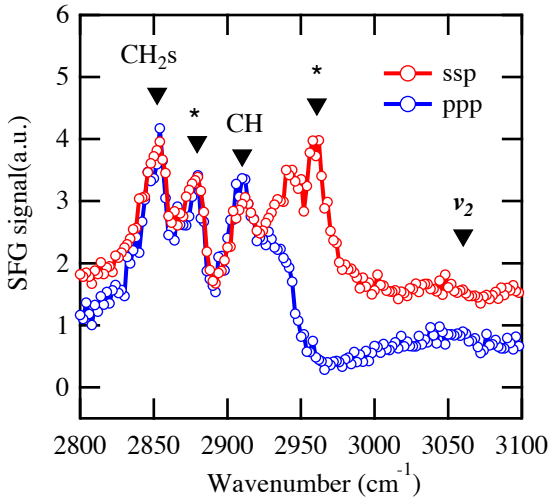

Fig. 2-S1: SFG spectra from the *ssp* and *ppp* polarization combinations for the flattened layer derived from the dip-coating film annealed at 150 °C for 144h. The assignments of the respective peaks are described in the main text.

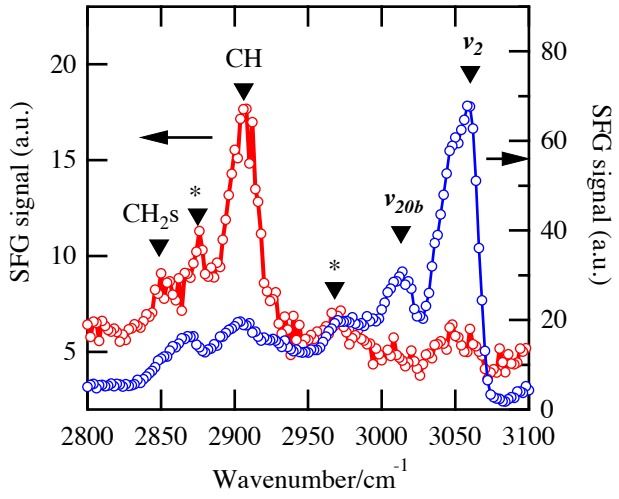

Fig. 2-S2: SFG spectra for the PS spin-cast film annealed for 3 h (blue) and 144 h (red) at 150 °C with the *ssp* polarization combination. The SFG data for 3 h annealing is from Ref. 28. The assignments of the respective peaks are described in the main text. Note that the peak around 3020 cm^{-1} is attributed to the contribution from the ν_{20b} vibrational mode of phenyl rings[9,11].

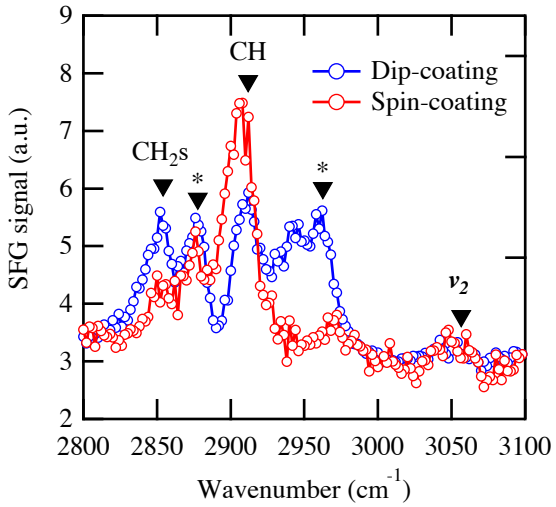

Fig. 2-S3: SFG spectra from the *ssp* polarization combination for the interfacial sublayers derived from the spin-coating and dip-coating films annealed at 150 °C for 144h. The assignments of the respective peaks are described in the main text.

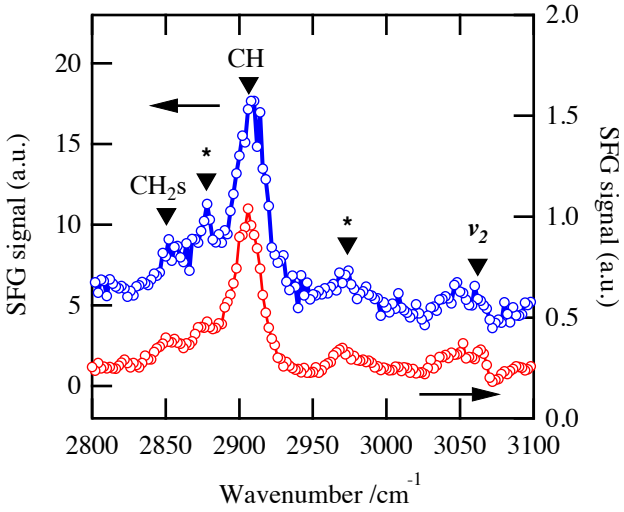

Fig. 2-S4: Comparison of the SFG spectra from the *ssp* polarization combinations for the sandwiched (blue) (bilayers) and (b) uncapped (single) (red) flattened layer derived from the spin-coating film annealed at 150 °C for 144h. The assignments of the respective peaks are described in the main text.

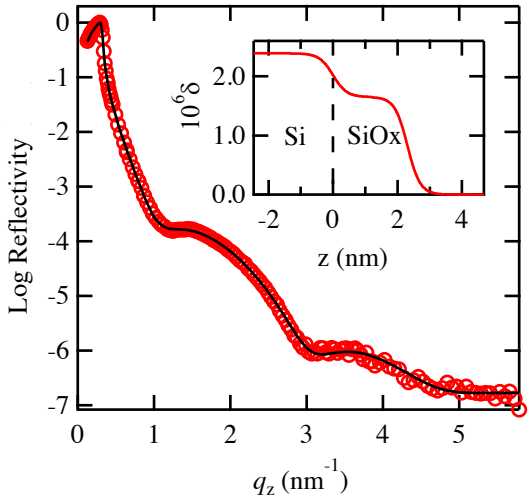

Fig. 2-S5: XR curve of the cleaned SiO_x/Si substrate. The black solid line corresponds to the best-fit to the data based on the dispersion (δ) profile against the distance (z) from the interface between silicon substrate and native oxide layer (SiO_x/Si interface) as shown in the inset. The dotted line in the inset corresponds to the SiO_x/Si interface.

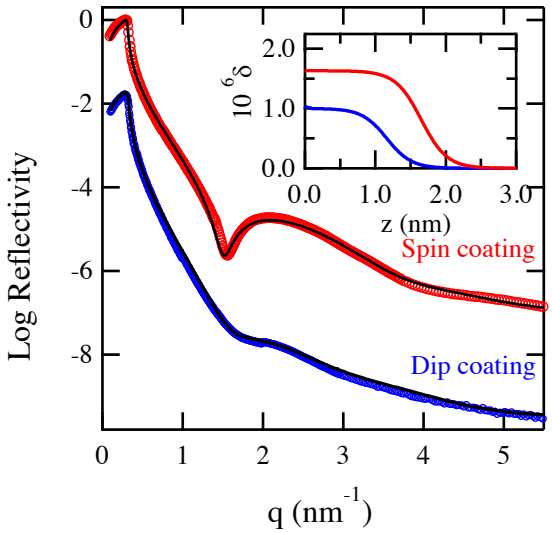

Fig. 2-S6: XR curves of the quasiequilibrium flattened layers. The solid lines correspond to the best-fit to the data based on the dispersion (δ) profiles against the distance (z) from the SiOx surface shown in the (b): red line, the flattened layer derived from the spin-coated film with the X-ray energy (E) of 10.5 keV; blue line, the flattened layer derived from the dip-coated film with E=11.25 keV. The δ values of the bulk PS are 1.85×10^{-6} for E=11.25 keV and 2.12×10^{-6} for E= 10.5 keV. The curves are shifted vertically for clarity.

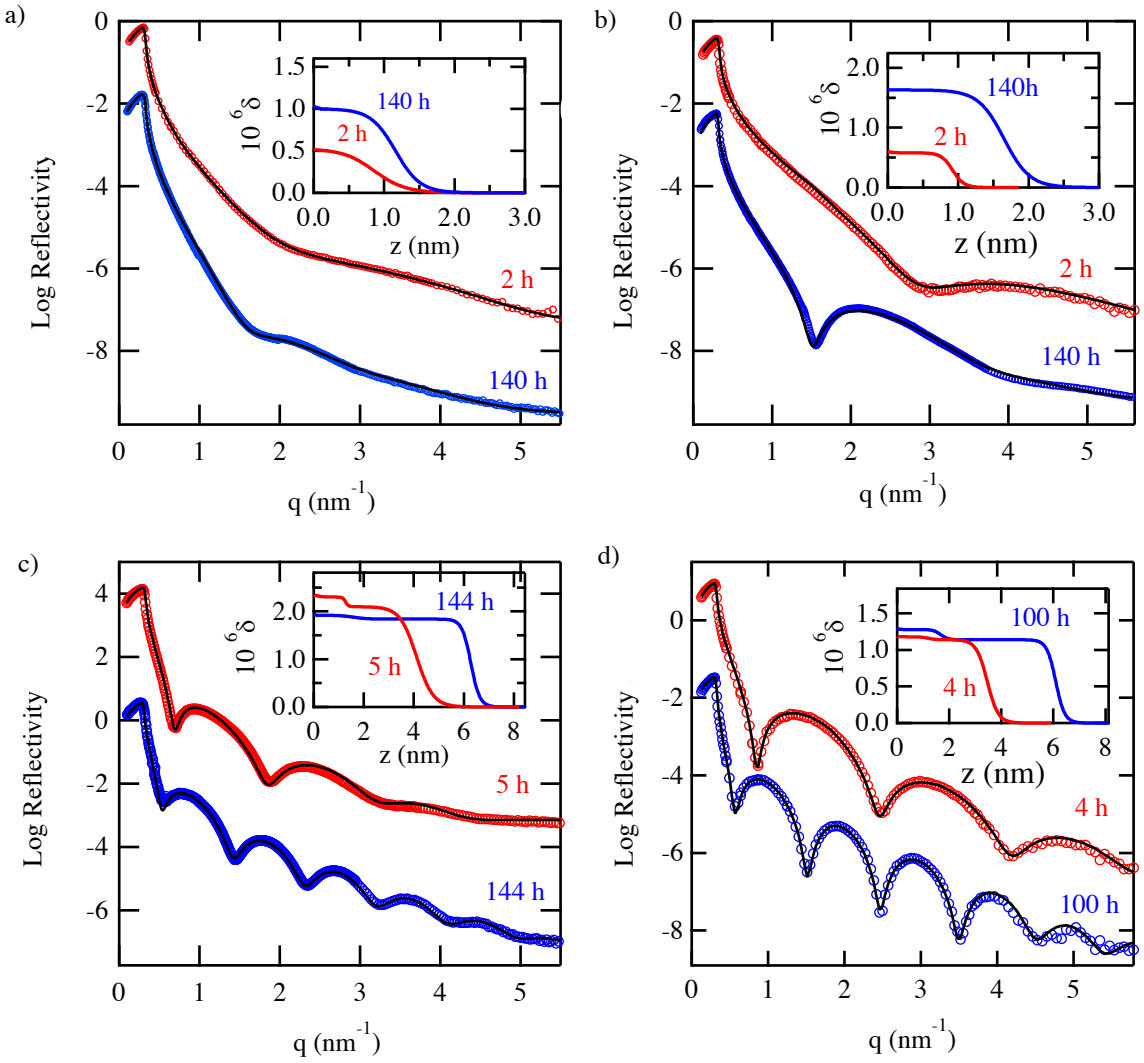

Fig. 2-S7: Representative time dependence of the XR curves of the flattened layers derived from (a) the dip-coating films with E =14.2 keV (red) and E =11.25 keV (blue) and (b) spin-coating films with E=14.2 keV (red) and E=10.5 keV (blue) and the interfacial sublayers from (c) the dip-coating films with E =10.5 keV (red) and E =11.25 keV (blue) (d) the spin-coating films with E=14.2 keV. The numbers displayed in the figures correspond to the annealing time. The solid lines correspond to the best-fits to the data based on the dispersion (δ) profiles against the distance (z) from the SiOx surface shown in the inset. The δ values of the bulk PS are 2.12×10^{-6} for E= 10.5 keV, 1.85×10^{-6} for E=11.25 keV, and 1.14×10^{-6} for E= 14.2 keV. It should be noted that there are two different PS layers with different densities for the interfacial sublayer. The choice of the two-layer model was determined by the corresponding Fourier transformation profile of the XR profile. The details of the XR analysis for the PS interfacial sublayers in conjunction with the FT method have been described elsewhere [3,5]. The curves are shifted vertically for clarity.

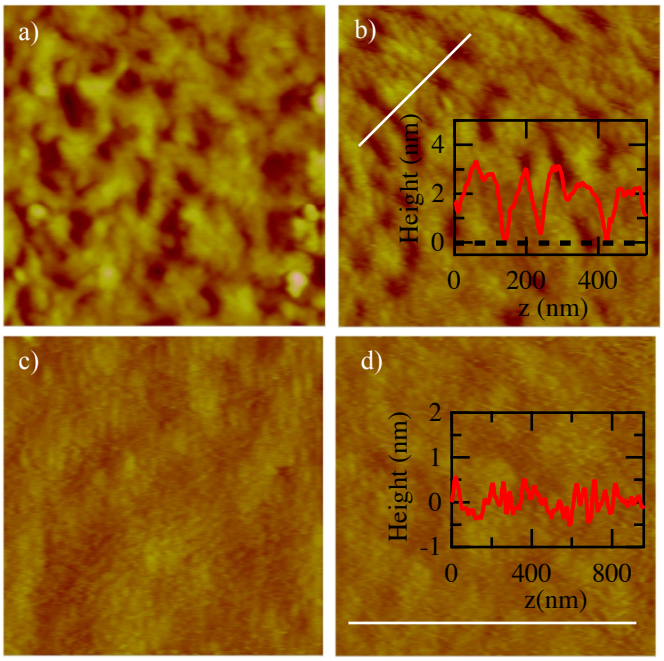

Fig. 2-S8 AFM height images of the PS flattened layer surface derived from (a) the dip coating film and (b) the spin-coating film and the interfacial sublayers derived from (c) the dip coating film and (d) the spin-coating film after annealing at 150°C for 144 h. The scan sizes and height scales are 1 μm × 1 μm and 0 - 6 nm for all the images, respectively. The insets of the images (b) and (d) correspond to the height profiles along the white lines in (b) and (d). The dotted line corresponds to the SiO_x surface.

Surface coverage of the flattened layers. In order to estimate the surface coverage (ϕ_p) of the flattened layers, a bearing area analysis was utilized using the NanoScope Analysis software (version 1.40, Bruker) that we have established previously[32]. A bearing area gives a percentage of the surface above a critical threshold. For this analysis, the AFM height images were used and we set the critical threshold to 0 nm at the

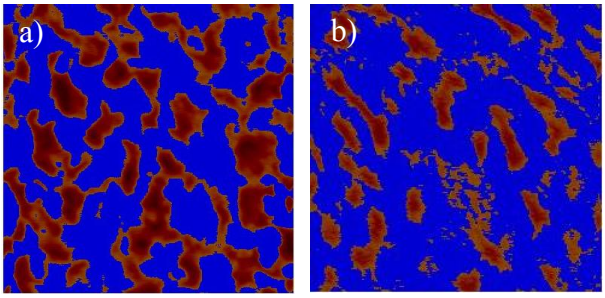

Fig.2-S9: Bearing area analysis results of the AFM images shown in Fig 2-S8 (a) (left) and Fig. 2-S8 (b) (right). The areas occupied by the polymer (bearing areas) are colored in blue.

polymer/SiO_2 interface. We independently preformed a scratch test to find the interface. Fig. 2-S9 shows the representative bearing analysis results using the AFM images shown in Fig. 2-S8 (a) of the Supporting Information. An average ϕ_p value of 48 % (± 5 %) was estimated for the flattened layer derived from the dip-coating film based on several AFM images at different spots of the film. The Φ_p value for the flattened layer derived from the spin-coating film was estimated to be 70 ± 5%.

The observed dispersion value of the flattened layer (δ_{obs}) is given by:

$$\delta_{obs} = \delta_{PS} \times \phi_p + \delta_{air} \times (1 - \phi_p) \quad \text{(S1)}$$

where δ_{ps} and δ_{air} is the dispersion value of the PS flattened layer and air, respectively. Eq. (S1) with the given δ_{air} (which can be approximated to zero since the value is much smaller than δ_{ps}), δ_p, and δ_{obs} values gives us $\delta_{ps} = 2\times10^{-6}$ for the flattened layer derived from the dip-coating film and $\delta_{ps} = 2.4\times10^{-6}$ for the flattened layer derived from the spin-coating film, respectively. This higher δ_{ps} value of the flattened layer (by about 10%) derived from the spin-coating film is consistent with the previous experimental[22, 25, 32] and simulational findings[114, 140], while the δ_{ps} value of the flattened layer derived from the dip-coating film is nearly the same as the bulk $\delta_{ps,}$. At this point, it is not yet conclusive whether the high-density flattened layer is also formed at the polymer-solid interface of the dip-coating film. However, we should emphasize the fact that the lateral correlation length of the textures seen in the flattened layer is less than the coherent length of X-ray beams at the sample position (~ 1 μm in the present case). Therefore, X-rays are sensitive to the textures and would interfere with them, possibly causing a drastic change in the "amplitude" of Kiessig oscillation fringes. This would make the accuracy of the data fitting (for the density and roughness of the flattened layer) somewhat ambiguous, while the thickness can be independently and still accurately determined from the "period" of the oscillation fringes. Hence, it may be

difficult to obtain an accurate δ value for the flattened layers with low surface coverage. Further experiments need to be done to clarify the issue.

SFG signal from methyl groups. According to a previous report by Müller-Buschbaum and co-workers[141], it was demonstrated that residual toluene molecules are bound at the substrate interface of PS spin-cast films even after thermal annealing, which may give signals from methyl groups. To rule out this possibility, we independently prepared spin-coating and dip-coating PS (M_w=290,000 g/mol) films using deuterated toluene as a solvent. The films were then annealed at 150 °C for 96 h, which was a much longer annealing time compared to that (8h at 120 °C and 160 °C) used in the literature[141] to evaporate the solvent completely. The SFG experiments clearly detected the signals at 2960 cm^{-1}, which is attributed to the C-H anti-stretching vibration of methyl groups. Thus, it is reasonable to conclude that the SFG peaks (indicated with asterisks in Fig. 2-2) are not from any residual solvent molecules. In addition, as reported previously[127], we characterized a film of deuterated PS (dPS) synthesized by sodium naphthalenide as a bifunctional polymerization initiator so that there were no methyl groups in the polymer chains. The SFG results illuminated no signals from methyl groups in the dPS thin film. Hence, it is reasonable to conclude that the observation of the signal from methyl groups indicates that a fragment of the initiator, Sec-BuLi, is segregated at the interface.

Liquid contact angle measurements for SiOx/Si and quartz surfaces. Static contact angle measurements with two liquids (water and glycerol) were carried out using a CAM 200 optical contact angle meter (KSV instruments, Ltd.) equipped with a video camera. A static contact angle (θ) of a film surface was determined based on the three-phase contact line with a 2 μL liquid droplet. All the results were obtained by averaging data from at least 5 individual samples and 10 readings per sample at different locations. It was found that the static contact angle of the SiOx/Si

is $\theta = (18 \pm 1)°$ for glycerol, which is in good agreement with that of that the quartz substrate ($\theta = (20 \pm 1)°$) for glycerol, which is also in good agreement with a previous result ($\theta = 26$ ° for glycerol)[142]. Since, the cleaned quartz prism and the SiOx/Si substrate showed very similar contact angle results, the different substrates used in the above experiments have no significant effect on the resultant adsorbed layers prepared on the different solids.

Chapter 3

Two-dimensional flattened structures of block copolymers on solid surfaces

3.1: Abstract: Block copolymers (BCP) thin films offer a simple and effective route to fabricate highly ordered periodic microdomain structures. However, it is known that preferential interactions between the blocks and the substrate and air cause the microdomains to orient parallel to the interfaces, resulting in a multilayered structure. We here report that one block coexist side-by-side with the other block on solid substrates with highly specific interactions, resulting in a novel two-dimensional (2d) flattened structure at the nanometer scale. Cylinder-forming polystyrene-block-poly(4-vinylpyridine) diblock copolymer and lamellar-forming poly (styrene-block-butadiene-block-styrene) triblock copolymer polystyrene-block-poly(4-vinylpyridine) were used as models. In order to reveal the buried interfacial flattened structures, the following experimental protocols were utilized: the BCP monolayer films were annealed under vacuum at $T > T_g$ of the blocks (to equilibrate the melts); vitrification of the annealed BCP films via rapid quench to room temperature; subsequent intensive solvent leaching (to remove unadsorbed chains) with chloroform, a non-selective good solvent for the blocks. A suite of surface-sensitive techniques demonstrate that both blocks lie flat on the substrate, forming the 2d randomly phase-separated structure irrespective of their microdomain structures and interfacial energetics.

3.2: Introduction:

Smart material interfaces in a variety of applications, such as those used for photolithography, removable inks, healable surfaces, and contact adhesives, demand control over complex interfacial processes, often involving adsorbed polymers [143]. Like any thermodynamic process, polymer adsorption on a surface is governed by entropic and enthalpic contributions to the free energy. In case of supported BCP thin films, interfacial energetics at the polymer-air and polymer-substrate interfaces play a crucial role in controlling the orientation and ordering of microdomain structures[56, 57]. In general, preferential interactions between one of blocks and the substrate or free surface will induce enrichment of the block with the lowest surface energy at the respective surface, resulting in parallel alignment of microstructure orientation[144-147]. However, the situation is complicated when thickness of a BCP film is less than the equilibrium interdomain spacing (L_d); the surface-parallel lamellar or cylinder orientation would incur an entropic penalty; microdomains oriented perpendicular to the film surface plane are formed instead [148-151]. In this study, polystyrene (PS)-based cylinder-forming or lamellar-forming block copolymers prepared on silicon (Si) substrates were used as models. We found that both the non-PS blocks, which have stronger affinity to the solid substrate than the PS block, and the PS block adsorb on the substrate surface simultaneously and coexist side-by-side on the solid, resulting in a few nanometers thick flattened layer with randomly phase-separated structure having the characteristic length of about 10 nm. Thus, the driving force for the development of such chain conformations is the total enthalpic gain due to an increase in solid-segment contacts that overcomes a loss in the conformational entropy of the adsorbed polymer chain[115, 116, 152].

3.3: Materials and experimental techniques:

Two different polystyrene (PS)-based block copolymers with varying PS contents were prepared on Si substrates as model systems: poly (styrene-*block*-4-vinylpyridine) (PS-*b*-P4VP, M_w=41,000 g/mol, M_w/M_n=1.1, Polymer Source Co.) and poly (styrene-*block*-butadiene-*block*-styrene) (SBS, M_w= 85,000 g/mol, M_w/M_n=1.4, Asahi-Kasei Chemical Corp.). The volume fractions of the PS component are 0.81 for PS-*b*-P4VP and 0.64 for SBS, respectively. We confirmed that bulk PS-b-P4VP displays hexagonally packed cylindrical microdomain structures, while SBS displays lamellar microdomain structures based on small angle X-ray scattering (SAXS) results (Supporting Information). The interdomain spacing (L_d) at room temperature was determined to be 36 nm for PS-*b*-P4VP and 29 nm for SBS, respectively. Si substrates (purchased from University Wafer Inc.) were pre-cleaned using a hot piranha solution (i.e., a mixture of H_2SO_4 and H_2O_2, *caution: a* piranha solution *is highly corrosive upon contact with skin or eyes and is an explosion hazard when mixed with organic chemicals/materials; Extreme care should be taken when handing it*) for 30 min, and were subsequently rinsed with deionized water thoroughly. We previously confirmed that the native oxide (SiO_x) layer after cleaning had a thickness of d_{SiOx} = 2.4 nm[153] (hereafter assigned as "non-treated Si"). The piranha solution-cleaned Si wafers were further immersed in an aqueous solution of hydrogen fluoride (HF) for 20s to remove the SiO_x layer (hereafter assigned as "HF-etched Si"). However, we confirmed that a thin SiO_x layer of 1.3 nm in thickness was reproduced even immediately after HF etching due to atmospheric oxygen and moisture[41]. A series of SBS monolayers with film thicknesses (h) of $h = L_d$ were spun cast from toluene solutions onto the HF-etched Si substrates, while PS-b-P4VP thin films with $h = L_d$ were spin coated from chloroform solutions onto the non-treated Si substrates because of the strong affinity of P4VP to the SiO_x layer. The thicknesses of the spin-cast thin films were determined by

an ellipsometer (Rudolf Auto EL-II) with the fixed refractive indices of 1.53 and 1.59[50] for SBS and PS-b-P4VP, respectively. According to previous results[68, 154, 155], PB and P4VP have a greater affinity to SiO_x than PS. On the other hand, Knoll and co-workers[156] showed that PB (γ_{PB}=31 mN/m) has a lower surface energy than PS (γ_{PS}=41 mN/m) at the polymer-air interface, while P4VP has a higher surface energy at the polymer-air interface than PS[157]. Hence, it is reasonable to suppose that SBS exhibits a symmetric wetting condition, while PS-b-P4VP presents an asymmetric wetting condition.

In order to uncover the interfacial structure, we used the established Guiselin's protocol[158]. In this method, a melt was equilibrated against a solid surface; unadsorbed chains can be then removed by a good solvent, while the adsorbed chains are assumed to maintain the same conformation due to the irreversible freezing experienced through multiple solid-segment contacts. Several research groups have already demonstrated that Guiselin approach is practical for revealing the buried interfacial structures for various homopolymers[13, 17, 20, 24, 41, 45, 159-167]. Following the protocol, the spin-cast BCP thin films were annealed at 150 °C for SBS and at 190 °C for PS-b-P4VP, both of which are above the individual homopolymer bulk glass transition temperatures, for prolonged periods of time (up to 300 h) in a vacuum oven at 10^{-3} Torr. Based on previous knowledge about the flattened layer formation of the constituting homopolymers[41], we leached the annealed BCP films with chloroform ($CHCl_3$), a good solvent for the individual blocks, at room temperature until the thickness of the residual layer remained unchanged (at least 10 times of 30 min-leaching). Note that the experiments were carried out in continually replenished solvent to facilitate desorption kinetics[143]. The resultant flattened layers were dried at high temperatures (150 °C for SBS and 190 °C for PS-b-P4VP) for 24h under vacuum to remove any excess solvent before further experiments.

3.4: Results and discussion:

We start with the structural characterization of the SBS flattened layer. Fig. 3-1 shows the XR profile of the SBS flattened layer with the annealing time (t_{an}) of 100 h. We utilized a three-layer model (a Si substrate, a SiO_x layer, and a SBS layer) to fit the experimental XR data. The details of the measurement and the fitting procedure are described in Supporting Information. A least-square fit (the black solid line) to the XR profile was performed using the dispersion (δ) profile shown in the inset of Fig. 3-1. The thickness of the quasi-equilibrium SBS flattened layer obtained from the fit is 1.5 ± 0.2 nm. Note that since the lateral correlation length of the textures in the flattened layer is ~ 10 nm (as will be discussed later), X-rays are sensitive to the texture structure and would interfere with them, possibly causing a drastic change in the "amplitude" of Kiessig oscillation fringes. This would make the accuracy of the data fitting (for the density and roughness of the flattened layer) somewhat ambiguous, while the thickness can be independently and still accurately determined from the "period" of the oscillation fringes. Hence, it is inconclusive whether a high-density flattened layer is formed at the polymer-solid interface. It is also important to mention that the quasi-equilibrium SBS flattened layer thickness was nearly equivalent to those of the PS or PB homopolymer flattened layers previously reported[41].

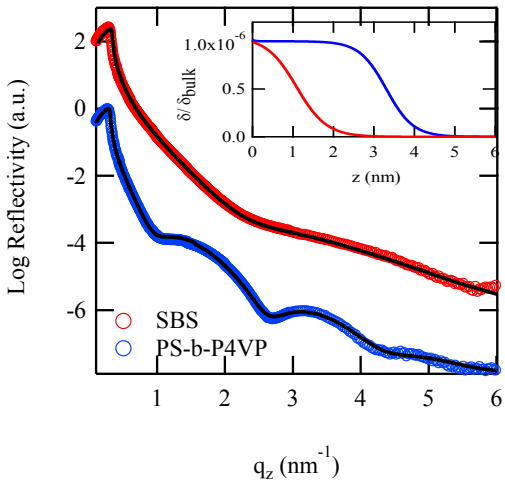

Fig. 3-1: XR profiles of the SBS and PS-b-P4VP flattened layers. The solid lines represent the best fits to the data based on the dispersion profiles shown in the inset.

Fig. 3-2 shows the time dependence of the film thicknesses of the flattened layers derived from the annealed spin-cast films. From the figure, we can see that the growth of the flattened layer reaches a plateau region after the cross over time (t_{cross})[32]. The t_{cross} values of 2 h for SBS is

nearly identical to those of the respective homopolymer flattened layers, which correspond to the time when the substrate surface is fully covered[41]. The AFM images further verified that the Si substrate was homogeneously covered with the SBS polymer after t > t_{cross} (Fig. 3-2(a)), but the detailed morphology of the individual blocks on the substrate was not clearly observed. To further visualize the structure, we stained the PB blocks with OsO_4 selectively and a SEM measurement was conducted. As shown in Fig. 3-3(b), the SEM image evidenced that the PB-rich regions (which appear bright in the image[68]) were dispersed in the matrix (which appear dark in the image).

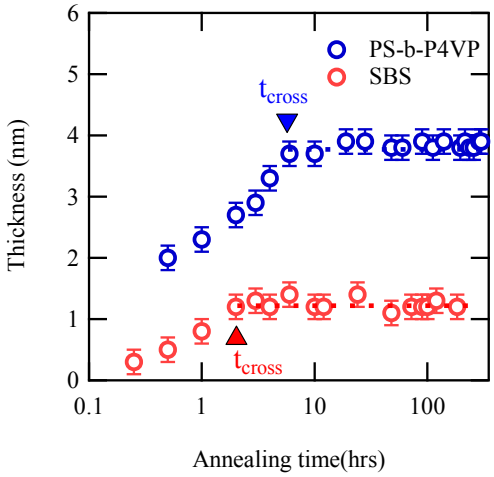

Fig. 3-2. Time evolution of the flattened layers derived from the PS-b-P4VP and SBS thin films. The crossover times (t_{cross}) for the PS-b-P4VP and SBS flattened layers are estimated to be 6h and 2h, respectively.

To further characterize the microscopic structure of the flattened layer, we utilized GISAXS. Fig. 3-3(d) shows the GISAXS profile of the SBS flattened layer with t_{an} =100 h. The details of the measurements are described in the Supporting Information. The 2d intensity profile was converted into the 1d profile along the q_{xy}-direction at around q_z = 0.1 nm^{-1}. From the figure, we can see a power law decay of the scattering intensity, i.e., $I(q_{xy}) \propto q_{xy}^{-3}$($q_{xy}$ is the in-plane scattering vector) at q_{xy} > 0.22 nm^{-1} and a deviation from the power law at the lower q_{xy} region. In conjunction with the SEM image, it may be reasonable to suppose that this power law scattering

arises from a randomly distributed two-dimensional (2d) two-phase system [168]. The Debye-Bueche (DB) model can be used to describe the scattering profile from such a random structure where the correlation is characterized by an inhomogeneity length (ξ)[169]. The DB equation for a 2d random structure is given as follows[168]:

$$I(q_{xy}) = \frac{C\xi^2}{(1+q_{xy}{}^2\xi^2)^{1.5}} \quad (1)$$

where C is a constant. The best-fit using eq. (1) to the GISAXS profile gave us ξ = 10.2 ± 0.3 nm. Hence, the size is reasonably comparable to that of the individual PB rich region in the SEM image (see, Fig. 3-3(b)). The critical question is therefore where are the PS chains are located within the 1.5 nm thick confinement space.

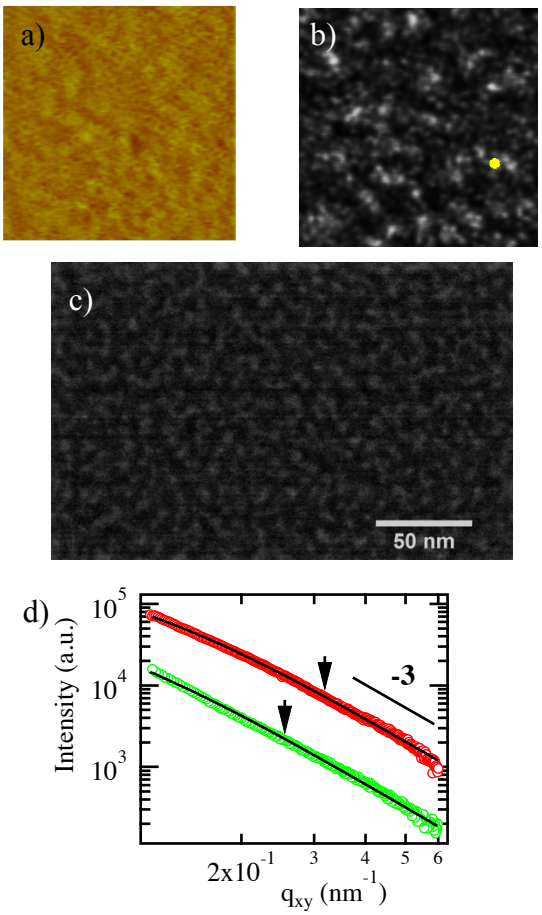

Fig. 3-3. (a) AFM phase image (1 μm × 1 μm size). SEM images of (b) the SBS flattened layer (0.25 μm × 0.25 μm) and (c) PS-b-P4VP flattened layer. The yellow circle in (b) corresponds to 10 nm in size. (d) GISAXS profiles from the SBS (red) and PS-b-P4VP (green) flattened layers. The arrows indicate the cut-off positions where we can see a deviation from the power law.

To answer the question, we investigated the local chain conformations of the SBS flattened chains using sum frequency generation spectroscopy (SFG). This technique takes advantage of the fact that generation of an SFG photon is forbidden in the centrosymmetric bulk, but is nonzero at interfaces where inversion symmetry is broken[120, 170]. The details of the SFG experiments are described in the Supporting Information. Since our previous results showed that the majority of SFG signals under *ssp* (SFG/s; visible/s;

and IR/p) and *ppp* (SFG/*p*; visible/*p*; and IR/*p*) polarization combinations for a PS thin film is attributed to the flattened chains[152], we measured the SFG signal from an annealed 29 nm-thick ($h = L_d$) SBS thin film prepared on a quartz prism without extracting the SBS flattened layer. We confirmed that (i) the resultant morphology and the film thickness of the SBS flattened layer on the non-HF Si substrates are similar to those on the HF-Si substrates and (ii) the contact angles of a quartz substrate and non-HF Si substrate are nearly identical[152]. Hence, the effect of the quartz substrate on the chain conformations can be ruled out.

Fig. 3-4 shows the SFG spectrum with the *ssp* polarization combination from the SBS film annealed at 150 °C for 96 h. From the figure we can see four peaks at 2836, 2906, 3030, and 3060 cm^{-1}, which are attributed to the contributions from the symmetric C-H stretching vibrations of methylene (CH_2s) groups, the C-H stretching vibration mode of methyne (CH) groups[43], the ν_{20b} vibrational mode and ν_2 vibrational mode of phenyl rings, respectively[170]. These peaks indicate the main chains and the phenyl groups of PS are directed toward the substrate surface, as reported previously[170, 171]. The phenyl rings are nearly parallel to the substrate but slight directed towards the substrate surface. This is consistent with a previous simulation result[171] and experimental result[170]. The interfacial ordering (tilting) of the backbone chains seems to arise from the bulky nature of the phenyl rings[171].

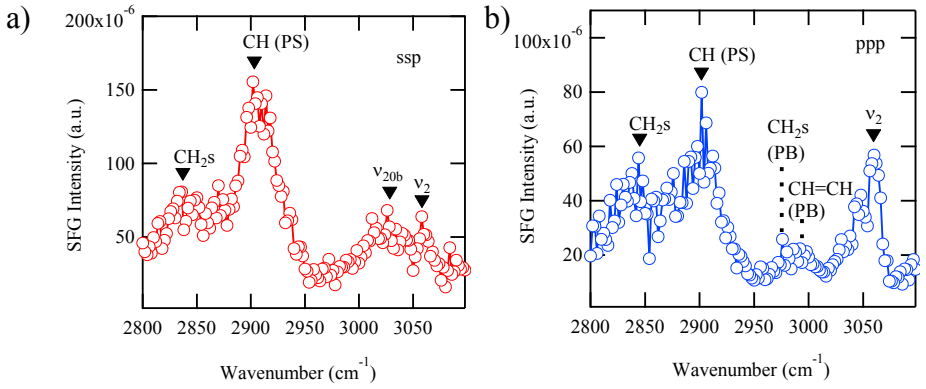

Fig. 3-4. SFG spectra for the SBS thin film using the (a) *ssp* and (b) *ppp* polarizarion combinations.

It should be noted that the peak at 2906 cm^{-1} may also be attributed to the contribution from the asymmetric C-H stretching vibrations of methylene (CH_2as) mode of a PB chain. However, as shown in Fig. 3-4(b), the CH_2s and CH=CH vibration modes of a PB chain in the SFG spectrum with the *ppp* (SFG/*p*; visible/*p*; and IR/*p*) polarization combination are observed at around 2980 and 3000 cm^{-1}, respectively, while both modes are not visible in the SFG spectrum with the *ssp* polarization combination. Given the fact that SFG measurements with the *ssp* and *ppp* polarization combinations are sensitive to chain orientations along the direction normal to the film surface and all directions, respectively[43], we may conclude that the adsorbed PB chains have the tendency to lie parallel to the planar substrate surface due to the adhesive interaction with the substrate. Fig. 3-5 shows the proposed chain orientations of the SBS chains at the substrate interface. As mentioned above, due to the bulky nature of the side chains, the PS backbone chains tend to have the tilt configuration in the direction normal to the substrate. Hence, the data implies that the formation of a surface directed wetting layer reported previously[68, 154, 172] does not take place. Furthermore, it is reasonable to suppose that a few nm confined space does not induce a disordered state of BCP previously reported[154]. Note that this flattened layer bears similarity to a reported uniformly thick "foot" (~ 1.5 nm in thickness) of various PS-based block copolymer thin films prepared from microdroplets[173], which was hypothesized to be a "precursor" film developed ahead of a macroscopic edge of a spreading homopolymer droplets on a smooth SiOx/Si substrate[174]. To see the generality of the buried adsorbed structure, we also characterized on the PS-b-P4VP flattened layer. The AFM image (Supporting information) further verified that the Si substrate was homogeneously covered with PS-b-P4VP after $t_{an} > t_{cross}$ =6h (Fig. 3-2). The XR result for the

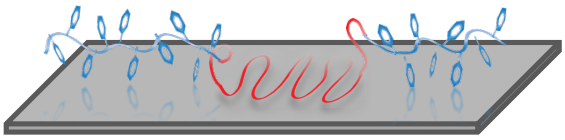

Fig. 3-5. Proposed SBS chain conformation on the substrate

flattened layer at $t_{an} > t_{cross}$ gave us the thickness of 3.5 ± 0.2 nm (Fig. 3-1). The δ value of the PS-b-P4VP flattened layer (shown in the inset of Fig 3-1) obtained from the best fit is similar to the bulk value. The final thickness at $t_{an} > t_{cross}$ is nearly equivalent to the thickness of the homopolymer P2VP flattened layer [41, 153]. To characterize the surface morphology, we stained the P4VP blocks with iodine (I_2) vapors selectively[175, 176] and imaged with SEM. As shown in Fig. 3-3(c), the SEM image demonstrated that the P4VP-rich regions (which appear bright in the image) are randomly phase-separated in the PS (darker areas in the image) matrix. The GISAXS profile for the PS-b-P4VP gave us $\xi = 13.4 \pm 0.3$ nm on the basis of the aforementioned DB model (Fig. 3-3(d)). Hence, we may draw the conclusion that the random two-phase structure is rather general at the BCP-solid interface regardless of the bulk microdomain structures and interfacial energetics. We further confirmed that the resultant 2D adsorbed structures do not depend on the original film thickness, at least $h = 4L_d$.

Previous simulation results for homopolymer adsorption from a dilute solution predicted that the time scale for early arriving polymer chains to lie flat on a solid is a few hundred nanoseconds[42, 177]. In fact, we found the formation of a very thin adsorbed layer (less than 1 nm in thickness) resulted from spin-casting alone without subsequent thermal annealing (Supporting information). Hence, it is likely that the initial (non-equilibrium) flattened chains form under solution conditions at the beginning of a spin-coating process rather than under melt conditions[160]. The adsorption kinetics of the flattened layer at $t > t_{cross}$ corresponds to a "collapse and zipping-down" process onto solids[39, 178] and the succeeding relaxation and re-arrangement of the flattened conformations toward their quasiequilibrium states in the melt. According to a mean-field theory study on adsorption of an asymmetric A-B diblock copolymer from a non-selective (good) solvent, the adsorbed layer is predicted to form a discontinuous "pancake" patchwork of individual A

chains in contact with a solid (the A block has a much stronger affinity to the solid than the B block), while the B block is stretched away from the solid surface, forming a brush in the good solvent[179]. Hence, we postulate that, as the solvent evaporates, the B block collapses onto the substrate surface rather than the A block to form minimal contacts between the two incompatible blocks[180]. As the evaporation proceeds further, the improvement of the segmental packing of the adsorbed A and B block chains takes place, as previously reported in the flattened process of homopolymer chains[113, 114]. As a consequence, the B block coexists side-by-side with the A block, resulting in the 2D adsorbed structure. Since the bulk R_g ($= \sqrt{N_A/6}a$) value of the P4VP block is estimated to be 2.4 nm, it may be reasonable to suppose that the P4VP rich domain (~10 nm in the average size) corresponds to aggregates composed of several P4VP blocks. Note that the polymer concentrations used for preparing the spin-cast BCP thin films (0.003g/ml for SBS and 0.004g/ml for PS-b-P4VP) are far below the respective overlap concentrations (0.025g/ml for SBS and 0.13g/ml for PS-b-P4VP) and we confirmed that the PS-*b*-P4VP and SBS copolymers existed as single chains in the dilute solutions using small-angle x-ray scattering.

In summary, the combined AFM and SEM results imply that (i) P4VP, which is a lower surface energy component at the substrate interface, do not cover the surface preferentially, and (ii) the PS chain, whose interaction with the non-treated Si is very weak[20], adsorb on the substrate surface concurrently.

3.5: Supporting information:

Experimental Techniques:

X-ray Reflectivity (XR) Measurements: X-ray reflectivity (XRR) measurements were conducted at the G2 beamline (at CHESS) to study the structures of the flattened SBS and PS-b-P4VP layers on Si substrates after the solvent-leaching process. The specular reflectivity was measured in air at room temperature as a function of the scattering vector in the perpendicular direction to the film surface, $q_z=(4\pi\sin\theta)/\lambda$ where θ is the incident angle and λ is the x-ray wavelength (λ=0.11 nm at CHESS). The XR data was fit by using a standard multilayer fitting routine for a dispersion value (δ in the x-ray refractive index) in conjunction with a Fourier method, a powerful tool to obtain detailed structures for low x-ray contrast polymer multilayers[181]. Note that δ is proportional to the density of a film. For λ=0.11 nm, the δ value of the bulk PS-b-P4VP is estimated to be $\delta_{bulk} = 1.5 \times 10^{-6}$ and δ value of the bulk SBS is estimated to be $\delta_{bulk} = 1.8 \times 10^{-6}$, the density of polymer is 0.9 g/cc for PS-b-P4VP and 1.05 g/cm^3 for SBS, respectively.

Atomic Force Microscopy (AFM) measurements: The surface morphologies of PS-b-P4VP/SBS films were studied by atomic force microscopy (AFM) (Veeco Multimode V and PARK NX20) at Center for Functional Nanomaterials (CFN) at BNL. Standard tapping mode measurements were conducted in air using a cantilever with a spring constant of 42 N/m and a resonant frequency of 204 - 497 kHz. The scan rate was 1.5 Hz with the scanning density of 512 lines per frame.

Scanning Electron Microscopy (SEM) measurements: PS-b-P4VP/SBS samples were characterized in a top down direction by SEM (Hitachi S4800 and *Magellan* 400) at CFN at BNL

and UMass Amherst Materials Research Science & Engineering Center (MRSEC) operating at 1kV-20kV.

X-ray photoelectron spectroscopy (XPS) measurements: XPS experiments were carried out in an ultrahigh vacuum (UHV) system (base pressures < 2 x 10^{-9} Torr) equipped with a hemispherical electron energy analyzer (SPECS, PHOIBOS 100) and a twin anode X-ray source (SPECS, XR50) with Al K_α (1486.6 eV) radiation was used at 10 kV and 30 mA. The angle between the analyzer and X-ray source was 45° and photoelectrons were collected along the sample surface normal. The XPS profiles were fit using XPST, an IgorPro fitting routine using a Gauss-Lorentzian sum function to approximate a Voigt profile after background corrections using a combination of Shirley and 'Pseudo-Tougaard' method.

Sum frequency generation (SFG) spectroscopy measurements: For the SFG experiments, the flattened layers prepared on the quartz prism was pressed together with another same polymer flattened layer prepared independently on a quartz window to suppress any signals from the polymer/air interface. We previously confirmed that such a sandwich configuration does not affect the chain conformations at the polymer melt-solid interface[152]. The details of the SFG set-up have been described elsewhere[43]. In short, visible (wavelength of 532 nm) and tunable infrared (IR) beams were introduced from the quartz prism side with incident angles of 70° and 50°, respectively. The measurements with *ssp* (SFG/*s*; visible/*s*; and IR/*p*) and *ppp* polarization combinations allow us to detect functional groups oriented only along the direction normal to the interface and all directions, respectively[43].

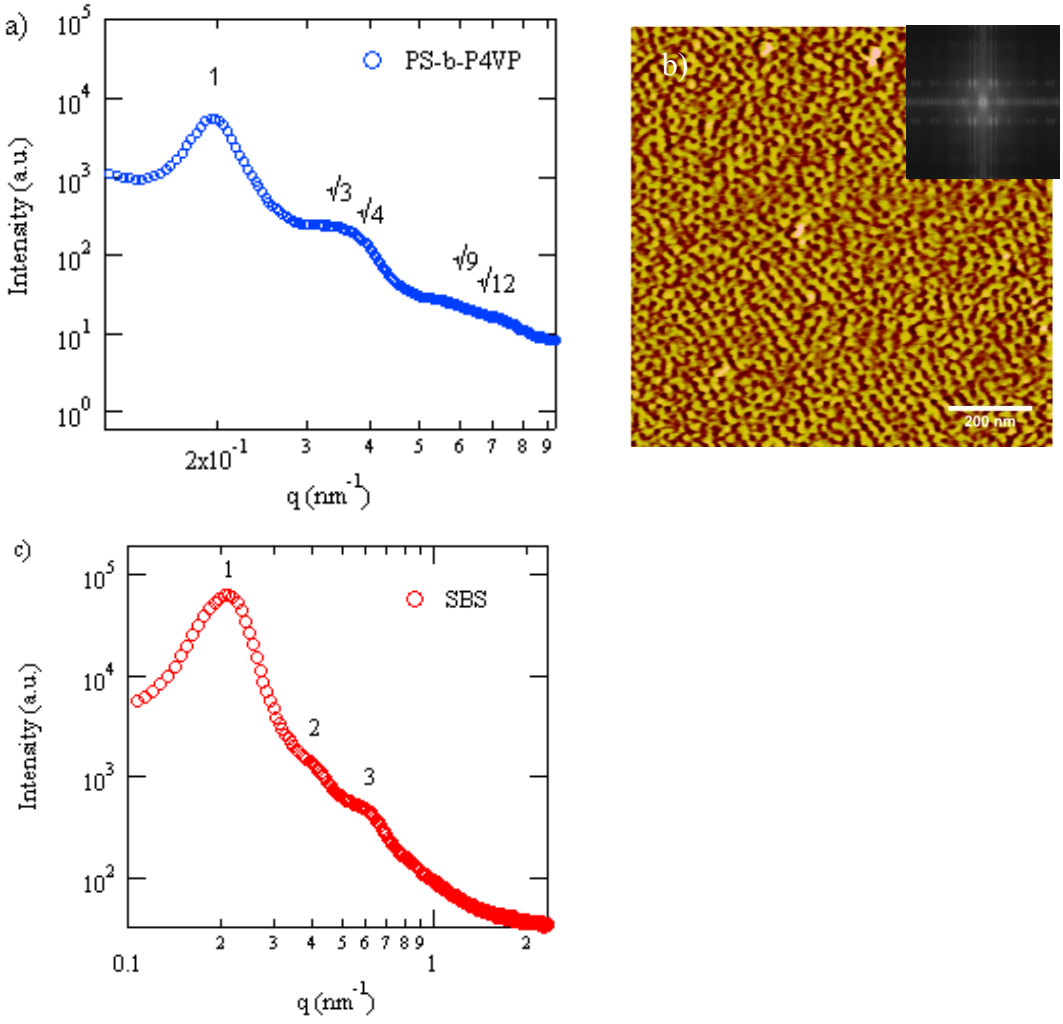

Figure 3-S1: Representative small angle x-ray scattering (SAXS) profile measured at 25°C in a cooling cycle after heating the bulk polymer to 200°C of a) PS-b-P4VP at X27C beamline at the National Synchrotron Light Source (NSLS), Brookhaven National Laboratory (BNL) using x-ray wavelength (λ)=0.1371nm. The bulk polymer shows hexagonally packed cylinder phase which was also confirmed by b) AFM phase image (inset FFT) of a monolayer film spun cast on non-treated silicon and annealed at 190°C for 6 h and surface reconstructed with ethanol. The P4VP cylinders appear as holes (darker) due to the surface reconstruction process. c) Bulk SBS using Bruker Nanostar U at Center for Functional Nanomaterials (CFN) at BNL at x-ray wavelength (λ=0.154nm). The bulk polymer shows a lamellar phase.

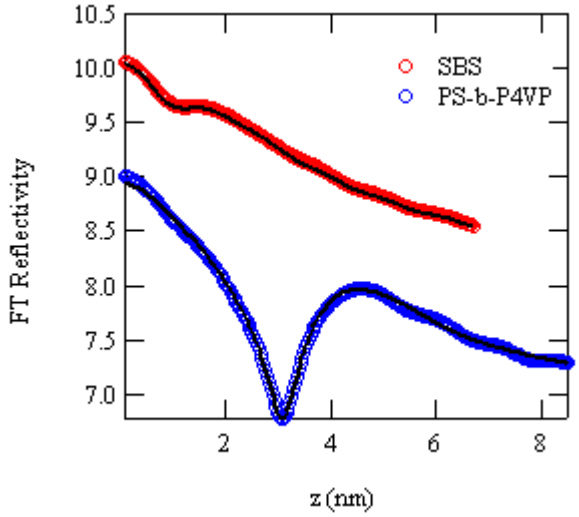

Fig 3-S2: Fourier transform (FT) of the reflectivity curves shown in Fig. 3-1 in the main text. The FT profiles show a peak (shown by the arrows) which corresponds to the total film thickness of the samples

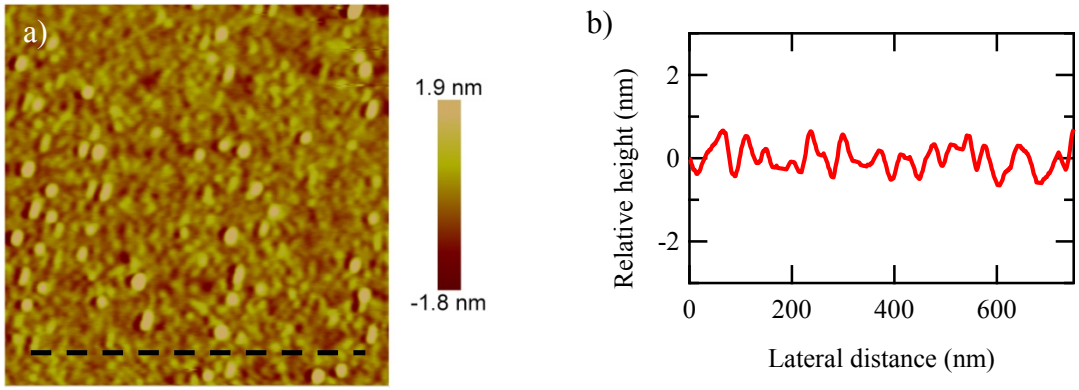

Fig 3-S3: a) AFM height image (1µm x 1µm) of a 'quasiequilibrium' PS-b-P4VP flattened layer b) the relative height profile along the black dashed line in Fig 3-S3 (a). The flattened layer homogeneously covers the Si substrate. The rms roughness of the flattened layer is ~0.1 nm.

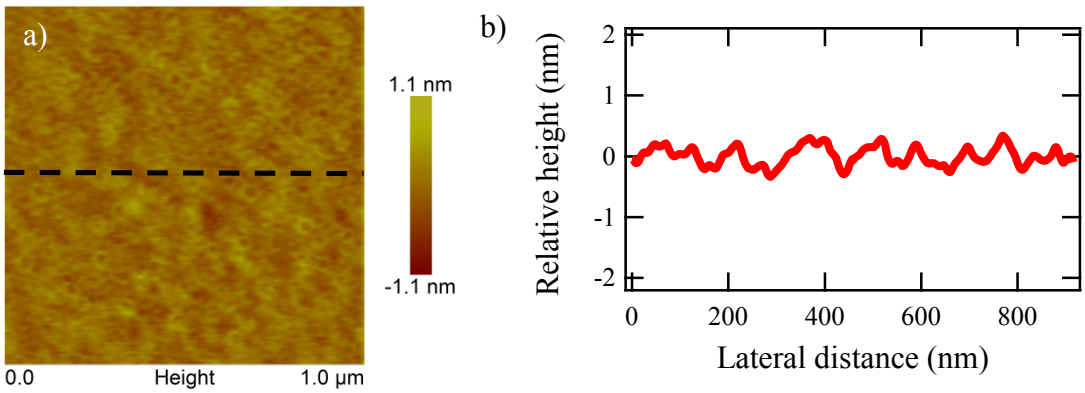

Fig 3-S4: AFM height image (1µm x 1µm) of a 'quasiequilibrium' SBS flattened layer b) the relative height profile along the black dashed line in Fig 3-S4 (a). The rms roughness of the flattened layer is ~0.25 nm.

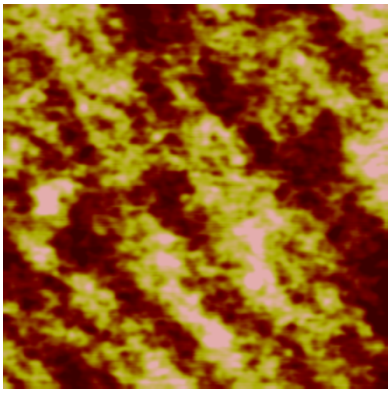

Fig 3-S5: AFM height image (1µm x 1µm) of the adsorbed layer obtained via solvent rinsing of the as-cast PS-b-P4VP with $CHCl_3$. The substrate surface was not homogeneously covered with the polymer with the darker areas corresponding to SiOx layer. The height scale of the AFM image shown is 0-1.6nm.

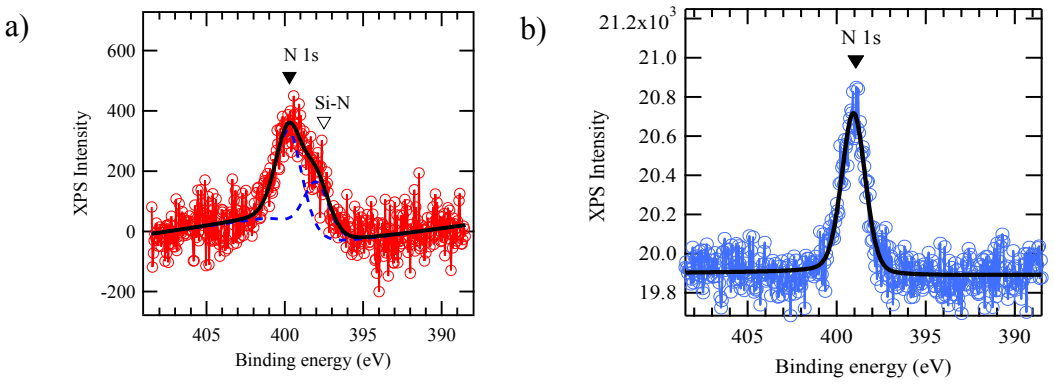

Fig 3-S6: N 1s XPS spectrum of a) PS-b-P4VP flattened layer; b) PS-b-P4VP 5nm spin cast film. The solid lines are the best fit to the XPS spectra using a Gauss-Lorentzian sum function to approximate a Voigt profile after background corrections using a combination of Shirley and 'Pseudo-Tougaard' method. The presence of two peaks in Fig. 3-S6(a) are denoted by the triangles (fitted with the blue dotted lines).

Fig. **3**-S6 (a) shows the N 1s XPS spectrum of the flattened layer derived from the thermally annealed PS-b-P4VP film. The N 1s spectrum clearly shows two peaks at 399.7 eV and 397.9 eV (shown by the triangles) with the component at 399.7 eV having a larger area (63% of the total area) instead of a singular N 1s peak in the XPS spectrum from PS-b-P4VP (Fig. 3-S4 (b)) spin cast film on the same substrate. The observation of two N 1s peaks demonstrates the presence of more than one bonding configuration. The characteristic N 1s peak position at 399.7 eV (similar peak position for N 1s was reported by Jiang et. al[125] for P4VP homopolymer) from the XPS spectrum is identical between the PS-b-P4VP flattened layer, PS-b-P4VP and P4VP spin cast films. The N 1s peak at 397.9 eV can be identified as a contribution from Si_3N_4 [123]. Since Si is less electronegative (Pauling electronegativity= 1.90) than N (Pauling electronegativity= 3.04), the N-Si bound atoms would have a smaller binding energy than the unbound N 1s atoms. Similar results were reported by Liu et al[182]. Therefore, our results indicate that the P4VP block is attached to the substrate.

The surface tension (γ) of the H−Si is quite different (48.71 mJ/m^2 for the dispersion part (γ_d) and 3.98 mJ/m^2 for the polar part (γ_p)[183]) from that of the B−Si (γ_d = 25.8 mJ/m^2 and γ_p = 25.8 mJ/m^2)[184]). The surface energies of different polymers used in this study and their dispersion and polar components are listed below.

Polymer	Surface tension (mJ/m^2)		
	γ	γ_D	γ_P
PS	40.6[41]	34.5[41]	6.1[41]
PMMA	41.1[41]	29.6[41]	11.5[41]
P4VP	50.5[185]	20.25	30.25
PB	41[186]	41	0

As summarized below, the interfacial energy (γls) between the polymer and the substrate were calculated based on the Owens−Wendt−Kaelble equation with the respective surface tensions. ($\gamma_{ls} = \gamma_l + \gamma_s - 2\left(\gamma_s^d \gamma_l^d\right)^{1/2} - 2\left(\gamma_s^p \gamma_l^p\right)^{1/2}$) ($\gamma_s^d$ and γ_s^p are the dispersion and polar parts of the surface energy of the solid, γ_l^d and γ_l^p are the dispersion and polar parts of the surface energy of the liquid). The interfacial energies between the respective blocks of different block copolymers used in this study were also calculated using the above equation.

γ_{ls} for PS/HF treated-Si = 1.45 mJ/m^2

γ_{ls} for PS/non treated-Si = 7.84 mJ/m^2

γ_{ls} for PB/ HF treated-Si = 4.32 mJ/m^2

γ_{ls} for PB/ non treated-Si = 27.56 mJ/m^2

γ_{ls} for PS/ P4VP = 11.07 mJ/m^2

γ_{ls} for PS/ PMMA = 1.04 mJ/m^2

γ_{ls} for PS/ PB = 6.3 mJ/m^2

γ_{ls} for PMMA/ non treated-Si = 3 mJ/m^2

γ_{ls} for P4VP/ non treated-Si = 0.5 mJ/m^2

Chapter 4

Heterogeneous structures and dynamics of block copolymer thin films induced by irreversibly adsorbed polymer chains

4.1: Abstract: Block copolymers (BCP) thin films have recently received significant attention because of their potential nano-technology applications including nanostructured membranes, nanoparticle templates, and high-density data storage media. For most of these applications, long-range order and control over microdomain orientations (either parallel or perpendicular to the substrate) within BCP films are of great importance. However, the structural dynamics of BCP in thin films and the ordering process of these microdomain structures are poorly understood. Here, we studied the dynamics of cylinders that were oriented normal to the substrate in polystyrene-block-poly(4-vinylpyridine) diblock copolymer thin films using high temperature grazing incidence x-ray photocorrelation spectroscopy (GI-XPCS). GI-XPCS results revealed that the dynamics of the standing cylinders is quite heterogeneous within the entire film. We found that this is attributed to the presence of an irreversibly adsorbed BCP layer which showed no favorable dynamics even at temperatures far above the individual glass transition temperatures of the blocks. Furthermore, we also revealed that the interfacial structure plays a crucial role in controlling the microdomain orientation in the entire film.

4.2: Introduction:

Block copolymers (BCP) have attracted increasing attention for various applications, often because of their ability to self-assemble into nanostructures, periodic and otherwise. Over the last decades, block copolymers (BCP) thin films offer a simple and effective route to fabricate highly ordered periodic microdomain structures, which are potentially useful in nanofabrication applications such as nanoparticle templates[47-49], nanostructured membranes[50-52], photovoltaic cells[53], low-*k* dielectrics[54], and high density data storage media[55]. For most of these applications, control over the orientations of microdomain structures is of great importance. In case of supported BCP thin films, interfacial energetics at the polymer-air and polymer-substrate interfaces play a crucial role in controlling the orientation and ordering of microdomain structure[56, 57]. In general, preferential interactions between one of blocks and the substrate or free surface will induce enrichment of the block with the lowest surface energy at the respective surface.[144-147]. Despite a tremendous amount of work on the phase behavior and static structures of BCPs in thin films, the structural dynamics of BCP in thin films are relatively little studied and poorly understood. It is because BCP dynamics compound the difficulties of polymer dynamics with the complications caused by nanoscale inhomogeneities associated with competing interfacial energies at different locations within the entire film, thereby giving rise to highly heterogeneous diffusivities and viscosities within the entire film. There is now a growing evidence that the air/polymer interface and polymer/substrate interface play crucial roles in these "nanoconfinement" effects. Although most previous work has revealed the deviations of "average" quantities of entire nanometer films from the bulks, it is expected that the local quantities within nanoconfined polymer thin films would be different from the average ones, depending on the interplay between these interfaces.

Here we studied the underlying polymer dynamics of a cylinder forming diblock copolymer using grazing incidence x-ray photocorrelation spectroscopy (GI-XPCS). During the last decade, the development of third generation synchrotron radiation sources has made it possible to extend photon correlation spectroscopy (PCS) from the optical region into the x-ray domain. This enables us to probe the dynamic properties of systems on molecular length scales as well as the use of optically dense samples that are not accessible for conventional PCS. XPCS has been extended into the sub-microsecond range of temporal resolution[76-78], and the advent of an x-ray free-electron laser would further provide a unique opportunity to identify chemical and biological phenomena with an unprecedented temporal resolution (femtosecond regime). Thus, XPCS has a great potential to impact the study of a variety of nonequilibrium phenomena. In the present study, we prepared cylinders that are oriented normal to the substrate surface via solvent vapor annealing[80]. The XPCS results evidenced the presence of an irreversibly adsorbed BCP layer at the substrate interface which showed no dynamics even at temperatures far above the respective glass transition temperatures of the blocks. Moreover, the effect of this adsorbed layer on the overall polymer dynamics in BCP thin films is discussed here.

4.3: Materials and experimental techniques:

Polystyrene (PS)-based di-block copolymer (BCP): poly (styrene-*block*-4-vinylpyridine) (PS-*b*-P4VP, M_w=41,000 g/mol, M_w/M_n=1.1, Polymer Source Co.) thin films were prepared on Si substrates as model systems. The volume fraction of the PS component in PS-*b*-P4VP is 0.81. We confirmed that bulk PS-b-P4VP displays hexagonally packed cylindrical microdomain structures based on small angle X-ray scattering (SAXS) results (Supporting information). The interdomain spacing (L_0) at room temperature was determined to be 36 nm for PS-*b*-P4VP. Silicon wafers (Si) (100) wafers (purchased from University Wafers Inc.) were cleaned by a modified Shirake

technique[187]. The wafers were cleaned by heating, uncovered, without stirring, for 20 min at 150 °C in aqueous hydrogen peroxide and ammonium hydroxide, rinsing with deionized water, followed by heating for 20 min in aqueous hydrogen peroxide and concentrated sulfuric acid. [*Caution: A solution of hydrogen peroxide and sulfuric acid is highly corrosive to skin and eyes and pose a risk of explosion when in contact with organic materials. Extreme care should be taken when handing it]*. The wafers were then rinsed at least five times with distilled water. This cleaning protocol removed organic contaminants and left the substrate surface covered with Si-OH groups[188]. XR results clarified that the resultant surface of the SiOx/Si was covered with a homogenous 2.4 nm thick oxide layer with a surface roughness of less than 0.5 nm (hereafter assigned as "non-treated Si")[9]. A series of PS-b-P4VP thin films with film thicknesses (h) of h = nL_0 were spun cast from chloroform solutions onto the non-treated Si substrates, where n is an integer. The thicknesses of the spin-cast thin films were determined by an ellipsometer (Rudolf Auto EL-II) with the fixed refractive index of 1.59[50] for PS-b-P4VP. According to previous results[68, 154, 155], P4VP have a greater affinity to SiO_x than PS. On the other hand, P4VP has a higher surface energy at the polymer-air interface than PS[157]. The thin films were solvent vapor annealed in chloroform ($CHCl_3$), a non-selective solvent for both blocks and subsequently in 1,4-dioxane, a selective solvent for PS block only at room temperature; following a protocol mentioned by Gowd and co-workers[80]. The thin films were thereafter "surface reconstructed" after solvent annealing using ethanol, which is a selective solvent for P4VP blocks only. The detailed solvent vapor annealing (SVA) and "surface reconstruction" (SR) process is outlined in the supporting information. "Surface reconstruction" enhances the contrast of the AFM images. Russell and co-workers have showed that such a "surface reconstruction" process with the use of a selective

solvent for PS-b-P4VP diblock copolymer thin films does not alter the order or orientation of the microdomains[47].

4.4: Results and discussion:

Fig.4-1 shows a representative AFM phase image of a monolayer PS-b-P4VP film after SVA and SR at optimum conditions. The darker "nanopores" in the AFM image represents the P4VP microdomains which were enhanced after SR. It is evident here that the P4VP microdomains are ordered in a hexagonally packed cylindrical morphology at the film surface (shown by the fast Fourier transformation (FFT) image in the inset).

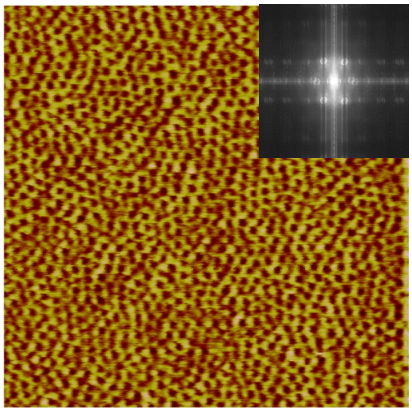

Figure 4-1: AFM phase image (1μm x 1μm) of SVA PS-b-P4VP monolayer film (inset: FFT of the phase image).

Firstly, we focused on the interfacial (substrate) structures in the upright cylinder forming PS-b-P4VP thin films. To reveal the buried interface of these SVA films, we used the established Guiselin's protocol[158]. In this method, polymer chains were equilibrated against a solid surface; unadsorbed chains thereafter can be removed by a good solvent, while the adsorbed chains are assumed to maintain the same conformation due to the irreversible freezing experienced through multiple solid-segment contacts. Several research groups have already demonstrated that Guiselin's approach is practical for revealing the buried interfacial structures for various homopolymers[13, 17, 20, 24, 41, 45, 159-167]. The SVA films were leached in fresh baths of toluene at 60°C (at least five times for 30 mins each time) and thereafter "surface

reconstructed" in ethanol. The solvent leaching process was optimized for extraction of the adsorbed layer. Fig. 4-2(a) shows the AFM phase image of the resultant adsorbed layer from SVA monolayer film. The P4VP microdomains (darker "nanopores") are perpendicularly oriented at the surface although the lateral ordering of the cylindrical microdomains is poor (inset: corresponding FFT). We studied the structure of the SVA adsorbed layer using X-ray reflectivity (XRR). Fig. 4-3 shows the XRR results of the SVA interfacial sublayer. A least-square fit (the black solid line) to the XR profile was performed using the dispersion (δ) profile shown in the inset plotted against the perpendicular distance from the substrate using a four-layer model consisting of: Si substrate, SiOx layer, a higher density layer and a bulk like density layer. The choice of the 4-layer model is based on the Fourier transform (FT) of the XR profile (Supporting information). The results showed that the adsorbed layer is comprised of two different nano-architectures at the substrate interface: a higher density (~10% higher than bulk) inner layer of thickness 2.4±0.2 nm and an outer bulk like density layer of thickness 4.4±0.2 nm. The details of the XRR data fitting procedure are outlined in the supporting information. This structure at the substrate is analogous to the nano-

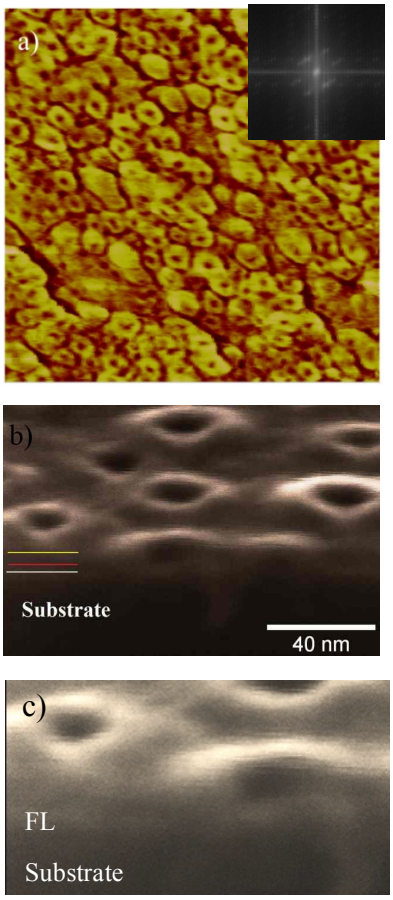

Figure 4-2: a) AFM phase image (1μm x 1μm) (inset: FFT of the phase image) b) cross-sectional SEM of SVA PS-b-P4VP adsorbed layer. The solid lines are guide to the eye: below the white line is the substrate (darkest); between white and red lines: flattened layer (FL) (brighter) and between red and yellow line: hollow perpendicular cylinder on the surface. c) Fig. 4-2 (b) is zoomed for better viewing purpose.

architectures of adsorbed layers from homopolymers[41, 45]. Hereafter, we assign the inner higher density layer as the "flattened layer" where both blocks lie flat on the substrate, forming the 2d randomly phase-separated structure (see Chapter 2) and the entire adsorbed layer comprising of the outer bulk-like density layer (loosely adsorbed chains) and the flattened layer as the interfacial sublayer (IS). Furthermore, to visualize the extent of the formation of the perpendicular P4VP cylinders on the substrate we performed a cross-sectional scanning electron microscope (SEM) (Fig. 4-2 (b) and (c)) measurement of the interfacial sublayer. The result showed that the perpendicular cylinders on the surface only propagate until the flattened layer which is clearly visible in the SEM image (Fig. 4-2 (c)). GISAXS 1D profile of the SVA adsorbed layer along q_y plotted in a double logarithmic scale (Fig. 4-4(a)) showed that the cylinders are arranged in a hexagonal lattice structure (evident from the peak ratio of 1: $\sqrt{3}$). An L_0= 32±1nm was calculated from the first peak position of q_y= 0.2nm^{-1} using $L_0=2\pi/q_y$. Thus, the structure of the blockcopolymer interfacial sublayer from SVA consisted of poorly ordered hexagonally packed perpendicular cylinders with a bulk L_0.

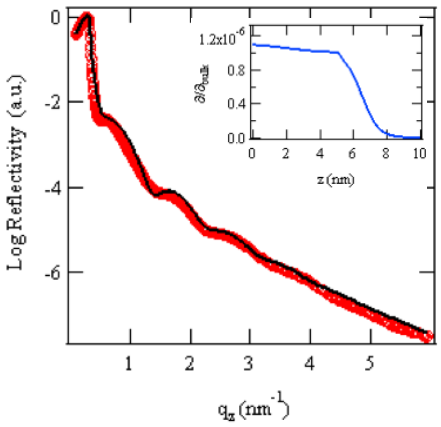

Figure 4-3. XRR profile of the SVA adsorbed layer. The black line is the best fit to the XR profile using the dispersion (δ) profile shown in the inset plotted against the perpendicular distance from the substrate.

To investigate the dynamics of the block copolymer interfacial sublayer at temperatures (T) more than the glass transition temperature (T_g) of the individual blocks, we performed high

temperature grazing incidence (GI) XPCS experiments under vacuum (~4.5*10^{-6} Torr). The details of the GI-XPCS experiment and data analysis is mentioned in the supporting information. GI-XPCS measures the normalized intensity-intensity time autocorrelation function, $g2(q_y, t) = \langle I(q_y,t')I(q_y,t'+t)\rangle / \langle I(q_y,t')\rangle^2$, where $I(q_y,t')$ refers to the scattering intensity at the in-plane wave vector transfer q_y and at time t'. The brackets < > refer to averages over time t' and t is the delay time. $g2(q_y,t)$ is related to the normalized intermediate structure factor (ISF) $[f(q_y,t)]$ via $g2(q_y, t) = 1 + A|f(q_y, t)|^2$, where A is the speckle contrast. $g2$ at each q_y was fitted by using a stretched exponential function of the ISF given as $f(q_y, t) = \exp[-(t/\tau)^{\alpha}]$, where τ and α ($0<\alpha<1$) are the characteristic relaxation time and the stretching exponent that characterizes the shape, respectively. The correlation function, g2, decays with increasing delay time (t), and converges to unity at long time. The characteristic decay time (τ) reflects the structural dynamics of the sample, in our case the polymer dynamics at the cylinder-cylinder length scales. We used an incident angle (θ=0.17°) which is higher than the critical angle (θ_c) for total external reflection (θ_c=0.14°) of PS-b-P4VP but lower than θ_c of Si (θ_c=0.2°) at X-ray energy of 9keV to visualize the dynamics within the entire polymer film. Hereafter, we refer this measurement configuration as "bulk mode". We performed XPCS

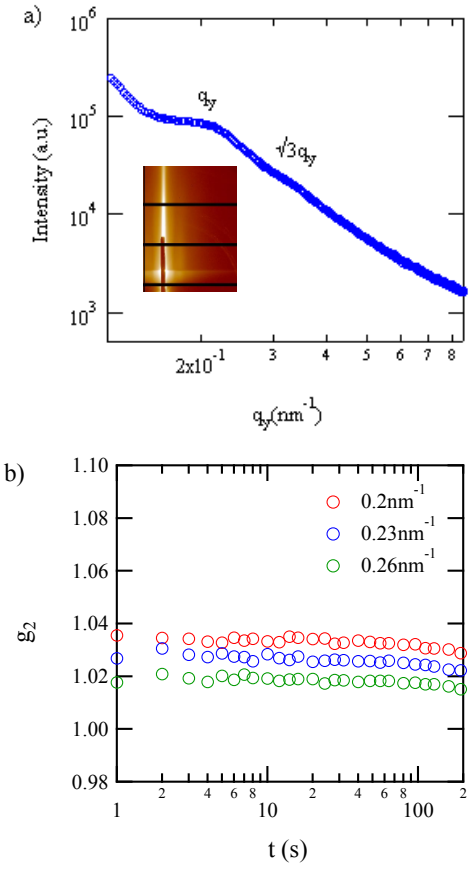

Figure 4-4: a) In-plane GISAXS line cut 1D profile (inset: 2D profile) of SVA interfacial sublayer at 25°C; q_y is the in-plane scattering vector. b) g2 function of SVA interfacial sublayer annealed at 190°C.

measurements at the vicinity of wave-vector q_y = 0.23 nm^{-1} which corresponds to the first order scattering maximum of the static structure factor (Fig. 4-4(a)), thereby probing directly the dynamics at length scales equal to inter-cylinder distance. Fig. 4-4(b) shows representative normalized intensity-intensity time autocorrelation (g_2) functions of the SVA interfacial sublayer at 190°C at different q_y. Hence, the g_2 functions do not decay at all within the time domain for the different q_y values, proving no dynamics of the standing cylinders even at T>>T_g of the individual blocks (Tg of PS~100°C; Tg of P4VP~142°C[189]).

These physically adsorbed chains in the interfacial sublayer can be considered as a ''polydispersed Guiselin brush''[158] where the chains are physically bound to the surface via multiple monomer-surface contacts such that the chain mobility would be greatly reduced. In fact, previous neutron reflectivity experiments for the PS interfacial sublayer proved that no dynamics of the loosely adsorbed chains is favorable even at T>>Tg[13]. In addition, recent XPCS results reported that chemically grafted polymer brushes showed no surface fluctuations even in a good solvent irrespective of polymer grafting density[190]. Hence, it is expected that the standing cylinders are not formed on top of the flattened layer but rather, the cylinders are still bound to the substrate (as shown in Fig. 4-5) and are immobile within the time window.

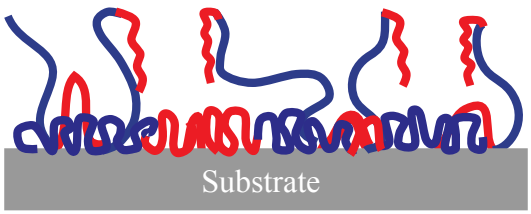

Figure 4-5. Schematic of SVA interfacial sublayer after SR.

Next, we studied the polymer dynamics of the standing cylinders formed within the SVA processed $4L_0$ and $2L_0$ PS-b-P4VP thin films at T>>T_g. in bulk mode. It is to be noted here that both $4L_0$ and $2L_0$ films solvent vapor annealed with $CHCl_3$ and 1,4-dioxane showed a similar perpendicular cylinder morphology at the surface with a characteristic cylinder-domain spacing of ~30nm as $1L_0$ (Fig 4-1). The AFM images are shown in Fig. 4-6((a) and (b)) respectively.

Although the surface morphology of the SVA $4L_0$ and $2L_0$ films look similar, GISAXS data (obtained in bulk mode shown in Fig. 4-6 (c)) showed that the overall ordering of the cylinders in the entire film is better in case of $4L_0$ film than $2L_0$. The static structure peaks from the $4L_0$ film reveal better microdomain orientations than the $2L_0$ film. Fig. 4-7 (a) shows the measured g2 functions as a function of the delay time (t) for the $4L_0$ and $2L_0$ PS-b-P4VP SVA films at 190°C at q_y=0.23 nm^{-1}, which is at the maximum of the structure factor peak. The results show that the g_2 functions for the $4L_0$ and $2L_0$ films do not decay completely within the experimental time (Fig. 4-7a). Rather, there is a plateau at t> 250 sec, implying the contributions from the immobile adsorbed chains. In fact, as shown in Fig. 4-7a, we confirmed that the plateau is in good agreement with that g2 function for the interfacial sublayer. Fig. 4-7(b) shows the corrected g_2 functions of the $2L_0$ and $4L_0$ thin films for the contribution of the interfacial sublayer. The profiles were reasonably fitted with a stretched exponential function with τ= 163s and α=0.36±0.02 for $4L_0$ and τ= 250s and α=0.8±0.1 for $2L_0$ films, respectively. Similar stretching exponential decay indicative of heterogeneous relaxation modes in asymmetric blockcopolymers were reported earlier[191, 192]. Jang et al.[191] and Mochrie et al.[192] have separately reported heterogeneous dynamical behavior in asymmetric BCP melt using transmission XPCS as the compositional fluctuations in BCP

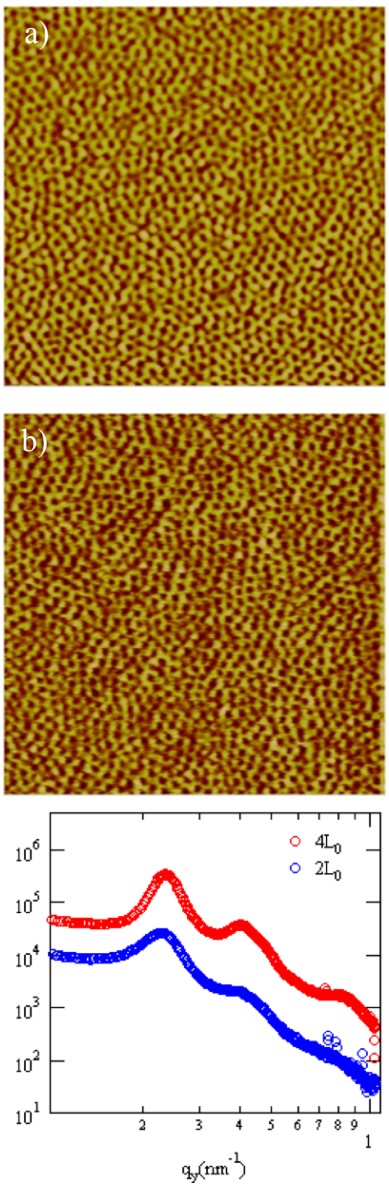

Fig. 4-6: AFM phase image (1µm x 1µm) of SVA PS-b-P4VP films a) $4L_0$ b) $2L_0$ c) In-plane GISAXS line cut 1D profiles from the two films.

undergoes reptation motion, the decay was expressed as a sum of exponentials which mimicked a stretched exponential function. In the present case, we hypothesize the origin of the heterogeneous modes of relaxation is the combined presence of a reduced viscosity polymer layer at the polymer/air interface and a "reduced mobility layer" near the substrate interface. Intriguingly, our data shows that the relaxation of polymer chains in case of $2L_0$ film is slower than $4L_0$ film.

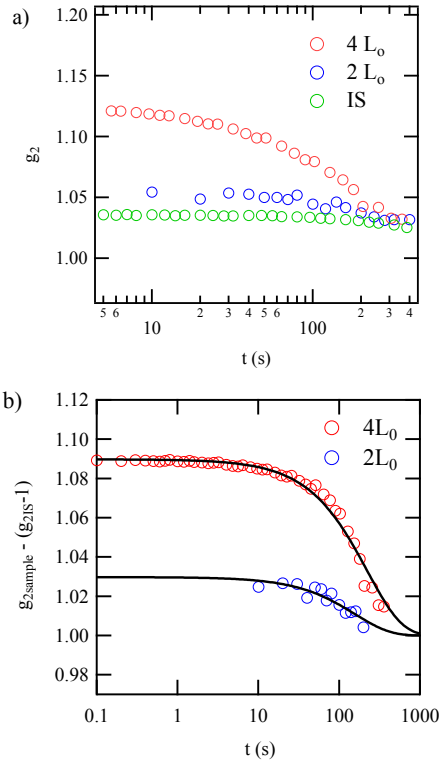

Fig. 4-7. a) Measured g2 functions as a function of the delay time (t) at 190°C for $4L_0$, $2L_0$ SVA films along with the SVA interfacial sublayer (IS) at q_y=0.23 nm^{-1}. b) Normalized g2 functions w.r.t to g_2 of IS. The solid black lines are the best fit using a stretched exponential function described in the text.

To further study the effect of the interfacial sublayer on the dynamics of the entire BCP film, we prepared bilayer films where we spin coated ~$2L_0$ and ~$4L_0$ films on the SVA interfacial sublayer. It is to be noted here that the total film thicknesses of the bilayers including the interfacial sublayer were kept equal to $2L_0$ and $4L_0$ respectively to avoid formation of islands and holes structure due to film thickness incommensurability[56]. The resultant bilayer films were solvent vapor annealed in $CHCl_3$ and 1,4-dioxane subsequently following the same procedure as mentioned earlier. The bilayer films showed a perpendicular cylinder morphology at the surface with a characteristic cylinder-domain spacing of ~30nm (Supporting information). XPCS results (Supporting information) show that the τ and α values for $4L_0$ and $2L_0$ bilayer films are similar to single layer films, respectively. Thus, the BCP dynamics in the bilayer films mimic the dynamics in the $4L_0$ and $2L_0$ films.

In case of BCP films during a SVA process, it is known that the polymer/air interface is the primary ordering front for cylinders[193], whereby the concentration of solvent at the surface is lowest during solvent evaporation and it creates a gradient in solvent concentration normal to the surface[194]. However, the present results indicate that the interface between the unadsorbed polymer chains and the interfacial sublayer play a crucial role as an additional cylinder ordering front, where the unadsorbed polymer chains are entangled with the interfacial sublayer and act as a "transition zone"[195] and thereby ensuring continuity in the mobility profile from the substrate to the bulk through chain entanglements[196]. Koga and co-workers revealed that the effect of the interfacial sublayer in amorphous or semicrystalline polymer thin films can propagate up to ~ 60 nm from the substrate surface into the film[13, 26]. We therefore postulate that the interfacial sublayer plays a neutral "substrate" and initiates the ordering of the microdomain structures, independent of the primary nucleation at the polymer/solvent interface. The polymer chains in the transition zone would then form the same cylinder orientation (i.e., upright orientation) as in the interfacial sublayer to minimize the free energy penalty at the polymer-polymer interface. Similar effect of the loosely adsorbed chains was observed in the formation of lamellar crystalline structures within PE or PEO thin films[26, 197]. In the present case, we thus hypothesize that the origin of the heterogeneous relaxation within the thin films is the effect of the irreversibly adsorbed polymer chains and its propagation into the film interior. When the film is thinner, the effect is more noticeable, as seen in the 2L0 films.

In summary, we have revealed the effects of the irreversibly adsorbed layer formed at the BCP/substrate interface on the inner structure and dynamics of the supported PS-b-P4VP thin films ($2L_0$ and $4L_0$ in thickness) with a perpendicular cylinder morphology via the solvent vapor annealing. The XPCS results revealed that the BCP adsorbed layer derived by the solvent leaching

process showed no dynamics even at T>>Tg of the individual blocks within the experimental time window. Moreover, the XPCS results of the BCP thin films clarified the dynamics of the standing cylinders is quite heterogeneous within the entire film and the dynamics was further retarded when the film thickness was thinner. We hypothesize that the adsorbed layer plays as an additional front in initiating the standing cylinder formation and the perturbation associated with the adsorbed layer propagates into the film interior, retarding the dynamics of the cylinder as well as the degree of the orientation within the film. Further studies with thermally annealed BCP films and different microdomains structures are currently in progress.

4.5: Supporting Information

Experimental techniques:

Solvent vapor annealing (SVA): The spin cast films were solvent vapor annealed in the vapors of chloroform ($CHCl_3$) (non-selective solvent) and 1,4-dioxane (a preferential solvent for PS block) in an air-tight chamber of 100cc volume at room temperature for vertical alignment of the cylindrical microdomains following the protocol described elsewhere[80, 198]. Nanoporous films, for better contrast, were obtained by "surface reconstruction" of SVA thin films in ethanol, a selective solvent for P4VP for 14 minutes[47]. The SVA conditions were optimized for maximum swelling of the films for all experiments.

X-ray Reflectivity (XRR) Measurements: X-ray reflectivity (XRR) measurements were conducted at the G2 beamline (at CHESS) to study the structure of the SVA PS-b-P4VP interfacial sublayer layer on Si substrates after the solvent-leaching process. The specular reflectivity was measured in air at room temperature as a function of the scattering vector in the perpendicular direction to the film surface, $q_z=(4\pi\sin\theta)/\lambda$ where θ is the incident angle and λ is the x-ray wavelength (λ=0.11 nm at CHESS). The XR data was fit by using a standard multilayer fitting routine for a dispersion value (δ in the x-ray refractive index) in conjunction with a Fourier method, a powerful tool to obtain detailed structures for low x-ray contrast polymer multilayers[181]. Note that δ is proportional to the density of a film. For λ=0.11 nm, the δ value of the bulk PS-b-P4VP is estimated to be $\delta_{bulk} = 1.5 \times 10^{-6}$, the density of polymer is 0.9 g/cc.

Grazing incidence small angle X-ray scattering (GISAXS): Grazing incidence small angle X-ray scattering (GISAXS) measurements were carried out at X9 beamline at the National

Synchrotron Light Source (NSLS), Brookhaven National Laboratory (BNL) and at G3 beamline at Cornell High Energy Synchrotron Source (CHESS). Two-dimensional scattering patterns were collected by using a MAR-CCD area or PILATUS 300k detector with a sample-to-detector distance of 5.016 m (at NSLS) and 2.719 m (at CHESS). All measurements at NSLS were carried out under vacuum (~10^{-3} Torr) at room temperature and the exposure time was fixed to 200 sec. The measurements at CHESS were conducted under ambient conditions with exposure time of 50 sec. The two-dimensional scattering patterns were converted to 1-dimensional (1D) scattering intensity (I (q_y)) plotted against q_y, defined by $q_y = (4\pi/\lambda) \sin(\theta/2)$ with λ and θ being the wavelength of the incident X-ray and the scattering angle respectively and where q_y is the scattering vector parallel to the film surface, after background scattering corrections. Silver behenate powder was used as a standard for data conversion to q-space.

Atomic Force Microscopy (AFM) measurements: The surface morphologies of PS-b-P4VP films were studied by atomic force microscopy (AFM) (Veeco Multimode V and PARK NX20) at Center for Functional Nanomaterials (CFN) at BNL. Standard tapping mode measurements were conducted in air using a cantilever with a spring constant of 42 N/m and a resonant frequency of 204 - 497 kHz. The scan rate was 1.5 Hz with the scanning density of 512 lines per frame.

II-3. X-ray photocorrelation spectroscopy (XPCS) measurements.

XPCS experiments were performed at beamline 11-ID at NSLS-II, BNL using a Dectris Eiger 4M detector which yielded $g2(q_y,t)$ where the magnitude of the scattering vector, q_y is defined by $q_y = (4\pi/\lambda) \sin(\theta/2)$ with λ and θ being the wavelength of the incident X-ray and the scattering angle respectively. The sample to detector distance was 4.84m. Silver behenate (AgBe) powder was used as a standard for data conversion to q_y-space. A double crystal Si (111) monochromator was

used to select 9 keV X-rays, having a relative bandwidth $\Delta\lambda/\lambda \approx 10^{-4}$. A Si mirror downstream of the monochromator was used to suppress higher energy X-rays from the monochromator. A transversely coherent beam was defined by slit blades with highly polished cylindrical edges. The slit size was 10 x 10 μm^2. A set of guard slits was placed just upstream of the sample to block the parasitic scattering due to diffraction from the beam-defining slit. A q value ranging from 0.005 to 1 nm^{-1} was accessible. Focusing on the dynamics, we collected speckle patterns every 1-10 sec, being limited on the long-time side only by the overall instrumental stability yielding an upper limit of a few hours in the accessible timescales. In order to avoid radiation damage, the sample exposure over the total correlation time was limited to less than 10 minutes. For the data analysis we proceeded as follows: first, individual pixels of the Dectris Eiger 4M detector were grouped in 15-25 q_y-bins according to the values of their in-plane momentum transfer q_y. Subsequently, every q_y-bin was filtered by excluding those pixels with average signals or standard deviations significantly different from the average values. The intensity-intensity time autocorrelation function, $g2(q_y, t)$ is calculated by taking an average of the pixels in the respective q_y-bins.

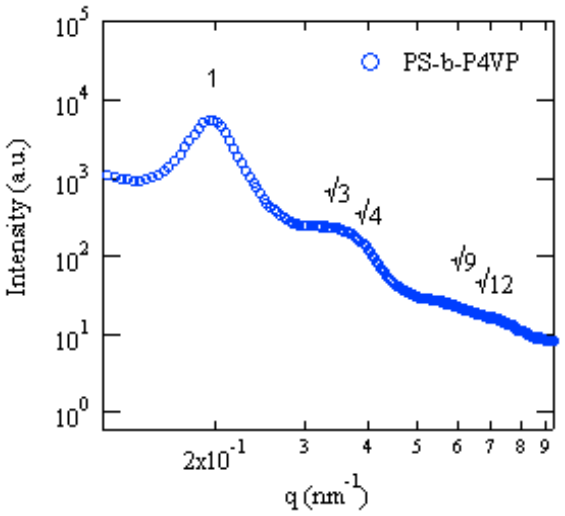

Figure 4-S1: Representative small angle x-ray scattering (SAXS) profile measured at 25℃ in a cooling cycle after heating the bulk polymer to 200℃ of PS-b-P4VP at X27C beamline at the National Synchrotron Light Source (NSLS), Brookhaven National Laboratory (BNL) at x-ray wavelength (λ)=0.1371nm. The bulk polymer shows hexagonally packed cylinder phase.

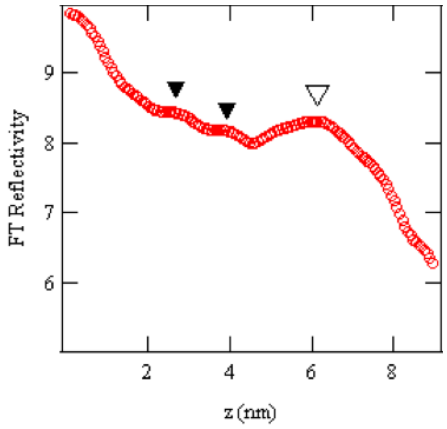

Figure 4-S2: Corresponding FT of the XR profile shown in Fig. 4-3 of the main text confirms the presence of two separate layers (shown by the filled triangles) and the total film thickness (shown by the empty triangle).

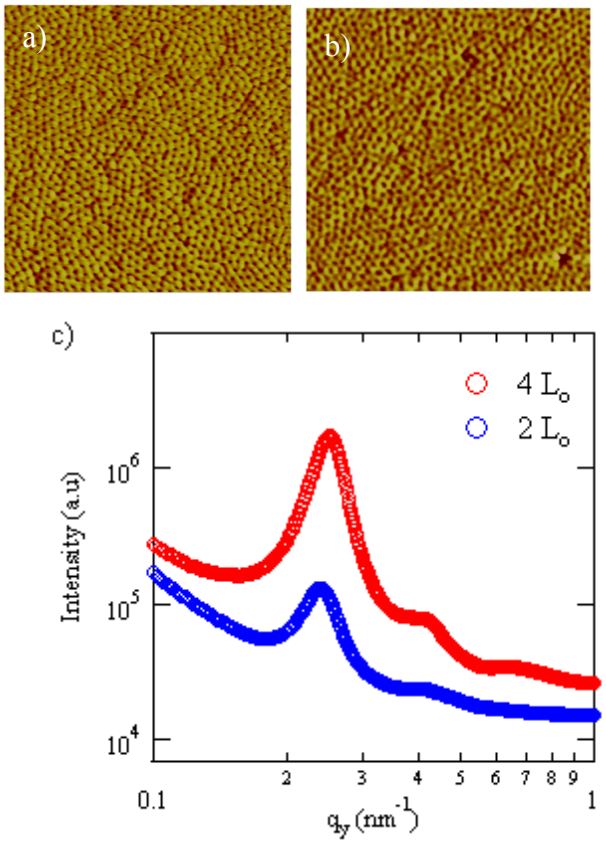

Figure 4-S3: AFM phase image (1µm x 1µm) of PS-b-P4VP films on SVA interfacial sublayer a) $4L_0$ b) $2L_0$ c) In-plane GISAXS line cut 1D profiles from the two bilayer films. GISAXS profiles were measured in bulk mode.

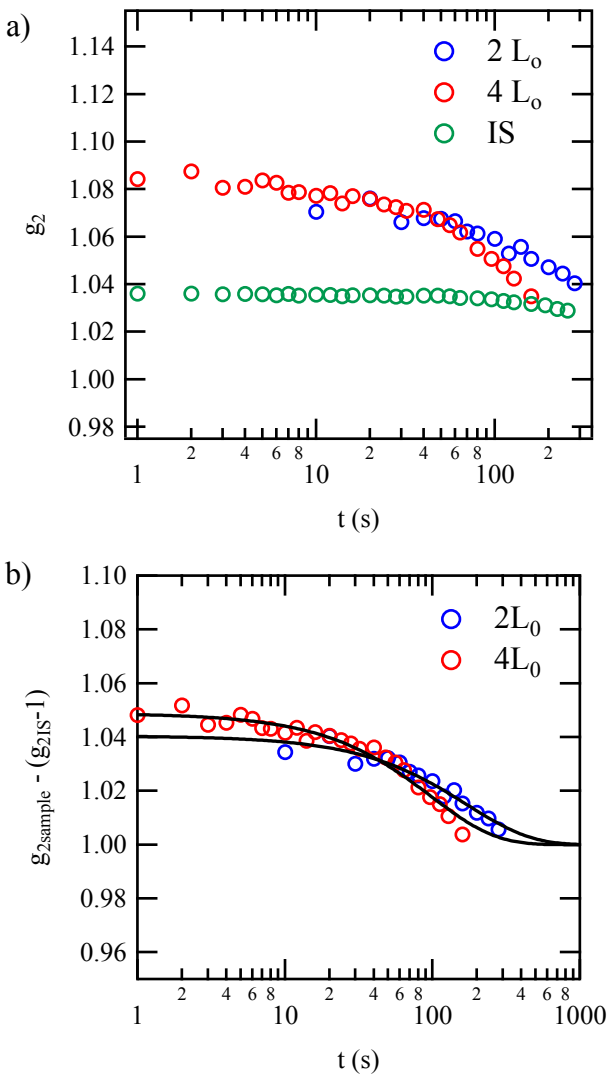

Figure. 4-S4. a) Measured g2 functions as a function of the delay time (t) at 190°C for $4L_0$, $2L_0$ SVA films on the SVA interfacial sublayer (IS) at q_y=0.23 nm^{-1}. b) Normalized g2 functions w.r.t to g_2 of IS. The solid black lines are the best fit using a stretched exponential function described in the text. The profiles were best fitted with τ= 123s and α=0.6 for $4L_0$ and τ= 273s and α=0.8 for $2L_0$ films, respectively

Chapter 5

Structural origin of anti-fouling characteristics of polymer chains strongly adsorbed on solids

5.1: Abstract: We here report a radically new paradigm of designing a polymeric coating layer of a few nanometers thick ("polymer nanolayer") with anti-biofouling properties. The anti-biofouling properties of this polymer nanolayer are considered to be of structural origin and is general to various polymer systems regardless of interactions with water molecules or biological molecules. Furthermore, the preparation of the polymer nanolayers is simple (i.e., no sophisticated chemistry involved) and versatile (i.e., presents many choices of solid-polymer pairs and film preparation methods). Additionally, the polymer nanolayers are stable even in good solvents. We hypothesize that the origin of the antifouling property is the nanoarchitecture of this polymer nanolayer whereby the large number of segment/solid contacts are the key factor in determining biomolecule resistance. This finding facilitates a simple and "universal" polymer structure-based design of an anti-biofouling surface using synthetic commodity polymers.

5.2:Introduction

Biofouling or biocontamination is undesirable in a wide range of applications, such as surgical equipment and protective apparel in hospitals[81, 82], medical implants[81-84], biosensors[85], textiles[86, 87], food packaging[88] and food storage[89], water purification systems[90], and marine and industrial equipment[90, 91]. Biofouling can be characterized into two broad categories: microfouling which involves proteins or bacteria and macrofouling due to barnacles or mussels. Anti-protein fouling is beneficial for in vitro diagnostics, where adsorption of protein molecules can compromise the sensitivity of the diagnostic and in vivo applications, such as biomedical implants where protein adsorption can lead to undesirable events that can include thrombus formation or fibrosis and scar tissue formation[92]. Moreover, protein adsorption on the surfaces of biological implants provides a conditioning layer for microbial colonization and subsequent biofilm formation which provides an associated risk of infection[93]. The most common approach to reduce protein adsorption on a surface is via a coating of poly(ethylene glycol) (PEG)[92]. Chemically or covalently grafted long chain PEGs with high grafting density on surfaces showed the highest reduction of adsorption of proteins, but most of these approaches to surface modification with PEG or PEG-containing copolymers do not reduce the adsorption of proteins below the nominal limit of several ng cm^{-2}, which is considered a useful operational definition for protein resistance as it is the approximate limit-of-detection (LOD) of most label-free interfacial detection techniques, such as surface plasmon resonance (SPR)[92]. Physisorption process of polymer chains has encountered very limited success in reducing protein adsorption due to the low surface density of PEG chains on the surface (<4 mg cm^{-2})[199], because of the excluded-volume effect[200]. Moreover, it is reported that hydrophilic materials are more resistant to biofouling than hydrophobic ones due to easier displacement of water molecules on hydrophobic surfaces[105, 106]. Thus, there is a present

need for the development of novel anti-fouling coatings to resist nonspecific protein adsorption and cell adhesion irrespective of hydrophobicity.

Long term surface stability of anti-fouling coatings in biomedical applications such as medical implants, contact lenses, drug delivery as well as in marine applications are of utmost importance. Hydrophilic PEG and PEG derivatives, the most thoroughly studied anti-fouling coating materials, have limited use in marine applications due to rapid oxidation of their backbone in the presence of oxygen and transition ion metals present in seawater[95,96]. Moreover, in cases where polymeric brushes display sufficient hydrolytic stability in their main chain, problems may arise at the anchoring point of the brush. This problem is particularly visible for hydrophilic brushes chemically or covalently end tethered on silicon oxide substrates (silicon, glass, and quartz) and anchored to the surface by siloxane bonds (Si−O−Si)[97, 98]. In a hydrophilic environment, the hydrolytic stability of the siloxane bond is compromised because the water is drawn directly to the interface. In the presence of water, a hydrolysis equilibrium between siloxane and silanol (Si−OH) groups is established[99,100]. The equilibrium favors the formation of the siloxane groups, the activation energy for this process can be drastically lowered at acidic and alkaline pH values[100-104]. Also, the generation of strong osmotic pressure at the glass/silane interface is presumed to promote the hydrolytic cleavage of siloxane as a consequence of the mechanochemical effect of tensile stress applied to the siloxane bond[98, 100].

It is also believed that the local structure of water near the polymer surface or in a polymer matrix plays a crucial role in determining their biocompatibility/bioinertness[201-203]. The water barrier mechanism[204, 205] arises due to the formation of interfacial water molecules which strongly interact with the surface of the hydrophilic polymer, acting as a barrier against proteins which approach the polymer surface, since large energy is required to break the strong hydrogen

network[204, 205]. Nagasawa and co-workers[206] recently reported the effects of polymer-water interactions on suppression of BSA protein adsorption. They synthesized various types of surfaces (hydrophilic, hydrophobic, anionic, cationic, and zwitterionic) using end-grafted polymer brushes. Their results validated that the better the interaction between water and the polymer brush, the less protein adsorption on the brush surface, which is consistent with the above water barrier mechanism. Tanaka and co-workers investigated the structure of water in hydrated poly(2-methoxyethylacrylate) (PMEA) by using NMR[207], DSC[208], and X-ray diffraction[209, 210]. As a result, they indicated that the water involved in these hydrated polymer matrices can be classified into three types: (i) "free water/freezing water" that barely interacts with a polymer chain, and crystallizes at around 0 °C (i.e., the bulk water); (ii) "tightly bound water/non-freezing bound water" that does not crystallize even below 0 °C due to a strong interaction with a polymer chain; (iii) "intermediate bound water/freezing bound water" which interacts with a polymer in an in-between way, i.e., stronger than free water, but weaker than the tightly bound water. Furthermore, they showed the predominant population of the intermediate bound water in the hydrated PMEA matrix, while a hydrated poly(2-hydroxyethyl methacrylate) (PHEMA) or other hydrophilic polymers which exhibited less biocompatibility than PMEA, possessed only a small population of the intermediate bound water[211]. Hence, they proposed that the population of the intermediate bound water can be used as a gauge of biocompatibility/bioinertness.

In this study, we proposed to use irreversibly adsorbed hydrophilic and hydrophobic polymer chains on silicon substrates extracted using the Giuselin's protocol[158]. Recently, we found that when unfunctionalized or uncharged homopolymer chains contact a solid surface, they favor an increase in the number of solid-segment contacts regardless of the magnitude of attractive solid-segment interactions[34, 166, 212-215]. This enthalpic gain is the driving force to overcome the

conformational entropy loss in the total free energy[25, 216]. As a result, the polymer chains self-assemble into a "flat" conformation on the solid via the equilibration process (hereafter assigned as "flattened chains"). Interestingly, the thickness of the flattened layer is much thinner (a few nanometers thick irrespective of chain lengths of a polymer[25, 217]) than the size of a random coil polymer dimension[217]. This increase in their solid-segment contacts further results in the improvement of the segmental packing of the flattened chains[25, 216], as predicted by simulation results[218, 219]. At the same time, we have established the approach to derive the lone flattened chains from polymer thin films using good solvents[41, 220]. This is possible as the flattened chains can maintain the same conformation even after the solvent leaching due to the irreversible freezing through many solid-segment contacts[221]. Moreover, our recent results demonstrated that the densely packed flattened chains are impenetrable even for chemically identical polymer chains, resulting in instability of a polymer thin film at the surface of the flattened chains (Fig. 5-1)[215].

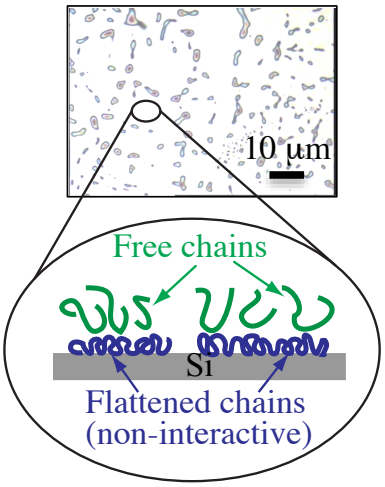

Fig. 5-1. Polymer dewetting on a solid occurs at the interface between free polymer chains and flattened chain, rather than at the solid-polymer interface, as schematically illustrated. The green chains in the illustration correspond to free polymer chains in the matrix of the film.

Here we propose to utilize the densely packed flattened chains as a simple and robust antifouling alternative coating in place of conventional end-grafted polymer coating that requires sophisticated chemistry. The results show that these flattened polymer layers could successfully repel both protein and bacteria from their surfaces irrespective of their hydrophobicity. The underlying mechanism of the anti-fouling characteristics of the adsorbed layers is discussed.

5.3: Materials and experimental techniques:

Two different polymers, poly (ethylene oxide) (PEO, average M_n = 20,000 g mol^{-1}, Sigma-Aldrich, product no. 83100) and poly (2-vinyl pyridine) (P2VP, M_w= 219,000 g/mol, M_w/M_n=1.11, Scientific Polymer Products, Inc.) were used for the present study. The advantages of these two polymer systems are two folds: (i) PEO is one of the most thoroughly studied "water-soluble polymers", while P2VP chains are categorized as a hydrophobic polymer under neutral or basic conditions[222]; (i) both polymers are strong interactive with glass or SiO_2 coated Si substrates, allowing for preparation of the homogenous flattened layers, which will be discussed later. Fluorescein isothiocyanate labeled bovine serum albumin (FITC-BSA) (albumin of M_w=66,000 g/mol labeled with FITC of M_w=389.4 g/mol (Protein Mods) in phosphate buffer saline (PBS, pH=7 and 0.04% sodium azide, the initial concentration of 30mg/ml) was used for the experiments. The stock protein solution was further diluted in dimethyl sulfoxide (DMSO) to prepare a resultant protein concentration of 1mg/ml in DMSO (Sigma-Aldrich, HPLC grade, ≥ 99.7%) for PEO thin films as controls. Si wafers (University Wafer Inc.) were cleaned using a hot piranha solution for 30 min, and subsequently rinsed with deionized water thoroughly. The cleaned Si wafers were then treated by a UV/ozone cleaner (UVOCS Inc.) for 30 min to create a homogenous 2.3 nm thick oxide layer[216]. Hereafter we assigned the UV-treated Si wafer as a "non-HF treated" substrate. A hydrogen-passivated silicon surface was created by dipping the silicon wafer cleaned by piranha solution in aqueous HF to remove any native oxide (SiO_2) layer immediately prior to spin coating with the polymer solution. [*Caution: HF is corrosive and causes severe burns to the eyes, skin, and respiratory tract. Extreme care should be taken when handing it*] (hereafter assigned as "HF-etched Si"). However, we confirmed that a thin SiO_x layer of 1.3 nm in thickness was reproduced even immediately after HF etching, possibly due to atmospheric oxygen and moisture[41]. We also

confirmed that the HF-etched Si has a very different hydrophobicity from that of the non-treated Si, as previously reported[9]. P2VP (50 nm thick) thin films were spin coated onto non-HF treated Si substrates from N,N-dimethyl formamide (DMF, Sigma-Aldrich, ACS reagent, > 99.8%) solutions, while 50 nm thick PEO thin films were spin coated onto HF-etched Si substrates from chlorobenzene (ACS, Macron Fine Chemicals) solutions. The thicknesses of the spin-cast thin films were measured by an ellipsometer (Rudolf Auto EL-II) with a fixed refractive index of 1.455 for PEO[29] and 1.590 for P2VP[223] respectively. To extract the flattened layers, we used the established Guiselin's protocol[158]. In this method, the melt was equilibrated against a solid surface; the unadsorbed chains were thereafter removed by a good solvent, while the flattened chains were assumed to maintain the same conformation due to the irreversible freezing experienced through multiple solid-segment contacts. Despite experimental difficulties, several research groups have proved that Guiselin approach is practical for studying the buried polymer-solid interface for various homopolymers[41,13, 17, 20, 24, 26, 45, 159, 160, 167]. The spin-cast polymer thin films were annealed at 85 °C for PEO and 190 °C for P2VP, both of which temperatures are far above the individual homopolymer bulk glass transition temperature (T_g) values, for prolonged periods of time (up to 300 h) in a vacuum oven at 10^{-3} Torr. Based on previous knowledge about the flattened layer formation for the two homopolymers[32, 197], we leached the annealed PEO and P2VP films with chlorobenzene and DMF, respectively, at room temperature until the thickness of the residual layer remained unchanged (at least 10 times of 30 min-leaching). All the resultant flattened layers were post-annealed at the same temperatures as those used for pre-annealing under vacuum overnight to remove any excess solvent molecules. The flattened layer coated substrates were incubated in the protein solution for 30 min, extracted and rinsed with DMSO and thereafter dried with a gentle nitrogen stream.

5.4: Results and Discussion.

Fig. 5-2 shows the growth curve of the flattened layer derived from a series of annealed PEO films. From the figure, we can see that the adsorbed layer grows as the annealing time increases and crossovers to a plateau (i.e., a "quasiequilibrium" state) after ~ 6h (denoted by t_{cross}). The morphology of the PEO flattened layer measured using AFM (Supporting information) showed that the flattened chains homogeneously covered the silicon substrate. However, we confirmed that no crystalline structures existed, as reported previously[197]. The thickness of the quasi-equilibrium flattened layer at t > 6h was estimated to be 2.4 nm and is consistent with that obtained from the X-ray reflectivity measurement[197]. Thus, we were able to extract the lone flattened layer using the leaching process mentioned earlier.

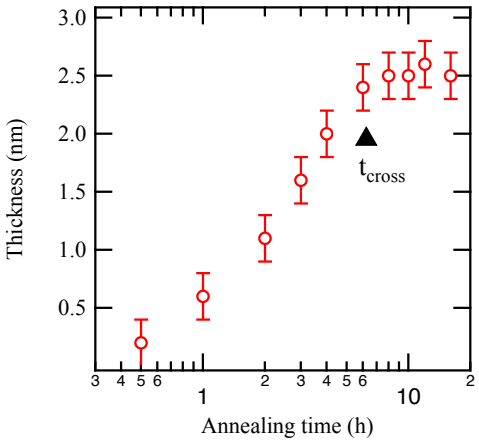

Fig. 5-2: Growth curve of the PEO flattened layer as a function of annealing time at t=85°C.

It is known that thermal annealing promotes the irreversible adsorption of (uncharged) polymer chains even onto weakly attractive surfaces,[115] forming three types of segment sequences, ''trains'', ''loops'', and ''tails''[224]. These physically adsorbed chains can be considered as a ''Guiselin brush''[158] where the chains are physically bound to the surface via multiple segments-solid contacts. It should also be emphasized that the flattened layer has a highly packed (i.e., high density ~ 10 % higher compared to the bulk) chain conformation[197].

Fig. 5-3 (c) shows the optical microscope (OM) images of the PEO flattened layer surface after the protein adsorption experiments with the FITC-labeled BSA protein molecules in DMSO.

As a control, we also measured the protein adsorption on a 50 nm-thick film as well as the bare Si substrate. The OM images for the control sample and bare Si evidenced a large number of the BSA molecules (which appear green on the image) adsorbed on the surfaces (Fig.5-3 (a) and (b)). On the contrary, the OM image proved the anti-fouling property of the flattened layer (Fig.5-3 (c)). We performed similar protein adsorption experiments with the FITC-labeled BSA protein molecules in phosphate-buffered saline (PBS) (pH=7) solution (a physiological buffer solution commonly used for biological research) and found that the PEO flattened layer repelled BSA completely, demonstrating the anti-fouling feature in the aqueous solutions as well.

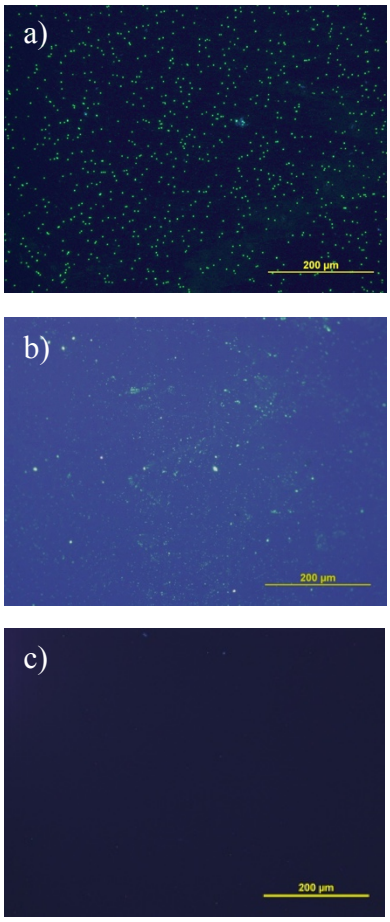

Fig. 5-3: Optical microscopy (OM) images: (a) 50nm spin coated film; (b) bare Si substrate; (c) flattened layer. BSA molecules appear green in the images.

Several theoretical studies have modeled the mechanism of protein resistance conferred by grafted PEG[225-228]. Jeon and co-workers[225] considered that a protein was modeled as a block of infinite length placed parallel to a PEG-functionalized surface, separated by the polymer chains and water. According to their studies, the approach of the protein towards the PEG grafted substrate results in compression of the PEG chains, leading to repulsive elastic forces. Additionally, the removal of water molecules from the hydrated polymer chains during compression creates a thermodynamically unfavorable osmotic penalty. These unfavorable elastic and osmotic stresses generate a repulsive force, the magnitude of which depends on the surface grafting density and chain length of the PEG chains[225, 226], as also predicted by Szleifer and co-workers using the single-chain mean field theory[226, 227].

On the other hand, Grunze and co-workers predicted that the protein resistance of grafted PEG chains depends on the chain conformation[228-231]. Their Monte Carlo simulations demonstrated that a PEG chain on gold, which forms a helical conformation, was inert to protein adsorption, while a PEG chain on silver, which results in a trans conformation, did not prevent protein adsorption[228]. Moreover, they suggested that the helical conformation interacts more with water molecules than the trans conformation, stressing the critical role of the polymer-water interaction in determining protein resistance[230, 231]. Recently, it was also shown that end-tethered polymer brushes do not show any surface height fluctuations even in a good solvent and thus act as a "solid" substrate[190]. Therefore, we hypothesize that the chain conformation and/or dynamics of the flattened layer in the presence of water is responsible for the anti-biofouling behavior.

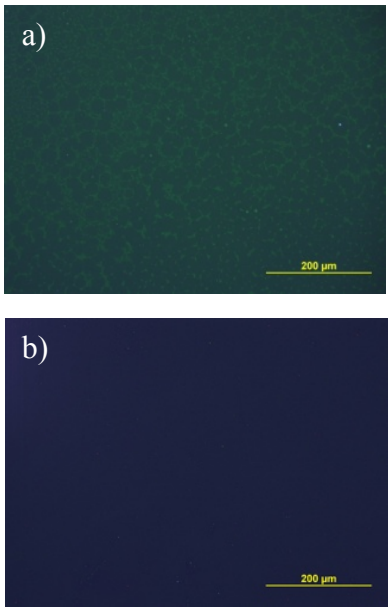

Fig. 5-4: OM image of BSA molecules adsorbed on the surface of P2VP a) 50 nm spin cast film b) flattened layer from PBS solutions.

The next question is whether a flattened layer composed of a hydrophobic polymer also shows the structure-induced antifouling property. Hydrophobic polymers are crucial in many biomedical applications such as drug delivery[87], polymer scaffolds[232], biomedical device fabrication, biological synthesis and analysis, disease diagnostics, DNA sequencing, and biosensors[233-236]. However, hydrophobic polymers suffer serious fouling problems which limit its practical use in biomedical applications due to low wettability and nonspecific protein/hydrophobic analyte adsorption and cell/bacterial adhesion. Poly(2-vinylpyridine) (P2VP) is an attractive hydrophobic polymer for applications like pH-sensitive systems[222,50]. We used P2VP flattened layers as a model hydrophobic polymer. It

should be noted that P2VP is hydrophobic under neutral or basic conditions, while the pyridine groups get protonated and become hydrophilic under acidic conditions[222]. Since the PBS solution used had pH=7, P2VP chains in PBS are considered as hydrophobic. We used the aforementioned protocol to prepare the flattened layer on the non-etched Si substrates. The thickness of the P2VP flattened layer was determined to be 3.0 ± 0.2 nm and the polymer chains homogeneously covered the substrate surface (Supporting information). The detailed structure and morphology of this flattened layer have been described elsewhere[32].

Fig. 5-4 (b) shows the OM image of the P2VP flattened layer surface after protein adsorption in the PBS solution along with a 50 nm-thick spin coated P2VP film (Fig. 5-4(a)). The protein adsorption results interestingly demonstrated that the P2VP flattened layer also repelled BSA completely, while the control P2VP spin-cast thin film (~ 50 nm in thickness) still showed BSA adsorption. Hence, the results prove that the interaction between the polymer and water is not critical for the emergence of the anti-fouling properties of the flattened layers. It was reported that hydrophobic surfaces adsorb higher amounts of BSA than hydrophilic surfaces[237]. This was confirmed by the present results: a higher percentage of area covered by BSA for the P2VP 50 nm-thick film than the PEO 50 nm thick films. We previously confirmed that the surface energy of the P2VP flattened layer is identical to that of the 50nm film[9]. As mentioned in the introduction, the formation of many solid-segment contacts forms the unique architecture of the flattened chain[217]. Hence, we postulate that the large number of segment/solid contacts are the key factor in determining protein resistance, as has been suggested by chemically end-grafted PEG monolayers[227].

Furthermore, as the bacteria adhesion mechanism is generally protein-mediated[238 239], it is expected that the flattened layers with the anti-biofouling properties would resist bacterial attachment and subsequent biofilm formation. To check the possibility, we used *Escherichia coli* (E-coli) as a model bacterium. The details of preparation of the bacterial solutions and adsorption experiments on polymer thin films are described in the supporting information. *E*. coli DH5α cultured on a nutrient agar (at 37°C for 10h) were transferred to 25mL of Lysogeny broth (LB). A 100μl aliquot of the bacteria suspension was pipetted out from the tube onto a clean petri dish. The PEO flattened layer was placed on top of the bacteria solution droplets with the polymer coated side down, to be in contact with the bacteria. The petri dish was thereafter covered and incubated at 37 °C for 30 min. The incubated flattened layer was rinsed gently in distilled water twice and dried under air flowing under a very low pressure. As shown in Fig. 5-5 (b), the PEO flattened layer repelled the bacteria completely, while E-coli strongly adsorbed onto the control 50 nm-thick PEO spin-cast film (Fig. 5-5(a)). The initial attachment of bacteria was believed to be mediated by recognition of components of a protein film by bacterial cells on the surface[240, 241]. As proved above, the flattened layers repel protein adsorption such that the incoming bacteria cells are not able to attach to the surface either. A similar correlation between adsorption of BSA molecules and E. Coli cells on polyethylene glycol (PEG) surfaces was reported earlier[242].

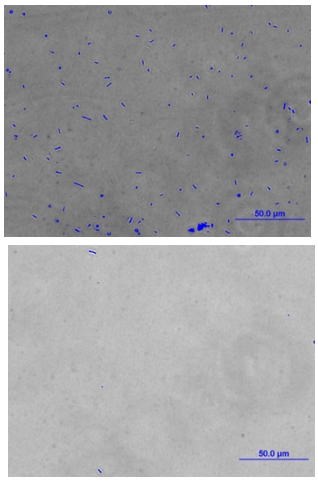

Fig. 5-5: OM image of E-coli adsorbed on the surface of PEO a) 50 nm spin cast film and b) flattened layer (bacteria are false colored by blue).

5.5: Summary

We demonstrated the novel anti-fouling characteristics of irreversibly adsorbed polymer nanolayers on solid substrates irrespective of their hydrophobicity. Our results show that the PEO and P2VP flattened layers could reduce model protein and bacteria adsorption on their surfaces significantly compared to the thin films. We postulate that the large number of segment/solid contacts are the key factor in determining protein resistance, as has been suggested by chemically end-grafted PEG monolayers[227]. Future work is needed to answer the following question:

(i) What are the chain architecture and local chain conformation of the flattened chains?

To understand the anti-fouling phenomenon as a whole, we also aim to reveal the structure and dynamics of the interfacial water independently. It is believed that the structure and dynamics of water are modified by the presence of solid surfaces[201-203]. The assessment of the perturbations of interfacial water structure and dynamics by hydrophilic surfaces is of fundamental interest since water plays a major role in a vast number of biological processes. The next question to be clarified is:

(ii) Does interfacial water[207-210] exist near the polymer surface? If so, is that dependent on the interaction between a polymer and water? What is the local structure and dynamics of the water molecules?

For this purpose, SFG experiments, which provide molecular level structural and dynamical information on the polymer chains and water molecules distinguishingly and quantitatively, will be performed.

Moreover, to realize the necessary attributes for this next-generation polymer-based coating technology, the third question to be addressed is:

(iii) What is the durability and stability of the flattened chains during multiple cycles of use in water?

For this, we will perform ex-situ AFM experiments to check the film stability (whether dewetting occurs after prolonged period of water immersion).

5.6: Supporting information

Optical Microscopy (OM) measurements: Optical microscopy measurements were carried out using an epifluorescent microscope (Olympus BX51) equipped with a fluorescein isothiocyanate (FITC) filter.

Atomic Force Microscopy (AFM) measurements: The surface morphologies of the polymer films were studied by atomic force microscopy (AFM) (Veeco Multimode V and Park NX20) at Center for Functional Nanomaterials (CFN) at BNL. Standard tapping mode measurements were conducted in air using a cantilever with a spring constant of 42 N/m and a resonant frequency of 204 - 497 kHz. The scan rate was 1 Hz with the scanning density of 512 lines per frame.

Bacteria experiments: The model bacteria, E.coli (*Escherichia Coli*) were thawed under room temperature and the nutrient agar medium in a petri dish was swabbed with e-coli bacteria. The petri dish was thereafter incubated in an incubator at 37°C overnight to help the e coli bacteria grow as colonies on the nutrient agar medium. Multiple swabs of E. coli culture from the nutrient agar petri dish is transferred into 25mL of Lysogeny broth (LB) medium in a centrifuge tube. 100µl of the bacteria solution was pipetted out from the tube on to a clean petri dish. The polymer films prepared om one side of the glass cover slips (glass cover slips cleaned with ethanol prior to experiments) were placed on the bacteria solution droplet with the polymer coated side in contact with the solution and the uncoated side facing the air surface. The petri dish was thereafter covered and incubated at 37°C for 30 minutes. Post incubation, the polymer films were rinsed gently in distilled water twice and dried under air flowing under a very low pressure.

Optical imaging for bacteria experiments: The bacteria were imaged using an Olympus BX51 microscope using a bright field configuration.

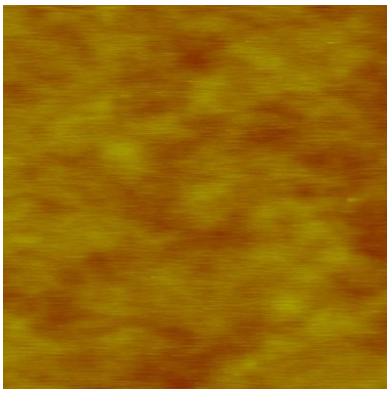

Fig. 5-S1: AFM height image (4 μm X 4 μm) of the "quasiequilibrium" PEO flattened layer.

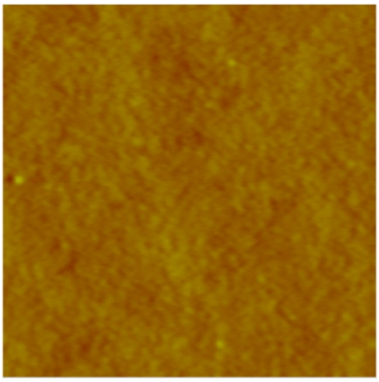

Fig. 5-S2: AFM height image (1 μm X 1 μm) of the "quasiequilibrium" P2VP flattened layer.

References

1. Walheim, S.; Schaffer, E.; Mlynek, J.; Steiner, U. Nanophase-separated polymer films as high-performance antireflection coatings. *Science* **1999,** 283 (5401), 520-2.
2. Forrest, S. R. The path to ubiquitous and low-cost organic electronic appliances on plastic. *Nature* **2004,** 428 (6986), 911-8 DOI: 10.1038/nature02498.
3. Ibn-Elhaj, M.; Schadt, M. Optical polymer thin films with isotropic and anisotropic nano-corrugated surface topologies. *Nature* **2001,** 410 (6830), 796-799.
4. Janata, J.; Josowicz, M. Conducting polymers in electronic chemical sensors. *Nat Mater* **2003,** 2 (1), 19-24 DOI: 10.1038/nmat768.
5. Lee, H.; Dellatore, S. M.; Miller, W. M.; Messersmith, P. B. Mussel-inspired surface chemistry for multifunctional coatings. *Science* **2007,** 318 (5849), 426-30 DOI: 10.1126/science.1147241.
6. Buchko, C. J.; Chen, L. C.; Shen, Y.; Martin, D. C. Processing and microstructural characterization of porous biocompatible protein polymer thin films. *Polymer* **1999,** 40 (26), 7397-7407.
7. Ulbricht, M. Advanced functional polymer membranes. *Polymer* **2006,** 47 (7), 2217-2262.
8. Peterson, S. L.; McDonald, A.; Gourley, P. L.; Sasaki, D. Y. Poly(dimethylsiloxane) thin films as biocompatible coatings for microfluidic devices: Cell culture and flow studies with glial cells. *J Biomed Mater Res A* **2005,** 72a (1), 10-18.
9. Jiang, N. S.; Wang, J. X.; Di, X. Y.; Cheung, J.; Zeng, W. D.; Endoh, M. K.; Koga, T.; Satija, S. K. Nanoscale adsorbed structures as a robust approach for tailoring polymer film stability. *Soft Matter* **2016,** 12 (6), 1801-1809.
10. Luengo, G.; Schmitt, F. J.; Hill, R.; Israelachvili, J. Thin film rheology and tribology of confined polymer melts: Contrasts with bulk properties. *Macromolecules* **1997,** 30 (8), 2482-2494.
11. Roth, C. B.; McNerny, K. L.; Jager, W. F.; Torkelson, J. M. Eliminating the enhanced mobility at the free surface of polystyrene: Fluorescence studies of the glass transition temperature in thin bilayer films of immiscible polymers. *Macromolecules* **2007,** 40 (7), 2568-2574.
12. Zheng, X.; Rafailovich, M. H.; Sokolov, J.; Strzhemechny, Y.; Schwarz, S. A.; Sauer, B. B.; Rubinstein, M. Long-range effects on polymer diffusion induced by a bounding interface. *Phys Rev Lett* **1997,** 79 (2), 241-244.
13. Koga, T.; Jiang, N.; Gin, P.; Endoh, M. K.; Narayanan, S.; Lurio, L. B.; Sinha, S. K. Impact of an Irreversibly Adsorbed Layer on Local Viscosity of Nanoconfined Polymer Melts. *Phys Rev Lett* **2011,** 107 (22).
14. Seemann, R.; Herminghaus, S.; Neto, C.; Schlagowski, S.; Podzimek, D.; Konrad, R.; Mantz, H.; Jacobs, K. Dynamics and structure formation in thin polymer melt films. *J Phys-Condens Mat* **2005,** 17 (9), S267-S290.
15. Reiter, G.; de Gennes, P. G. Spin-cast, thin, glassy polymer films: Highly metastable forms of matter. *Eur Phys J E* **2001,** 6 (1), 25-28.
16. Barbero, D. R.; Steiner, U. Nonequilibrium Polymer Rheology in Spin-Cast Films. *Phys Rev Lett* **2009,** 102 (24).

17. Napolitano, S.; Wubbenhorst, M. The lifetime of the deviations from bulk behaviour in polymers confined at the nanoscale. *Nat Commun* **2011,** 2.

18. Thomas, K. R.; Chenneviere, A.; Reiter, G.; Steiner, U. Nonequilibrium behavior of thin polymer films. *Phys Rev E* **2011,** 83 (2).

19. Raegen, A.; Chowdhury, M.; Calers, C.; Schmatulla, A.; Steiner, U.; Reiter, G. Aging of Thin Polymer Films Cast from a Near-Theta Solvent. *Phys Rev Lett* **2010,** 105 (22).
20. Fujii, Y.; Yang, Z. H.; Leach, J.; Atarashi, H.; Tanaka, K.; Tsui, O. K. C. Affinity of Polystyrene Films to Hydrogen-Passivated Silicon and Its Relevance to the T-g of the Films. *Macromolecules* **2009,** 42 (19), 7418-7422.
21. Napolitano, S.; Wubbenhorst, M. The lifetime of the deviations from bulk behaviour in polymers confined at the nanoscale. *Nat Commun* **2011,** 2, 260-266.

22. Durning, C. J.; O'Shaughness, B.; Sawhney, U.; Nguyen, D.; Majewski, J.; Smith, G. S. Adsorption of Poly(methyl methacrylate) Melts on Quartz. *Macromolecules* **1999,** 32 (20), 6772-6781 DOI: 10.1021/ma981785k.
23. Koga, T.; Jiang, N.; Gin, P.; Endoh, M. K.; Narayanan, S.; Lurio, L. B.; Sinha, S. K. Impact of an Irreversibly Adsorbed Layer on Local Viscosity of Nanoconfined Polymer Melts. *Phys Rev Lett* **2011,** 107, 225901.

24. Rotella, C.; Napolitano, S.; Vandendriessche, S.; Valev, V. K.; Verbiest, T.; Larkowska, M.; Kucharski, S.; Wubbenhorst, M. Adsorption Kinetics of Ultrathin Polymer Films in the Melt Probed by Dielectric Spectroscopy and Second-Harmonic Generation. *Langmuir* **2011,** 27 (22), 13533-13538.
25. Gin, P.; Jiang, N. S.; Liang, C.; Taniguchi, T.; Akgun, B.; Satija, S. K.; Endoh, M. K.; Koga, T. Revealed Architectures of Adsorbed Polymer Chains at Solid-Polymer Melt Interfaces. *Phys. Rev. Lett.* **2012,** 109 (26), DOI: 10.1103/PhysRevLett.109.265501.
26. Asada, M.; Jiang, N.; Sendogdular, L.; Gin, P.; Wang, Y.; Endoh, M. K.; Koga, T.; Fukuto, M.; Schultz, D.; Lee, M.; Li, X.; Wang, J.; Kikuchi, M.; Takahara, A. Heterogeneous Lamellar Structures Near the Polymer/Substrate Interface. *Macromolecules* **2012,** 45 (17), 7098-7106.
27. Napolitano, S.; Rotella, C.; Wübbenhorst, M. Can Thickness and Interfacial Interactions Univocally Determine the Behavior of Polymers Confined at the Nanoscale? *Acs Macro Lett* **2012,** 1 (10), 1189-1193 DOI: 10.1021/mz300432d.
28. Napolitano, S.; Capponi, S.; Vanroy, B. Glassy dynamics of soft matter under 1D confinement: how irreversible adsorption affects molecular packing, mobility gradients and orientational polarization in thin films. *Eur. Phys. J. E Soft Matter* **2013,** 36 (6), 61 DOI: 10.1140/epje/i2013-13061-8.
29. Asada, M.; Jiang, N. S.; Sendogdular, L.; Sokolov, J.; Endoh, M. K.; Koga, T.; Fukuto, M.; Yang, L.; Akgun, B.; Dimitrioug, M.; Satija, S. Melt crystallization/dewetting of ultrathin PEO films via carbon dioxide annealing: the effects of polymer adsorbed layers. *Soft Matter* **2014,** 10 (34), 6392-6403.
30. Vanroy, B.; Wübbenhorst, M.; Napolitano, S. Crystallization of thin polymer layers confined between two adsorbing walls. *Acs Macro Lett* **2013,** 2 (2), 168-172 DOI: 10.1021/mz300641x.
31. Housmans, C.; Sferrazza, M.; Napolitano, S. Kinetics of Irreversible Chain Adsorption. *Macromolecules* **2014,** 47, 3390-3393.

32. Jiang, N.; Shang, J.; Di, X.; Endoh, M. K.; Koga, T. Formation mechanism of high-density, flattened polymer nanolayers adsorbed on planar solids Macromolecules submitted. *Macromolecules* **2014,** 47, 2682-2689.
33. Martínez-Tong, D. E.; Vanroy, B.; Wübbenhorst, M.; Nogales, A.; Napolitano, S. Crystallization of Poly(l-lactide) Confined in Ultrathin Films: Competition between Finite Size Effects and Irreversible Chain Adsorption. *Macromolecules* **2014,** 47, 2354-2360.
34. Jiang, N.; Sendogdular, L.; Di, X.; Sen, M.; Gin, P.; Endoh, M. K.; Koga, T.; Akgun, B.; Dimitriou, M.; Satija, S. K. Effect of CO2 on a mobility gradient of polymer chains near an impenetrable solid *Macromolecules* **2015,** 48, 1795-1803.
35. Jiang, N.; Wang, J.; Di, X.; Cheung, J.; Zeng, W.; Endoh, M. K.; Koga, T.; Satija, S. K. Nanoscale interface structures for the stability of polymer thin films on solids. *Soft Matter, Accepted* **2015**.
36. Bal, J. K.; Beuvier, T.; Unni, A. B.; Panduro, E. A. C.; Vignaud, G.; Delorme, N.; Chebil, M. S.; Grohens, Y.; Gibaud, A. Stability of Polymer Ultrathin Films (<7 nm) Made by a Top-Down Approach. *Acs Nano* **2015,** 9 (8), 8184-8193 DOI: 10.1021/acsnano.5b02381.
37. Scheutjens, J. M. H. M.; Fleer, G. J. Statistical theory of the adsorption of interacting chain molecules. 2. Train, loop, and tail size distribution. *The Journal of Physical Chemistry* **1980,** 84 (2), 178-190 DOI: 10.1021/j100439a011.
38. Douglas, J. F.; Schneider, H. M.; Frantz, P.; Lipman, R.; Granick, S. The origin and characterization of conformational heterogeneity in adsorbed polymer layers. *J Phys-Condens Mat* **1997,** 9 (37), 7699-7718.
39. O'Shaughnessy, B.; Vavylonis, D. Irreversibility and polymer adsorption. *Phys Rev Lett* **2003,** 90 (5).
40. O'Shaughnessy, B.; Vavylonis, D. Irreversible adsorption from dilute polymer solutions. *Eur Phys J E* **2003,** 11 (3), 213-230.
41. Jiang, N. S.; Shang, J.; Di, X. Y.; Endoh, M. K.; Koga, T. Formation Mechanism of High-Density, Flattened Polymer Nano layers Adsorbed on Planar Solids. *Macromolecules* **2014,** 47 (8), 2682-2689.
42. Linse, P.; Kallrot, N. Polymer Adsorption from Bulk Solution onto Planar Surfaces: Effect of Polymer Flexibility and Surface Attraction in Good Solvent. *Macromolecules* **2010,** 43 (4), 2054-2068.
43. Tsuruta, H.; Fujii, Y.; Kai, N.; Kataoka, H.; Ishizone, T.; Doi, M.; Morita, H.; Tanaka, K. Local Conformation and Relaxation of Polystyrene at Substrate Interface. *Macromolecules* **2012,** 45 (11), 4643-4649.
44. Gin, P.; Jiang, N.; Liang, C.; Taniguchi, T.; Akgun, B.; Satija, S. K.; Endoh, M. K.; Koga, T. Revealed Architectures of Adsorbed Polymer Chains at Solid-Polymer Melt Interfaces. *Phys Rev Lett* **2012,** 109 (26), 265501.
45. Gin, P.; Jiang, N. S.; Liang, C.; Taniguchi, T.; Akgun, B.; Satija, S. K.; Endoh, M. K.; Koga, T. Revealed Architectures of Adsorbed Polymer Chains at Solid-Polymer Melt Interfaces. *Phys Rev Lett* **2012,** 109 (26).
46. Simha, R.; Frisch, H. L.; Eirich, F. R. The Adsorption of Flexible Macromolecules. *J Phys Chem-Us* **1953,** 57 (6), 584-589.
47. Park, S.; Wang, J. Y.; Kim, B.; Xu, J.; Russell, T. P. A simple route to highly oriented and ordered nanoporous block copolymer templates. *Acs Nano* **2008,** 2 (4), 766-772.
48. Cavicchi, K. A.; Russell, T. P. Solvent annealed thin films of asymmetric polyisoprene-polylactide diblock copolymers. *Macromolecules* **2007,** 40 (4), 1181-1186.

49. Deshmukh, R. D.; Buxton, G. A.; Clarke, N.; Composto, R. J. Nanoscale block copolymer templates decorated by nanoparticle arrays. *Macromolecules* **2007,** 40 (17), 6316-6324.
50. Sidorenko, A.; Tokarev, I.; Minko, S.; Stamm, M. Ordered reactive nanomembranes/nanotemplates from thin films of block copolymer supramolecular assembly. *J Am Chem Soc* **2003,** 125 (40), 12211-12216.
51. Phillip, W. A.; O'Neill, B.; Rodwogin, M.; Hillmyer, M. A.; Cussler, E. L. Self-Assembled Block Copolymer Thin Films as Water Filtration Membranes. *ACS Applied Materials & Interfaces* **2010,** 2 (3), 847-853 DOI: 10.1021/am900882t.
52. Drzal, P. L.; Halasa, A. F.; Kofinas, P. Microstructure orientation and nanoporous gas transport in semicrystalline block copolymer membranes. *Polymer* **2000,** 41 (12), 4671-4677.
53. Crossland, E. J. W.; Kamperman, M.; Nedelcu, M.; Ducati, C.; Wiesner, U.; Smilgies, D. M.; Toombes, G. E. S.; Hillmyer, M. A.; Ludwigs, S.; Steiner, U.; Snaith, H. J. A Bicontinuous Double Gyroid Hybrid Solar Cell. *Nano Lett* **2009,** 9 (8), 2807-2812.
54. Lee, B.; Yoon, J.; Oh, W.; Hwang, Y.; Heo, K.; Jin, K. S.; Kim, J.; Kim, K. W.; Ree, M. In-situ grazing incidence small-angle X-ray scattering studies on nanopore evolution in low-k organosilicate dielectric thin films. *Macromolecules* **2005,** 38 (8), 3395-3405.
55. Park, S.; Lee, D. H.; Xu, J.; Kim, B.; Hong, S. W.; Jeong, U.; Xu, T.; Russell, T. P. Macroscopic 10-Terabit-per-Square- Inch Arrays from Block Copolymers with Lateral Order. *Science* **2009,** 323 (5917), 1030-1033.
56. Albert, J. N. L.; Epps, T. H. Self-assembly of block copolymer thin films. *Mater Today* **2010,** 13 (6), 24-33.
57. Hamley, I. W. Ordering in thin films of block copolymers: Fundamentals to potential applications. *Prog Polym Sci* **2009,** 34 (11), 1161-1210.
58. Thurn-Albrecht, T.; Schotter, J.; Kastle, G. A.; Emley, N.; Shibauchi, T.; Krusin-Elbaum, L.; Guarini, K.; Black, C. T.; Tuominen, M. T.; Russell, T. P. Ultrahigh-Density Nanowire Arrays Grown in Self-Assembled Diblock Copolymer Templates. *Science* **2000,** 290, 2126-2129.
59. Albalak, R. J.; Thomas, E. L. Roll-Casting of block copolymers and of block copolymer-homopolymer blends. *J. Polym. Sci., Part B: Polym. Phys.* **1994,** 32, 341-350.
60. Angelescu, D. E.; Waller, J. H.; Adamson, D. H.; Deshpande, P.; Chou, S. Y.; Register, R. A.; Chaikin, P. M. Macroscopic Orientation of Block Copolymer Cylinders in Single-Layer Films by Shearing. *Adv. Mater.* **2004,** 16, 1736-1740.
61. Kim, S. O.; Solak, H. H.; Stoykovich, M. P.; Ferrier, N. J.; de Pablo, J. J.; Nealey, P. F. Epitaxial self-assembly of block copolymers on lithographically defined nanopatterned substrates. *Nature* **2003,** 424, 411-414.
62. Ruiz, R.; Kang, H.; Detcheverry, F. A.; Dobisz, E.; Kercher, D. S.; Albrecher, T. R.; de Pable, J. J.; Nealey, P. F. Density Multiplication and Improved Lithography by Directed Block Copolymer Assembly. *Science* **2008,** 321, 936-939.
63. Gong, J.; Ahn, H.; Kim, E.; Lee, H.; Park, S.; Lee, M.; Lee, S.; Kim, T.; Kwak, E. A.; Ryu, D. Y. Rapid structural reorganization in thin films of block copolymer self-assembly. *Soft Matter* **2012,** 8 (13), 3570-3575.
64. Sohn, B. H.; Yun, S. H. Perpendicular lamellae induced at the interface of neutral self-assembled monolayers in thin diblock copolymer films. *Polymer* **2002,** 43 (8), 2507-2512.
65. Huang, E.; Pruzinsky, S.; Russell, T. P.; Mays, J.; Hawker, C. J. Neutrality conditions for block copolymer systems on random copolymer brush surfaces. *Macromolecules* **1999,** 32 (16), 5299-5303.

66. Mansky, P.; Liu, Y.; Huang, E.; Russell, T. P.; Hawker, C. J. Controlling polymer-surface interactions with random copolymer brushes. *Science* **1997,** 275 (5305), 1458-1460.
67. Edwards, E. W.; Montague, M. F.; Solak, H. H.; Hawker, C. J.; Nealey, P. F. Precise control over molecular dimensions of block-copolymer domains using the interfacial energy of chemically nanopatterned substrates. *Adv Mater* **2004,** 16 (15), 1315-+.
68. Harrison, C.; Chaikin, P. M.; Huse, D. A.; Register, R. A.; Adamson, D. H.; Daniel, A.; Huang, E.; Mansky, P.; Russell, T. P.; Hawker, C. J.; Egolf, D. A.; Melnikov, I. V.; Bodenschatz, E. Reducing substrate pinning of block copolymer microdomains with a buffer layer of polymer brushes. *Macromolecules* **2000,** 33 (3), 857-865.
69. Yang, X. M.; Peters, R. D.; Nealey, P. F.; Solak, H. H.; Cerrina, F. Guided self-assembly of symmetric diblock copolymer films on chemically nanopatterned substrates. *Macromolecules* **2000,** 33 (26), 9575-9582.
70. Busch, P.; Posselt, D.; Smilgies, D.-M.; Rheinländer, B.; Kremer, F.; Papadakis, C. M. Lamellar diblock copolymer thin films investigated by tapping mode atomic force microscopy: Molar-mass dependence of surface ordering. *Macromolecules* **2003,** 36, 8717-8727.
71. Kim, S. H.; Misner, M. J.; Xu, T.; Kimura, M.; Russell, T. P. Highly oriented and ordered arrays from block copolymers via solvent evaporation. *Adv. Mater.* **2004,** 16, 226-231.
72. Hanley, K. J.; Lodge, T. P.; Huang, C. I. Phase behavior of a block copolymer in solvents of varying selectivity. *Macromolecules* **2000,** 33, 5918-5931.
73. Bosworth, J. K.; Paik, M. Y.; Ruiz, R.; Schwartz, E. L.; Huang, J. Q.; Ko, A. W.; Smilgies, D.-M.; Black, C. T.; Ober, C. K. Control of Self-Assembly of Lithographically Patternable Block Copolymer Films. *ACS Nano* **2008,** 2, 1396-1402.
74. Sinturel, C.; Vayer, M.; Morris, M.; Hillmyer, M. A. Solvent vapor annealing of block polymer thin films. *Macromolecules* **2013,** 46, 5399-5415.
75. Qiang, Z.; Zhang, L.; Stein, G. E.; Cavicchi, K. A.; Vogt, B. D. Unidirectional Alignment of Block Copolymer Films Induced by Expansion of a Permeable Elastomer during Solvent Vapor Annealing. *Macromolecules* **2014,** 47, 1109-1117.
76. Jiang, Z.; Mukhopadhyay, M. K.; Song, S.; Narayanan, S.; Lurio, L. B.; Kim, H.; Sinha, S. K. Entanglement Effects in Capillary Waves on Liquid Polymer Films. *Phys Rev Lett* **2008,** 101 (24).
77. Kim, H.; Ruhm, A.; Lurio, L. B.; Basu, J. K.; Lal, J.; Lumma, D.; Mochrie, S. G. J.; Sinha, S. K. Surface dynamics of polymer films. *Phys Rev Lett* **2003,** 90 (6).
78. Kim, H.; Ruhm, A.; Lurio, L. B.; Basu, J. K.; Lal, J.; Mochrie, S. G. J.; Sinha, S. K. Synchrotron radiation studies of the dynamics of polymer films. *J Phys-Condens Mat* **2004,** 16 (33), S3491-S3497.
79. Priestley, R. D.; Ellison, C. J.; Broadbelt, L. J.; Torkelson, J. M. Structural relaxation of polymer glasses at surfaces, interfaces, and in between. *Science* **2005,** 309 (5733), 456-9 DOI: 10.1126/science.1112217.
80. Gowd, E. B.; Koga, T.; Endoh, M. K.; Kumar, K.; Stamm, M. Pathways of cylindrical orientations in PS-b-P4VP diblock copolymer thin films upon solvent vapor annealing. *Soft Matter* **2014,** 10 (39), 7753-7761.
81. Donlan, R. M. Biofilm formation: a clinically relevant microbiological process. *Clin Infect Dis* **2001,** 33 (8), 1387-92 DOI: 10.1086/322972.
82. Pavithra, D.; Doble, M. Biofilm formation, bacterial adhesion and host response on polymeric implants--issues and prevention. *Biomed Mater* **2008,** 3 (3), 034003 DOI: 10.1088/1748-6041/3/3/034003.

83. Vasilev, K.; Cook, J.; Griesser, H. J. Antibacterial surfaces for biomedical devices. *Expert Rev Med Devices* **2009,** 6 (5), 553-67 DOI: 10.1586/erd.09.36.
84. Willcox, M. D.; Hume, E. B.; Aliwarga, Y.; Kumar, N.; Cole, N. A novel cationic-peptide coating for the prevention of microbial colonization on contact lenses. *J Appl Microbiol* **2008,** 105 (6), 1817-25 DOI: 10.1111/j.1365-2672.2008.03942.x.
85. Wisniewski, N.; Reichert, M. Methods for reducing biosensor membrane biofouling. *Colloids Surf B Biointerfaces* **2000,** 18 (3-4), 197-219.
86. Yang, C.; Liang, G. L.; Xu, K. M.; Gao, P.; Xu, B. Bactericidal functionalization of wrinkle-free fabrics via covalently bonding TiO2@Ag nanoconjugates. *J Mater Sci* **2009,** 44 (7), 1894-1901.
87. Abu-Diak, O. A. A., G.P.; Jones, D.S., *Fundamentals and applications of controlled release drug delivery*. Control Release Society: 2011.
88. Conte, A.; Buonocore, G. G.; Bevilacqua, A.; Sinigaglia, M.; Del Nobile, M. A. Immobilization of lysozyme on polyvinylalcohol films for active packaging applications. *J Food Protect* **2006,** 69 (4), 866-870.
89. Kenawy, E. R.; Worley, S. D.; Broughton, R. The chemistry and applications of antimicrobial polymers: A state-of-the-art review. *Biomacromolecules* **2007,** 8 (5), 1359-1384.
90. Asuri, P.; Karajanagi, S. S.; Kane, R. S.; Dordick, J. S. Polymer-nanotube-enzyme composites as active antifouling films. *Small* **2007,** 3 (1), 50-53.
91. Flemming, H. C. Biofouling in water systems - cases, causes and countermeasures. *Appl Microbiol Biot* **2002,** 59 (6), 629-640.
92. Hucknall, A.; Rangarajan, S.; Chilkoti, A. In Pursuit of Zero: Polymer Brushes that Resist the Adsorption of Proteins. *Adv Mater* **2009,** 21 (23), 2441-2446.
93. Banerjee, I.; Pangule, R. C.; Kane, R. S. Antifouling coatings: recent developments in the design of surfaces that prevent fouling by proteins, bacteria, and marine organisms. *Adv Mater* **2011,** 23 (6), 690-718 DOI: 10.1002/adma.201001215.
94. Copisarow, M. Marine Fouling and Its Prevention. *Science* **1945,** 101 (2625), 406-407.
95. Chapman, R. G.; Ostuni, E.; Takayama, S.; Holmlin, R. E.; Yan, L.; Whitesides, G. M. Surveying for surfaces that resist the adsorption of proteins. *J Am Chem Soc* **2000,** 122 (34), 8303-8304.
96. Ostuni, E.; Chapman, R. G.; Holmlin, R. E.; Takayama, S.; Whitesides, G. M. A survey of structure-property relationships of surfaces that resist the adsorption of protein. *Langmuir* **2001,** 17 (18), 5605-5620.
97. Paripovic, D.; Klok, H. A. Improving the Stability in Aqueous Media of Polymer Brushes Grafted from Silicon Oxide Substrates by Surface-Initiated Atom Transfer Radical Polymerization. *Macromol Chem Phys* **2011,** 212 (9), 950-958.
98. Tugulu, S.; Klok, H. A. Stability and nonfouling properties of poly(poly(ethylene glycol) methacrylate) brushes-under cell culture conditions. *Biomacromolecules* **2008,** 9 (3), 906-912.
99. Plueddemann, E. P., *Silane Coupling Agents*. Springer US: 1991.
100. Ishida, H., *Controlled Interphases in Glass Fiber and Particulate Reinforced Polymers: Structure of Silane Coupling Agents in Solutions and on Substrates.* Springer Netherlands: 1993; p 455.

101. Ishida, H.; Koenig, J. L. Effect of Hydrolysis and Drying on the Siloxane Bonds of a Silane Coupling Agent Deposited on E-Glass Fibers. *J Polym Sci Pol Phys* **1980,** 18 (2), 233-237.

102. Cypryk, M.; Apeloig, Y. Mechanism of the acid-catalyzed Si-O bond cleavage in siloxanes and siloxanols. A theoretical study. *Organometallics* **2002,** 21 (11), 2165-2175.
103. Wasserman, S. R.; Tao, Y. T.; Whitesides, G. M. Structure and Reactivity of Alkylsiloxane Monolayers Formed by Reaction of Alkyltrichlorosilanes on Silicon Substrates. *Langmuir* **1989,** 5 (4), 1074-1087.
104. Liberelle, B.; Giasson, S. Chemical end-grafting of homogeneous polystyrene monolayers on mica and silica surfaces. *Langmuir* **2007,** 23 (18), 9263-9270.
105. Wertz, C. F.; Santore, M. M. Fibrinogen adsorption on hydrophilic and hydrophobic surfaces: Geometrical and energetic aspects of interfacial relaxations. *Langmuir* **2002,** 18 (3), 706-715.
106. Rabe, M.; Verdes, D.; Seeger, S. Understanding protein adsorption phenomena at solid surfaces. *Adv Colloid Interfac* **2011,** 162 (1-2), 87-106.
107. Reiter, G.; de Gennes, P. G. *Eur. Phys. J. E* **2001,** 6, 25-28.
108. Seemann, R.; Herminghaus, S.; Neto, C.; Schlagowski, S.; Podzimek, D.; Konrad, R.; Mantz, H.; Jacobs, K. Dynamics and structure formation in thin polymer melt films. *J. Phys. Condens. Matter* **2005,** 17 (9), S267-S290.
109. Barbero, D. R.; Steiner, U. Nonequilibrium Polymer Rheology in Spin-Cast Films. *Phys Rev Lett* **2009,** 102 (24).

110. Thomas, K. R.; Chenneviere, A.; Reiter, G.; Steiner, U. Nonequilibrium behavior of thin polymer films. *Phys. Rev. E* **2011,** 83 (2).

111. Chung, J. Y.; Chastek, T. Q.; Fasolka, M. J.; Ro, H. W.; Stafford, C. M. Quantifying Residual Stress in Nanoscale Thin Polymer Films via Surface Wrinkling. *Acs Nano* **2009,** 3 (4), 844-852 DOI: Doi 10.1021/Nn800853y.
112. Guiselin, O. Irreversible Adsorption of a Concentrated Polymer-Solution. *Europhys Lett* **1992,** 17 (3), 225-230 DOI: Doi 10.1209/0295-5075/17/3/007.
113. Yethiraj, A. Monte-Carlo Simulation of Confined Semiflexible Polymer Melts. *J Chem Phys* **1994,** 101 (3), 2489-2497.
114. Carrillo, J. M. Y.; Cheng, S. W.; Kumar, R.; Goswami, M.; Sokolov, A. P.; Sumpter, B. G. Untangling the Effects of Chain Rigidity on the Structure and Dynamics of Strongly Adsorbed Polymer Melts. *Macromolecules* **2015,** 48 (12), 4207-4219.
115. Fleer, G. J.; Cohen Stuart, M. A.; Scheutjens, J. M. H. M.; Cosgrove, T.; Vincent, B., *Polymers at Interfaces*. Chapman and Hall: London, 1993.
116. Scheutjens, J. M. H. M.; Fleer, G. J. Statistical-Theory of the Adsorption of Interacting Chain Molecules .2. Train, Loop, and Tail Size Distribution. *J Phys Chem-Us* **1980,** 84 (2), 178-190.
117. Gautam, K. S.; Schwab, A. D.; Dhinojwala, A.; Zhang, D.; Dougal, S. M.; Yeganeh, M. S. Molecular structure of polystyrene at air/polymer and solid/polymer interfaces. *Phys Rev Lett* **2000,** 85 (18), 3854-3857 DOI: DOI 10.1103/PhysRevLett.85.3854.
118. Shen, Y. R. Surface-Properties Probed by 2nd-Harmonic and Sum-Frequency Generation. *Nature* **1989,** 337 (6207), 519-525 DOI: Doi 10.1038/337519a0.
119. Chen, Z.; Shen, Y. R.; Somorjai, G. A. Studies of polymer surfaces by sum frequency generation vibrational spectroscopy. *Annu Rev Phys Chem* **2002,** 53, 437-465 DOI: DOI 10.1146/annurev.physchem.53.091801.115126.

120. Frank, C. W.; Rao, V.; Despotopoulou, M. M.; Pease, R. F. W.; Hinsberg, W. D.; Miller, R. D.; Rabolt, J. F. Structure in thin and ultrathin spin-cast polymer films. *Science* **1996,** 273 (5277), 912-915 DOI: DOI 10.1126/science.273.5277.912.
121. Tatek, Y. B.; Tsige, M. Structural properties of atactic polystyrene adsorbed onto solid surfaces. *J Chem Phys* **2011,** 135 (17).

122. O'Shaughnessy, B.; Vavylonis, D. Irreversibility and polymer adsorption. *Phys Rev Lett* **2003,** 90 (5).
123. Naumkin, A. K.-V., A.; Gaarenstroom, S.; Powell, C., NIST X-ray Photoelectron Spectroscopy Database, Version 4.1. National Institute of Standards and Technology, Gaithersburg: 2012.
124. Zajac, R.; Chakrabarti, A. Irreversible polymer adsorption from semidilute and moderately dense solutions. *Phys. Rev. E* **1995,** 52 (6), 6536-6549 DOI: 10.1103/PhysRevE.52.6536.
125. Jiang, X. Q.; Tanaka, K.; Takahara, A.; Nakahama, S.; Kajiyama, T. Chain end group-induced surface ordering in poly(styrene-b-4-vinylpyridine) symmetric diblock copolymer films. *Polym J* **1999,** 31 (11), 1015-1020.
126. Barnette, A. L.; Bradley, L. C.; Veres, B. D.; Schreiner, E. P.; Park, Y. B.; Park, J.; Park, S.; Kim, S. H. Selective detection of crystalline cellulose in plant cell walls with sum-frequency-generation (SFG) vibration spectroscopy. *Biomacromolecules* **2011,** 12, 2434-2439.
127. Horinouchi, A.; Yamada, N. L.; Tanaka, K. Aggregation States of Polystyrene at Nonsolvent Interfaces. *Langumuir* **2014,** 30, 6565-6570.
128. Elman, J. F.; Jobs, B. D.; Long, T. E.; Koberstein, J. T. A Neutron Reflectivity Investigation of Surface and Interface Segregation of Polymer Functional End Groups. *Macromolecules* **1994,** 27, 5341-5349.
129. Kumar, S. K.; Vacatello, M.; Yoon, D. Y. *J Chem Phys* **1988,** 89, 5206−5215.
130. Yethiraj, A.; Hall, C. K. *J Chem Phys* **1989,** 91, 4827−4837.
131. Bitsanis, I.; Hadziioannou, G. *J Chem Phys* **1990,** 92, 3827-3847.
132. Walton, D. G.; Mayes, A. M. *Phys. Rev. E* **1996,** 54, 2811−2815.
133. Calchera, A. R.; Curtis, A. D.; Patterson, J. E. Plasma Treatment of Polystyrene Thin Films Affects More Than the Surface. *ACS Appl. Mater. Interfaces* **2012,** 4, 3493-3499.
134. Wong, D.; Jalbert, C. A.; P. A. V., O. R.-M.; Koberstein, J. T. Surface Dynamics of Polymer Glasses: Sub‑Tg Surface Reorganization in End-Functional Polymers. *Macromolecules* **2012,** 45, 7973-7984.
135. Wilson, P. T.; Richter, L. J.; Wallace, W. E.; Briggman, K. A.; Stephenson, J. C. Correlation of molecular orientation with adhesion at polystyrene/solid interfaces. *Chem Phys Lett* **2002,** 363 (1-2), 161-168.

136. Kraus, J.; Müller-Buschbaum, P.; Kuhlmann, T.; Schubert, D. W.; Stamm, M. Con¯nement effects on the chain conformationin thin polymer Flms. *Europhys Lett* **2000,** 49, 210-216.
137. Doumenc, F.; Guerrier, B.; Allain, C. Aging and history effects in solvent-induced glass transition of polymer films. *Europhys Lett* **2006,** 76 (4), 630-636.
138. Lu, Y. J.; Xia, H. W.; Zhang, G. Z.; Wu, C. *J. Mater. Chem.* **2009,** 19, 5952-5955.
139. Seeck, O. H.; Kaendler, I. D.; Tolan, M.; Shin, K.; Rafailovich, M. H.; Sokolov, J.; Kolb, R. Analysis of x-ray reflectivity data from low-contrast polymer bilayer systems using a Fourier method. *Appl Phys Lett* **2000,** 76 (19), 2713-2715 DOI: Doi 10.1063/1.126452.

140. Kallrot, N.; Dahlqvist, M.; Linse, P. Dynamics of Polymer Adsorption from Bulk Solution onto Planar Surfaces. *Macromolecules* **2009,** 42 (10), 3641-3649.
141. Perlich, J.; Körstgens, V.; Metwalli, E.; Schulz, L.; Georgii, R.; Müller-Buschbaum, P. Solvent Content in Thin Spin-Coated Polystyrene Homopolymer Films. *Macromolecules* **2009,** 42, 337-344.
142. Janczuk, B.; Zdziennicka, A. *J. Mater. Sci.* **1994,** 29, 3559-3564.
143. Santore, M. Dynamics in adsorbed homopolymer layers: Understanding complexity from simple starting points. *Current Opinion in Colloid & Interface Science* **2005,** 10 (3-4), 176-183.
144. Matsen, M. W.; Schick, M. Stable and Unstable Phases of a Diblock Copolymer Melt. *Phys Rev Lett* **1994,** 72 (16), 2660-2663.
145. Khandpur, A. K.; Forster, S.; Bates, F. S.; Hamley, I. W.; Ryan, A. J.; Bras, W.; Almdal, K.; Mortensen, K. Polyisoprene-polystyrene diblock copolymer phase diagram near the order-disorder transition. *Macromolecules* **1995,** 28 (26), 8796-8806.
146. Segalman, R. A. Patterning with block copolymer thin films. *Mat Sci Eng R* **2005,** 48 (6), 191-226.
147. Jung, Y. S.; Ross, C. A. Orientation-controlled self-assembled nanolithography using a polystyrene-polydimethylsiloxane block copolymer. *Nano Lett* **2007,** 7 (7), 2046-2050.
148. Walton, D. G.; Kellogg, G. J.; Mayes, A. M.; Lambody, P.; Russell, T. P. A free energy model for confined diblock copolymers. *Macromolecules* **1994,** 27, 6225-6228.
149. Vandijk, M. A.; Vandenborg, R. Ordering Phenomena in Thin Block-Copolymer Films Studied Using Atomic-Force Microscopy. *Macromolecules* **1995,** 28, 6773-6778.
150. Kellogg, G. J.; Walton, D. G.; Mayes, A. M.; Lambooy, P.; Russell, T. P.; Gallagher, P. D.; Satija, S. K. Observed Surface Energy Effects in Confined Diblock Copolymers. *Phys. Rev. Lett.* **1996,** 76, 2503.
151. Nikoubashman, A.; Register, R. A.; Panagiotopoulos, A. Z. Self-Assembly of Cylinder-Forming Diblock Copolymer Thin Films. *Macromolecules* **2013,** 46, 6651-6658.
152. Sen, M.; Jiang, N.; Cheung, J.; Endoh, M. K.; Koge, T.; Kawaguchi, D.; Tanaka, K. Flattening Process of Polymer Chains Irreversibly Adsorbed on a Solid. *Acs Macro Lett* **2016,** 5 (4), 504-508.
153. Jiang, N.; Wang, J.; Di, X.; Cheung, J.; Zeng, W.; Endoh, M. K.; Koga, T.; Satija, S. K. Nanoscale adsorbed structures as a robust approach for tailoring polymer film stability *Soft Matter* **2016,** 12, 1801-1809.
154. Knoll, A.; Horvat, A.; Lyakhova, K. S.; Krausch, G.; Sevink, G. J. A.; Zvelindovsky, A. V.; Magerle, R. Phase behavior in thin films of cylinder-forming block copolymers. *Phys Rev Lett* **2002,** 89 (3).
155. Tsarkova, L. A., *Structure and Dynamics of Cylinder Forming Block Copolymers in Thin Films*. Springer: 2007; p 231-265.
156. Knoll, A.; Magerle, R.; Krausch, G. *Macromolecules* **2001,** 34, 4159-4165.
157. Jiang, X.; Tanaka, K.; Takahara, A.; Kajiyama, T. Effect of chain end group hydrophobicity on surface aggregation structure of poly(styrene-block-4-vinylpyridine) symmetric diblock copolymer films. *Polymer* **1998,** 39 (12), 2615-2620.
158. Guiselin, O. Irreversible Adsorption of a Concentrated Polymer-Solution. *Europhys Lett* **1992,** 17 (3), 225-230.
159. Housmans, C.; Sferrazza, M.; Napolitano, S. Kinetics of Irreversible Chain Adsorption. *Macromolecules* **2014,** 47 (10), 3390-3393.

160. Durning, C. J.; O'Shaughnessy, B.; Sawhney, U.; Nguyen, D.; Majewski, J.; Smith, G. S. Adsorption of poly(methyl methacrylate) melts on quartz. *Macromolecules* **1999,** 32 (20), 6772-6781.
161. Napolitano, S.; Wubbenhorst, M. Dielectric Signature of a Dead layer in Ultrathin films of nonpolar polymer. *J. Phys. Chem. B* **2007,** 111, 9197-9199.
162. Napolitano, S.; Prevosto, D.; Lucchesi, M.; Pingue, P.; D'Acunto, M.; Rolla, P. Structural relaxation dynamics of PET films. *Langmuir* **2007,** 23, 2103-2109.
163. Napolitano, S.; Lupascu, V.; Wubbenhorst, M. Temperature dependence of the deviations from bulk behavior in ultrathin polymer films. *Macromolecules* **2008,** 41, 1061-1063.
164. Rotella, C.; Napolitano, S.; De Cremer, L.; Koeckelberghs, G.; Wubbenhorst, M. Distribution of Segmental Mobility in Ultrathin Polymer Films. *Macromolecules* **2010,** 43, 8686-8691.
165. Napolitano, S.; Rotella, C.; Wubbenhorst, M. Is the Reduction in Tracer Diffusivity under Nanoscopic Confinement Related to a Frustrated Segmental Mobility? *Macromol. Rapid Commun.* **2011,** 32, 844-848.
166. Asada, M.; Jiang, N.; Sendogdular, L.; Gin, P.; Wang, Y.; Endoh, M. K.; Koga, T.; Fukuto, M.; Schultz, D.; Lee, M.; Li, X.; Wang, J.; Kikuchi, M.; Takahara, A. Heterogeneous Lamellar Structures Near the Polymer/Substrate Interface. *Macromolecules* **2012,** 45, 7098-7106.
167. Shimomura, S.; Inutsuka, M.; Yamada, N. L.; Tanaka, K. Unswollen layer of cross-linked polyisoprene at the solid interface. *Polymer* **2016,** 105, 526-531.
168. Guinier, A. F., G., *Small angle scattering of x-rays*. John Wiley & Sons, Inc: 1955.
169. Debye, P.; Bueche, A. M. Scattering by an Inhomogeneous Solid. *J Appl Phys* **1949,** 20 (6), 518-525.
170. Gautam, K. S.; Schwab, A. D.; Dhinojwala, A.; Zhang, D.; Dougal, S. M.; Yeganeh, M. S. Molecular Structure of Polystyrene at Air/ Polymer and Solid /Polymer Interfaces. *Phys. Rev. Lett.* **2000,** 85, 3854-3857.
171. Tatek, Y. B.; Tsuge, M. Structural properties of atactic polystyrene adsorbed onto solid surfaces. *J Chem Phys* **2011,** 135, 174708.
172. Tsarkova, L.; Knoll, A.; Krausch, G.; Magerle, R. Substrate-induced phase transitions in thin films of cylinder-forming diblock copolymer melts. *Macromolecules* **2006,** 39 (10), 3608-3615.
173. Fasolka, M. J.; Banerjee, P.; Mayes, A. M.; Pickett, G.; Balazs, A. C. Morphology of Ultrathin Supported Diblock Copolymer Films: Theory and Experiment. *Macromolecules* **2000,** 33, 5702-5712.
174. Leger, L.; Erman, M.; Guinetpicard, A. M.; Ausserre, D.; Strazielle, C. Precursor Film Profiles of Spreading Liquid Drops. *Phys. Rev. Lett.* **1988,** 60, 2390.
175. Peinemann, K. V.; Abetz, V.; Simon, P. F. W. Asymmetric superstructure formed in a block copolymer via phase separation. *Nat Mater* **2007,** 6 (12), 992-996.
176. Vukovic, I.; ten Brinke, G.; Loos, K. Hexagonally Perforated Layer Morphology in PS-b-P4VP(PDP) Supramolecules. *Macromolecules* **2012,** 45 (23), 9409-9418.
177. Linse, P. Effect of solvent quality on the polymer adsorption from bulk solution onto planar surfaces. *Soft Matter* **2012,** 8, 5140-5150.
178. O'Shaughnessy, B.; Vavylonis, D. Irreversible adsorption from dilute polymer solutions. *Eur. Phys. J. E* **2003,** 11 (3), 213-230 DOI: 10.1140/epje/i2003-10015-9.

179. Marques, C. M.; Joanny, J. F. Block Copolymer Adsorption in a Nonselective Solvent. *Macromolecules* **1989,** 22, 1454-1458.
180. Hashimoto, T., Order-Disorder Transition in Block Polymers. In *Thermoplastic Elastomers*, 2nd ed.; Holden, G., Legge, N. R., Quirk, R., Schroeder, H. E., Hanser, M., Eds. Hanser Gardner Pubns: Cincinnati, 1996; pp 429-463.
181. Seeck, O. H.; Kaendler, I. D.; Tolan, M.; Shin, K.; Rafailovich, M. H.; Sokolov, J.; Kolb, R. Analysis of x-ray reflectivity data from low-contrast polymer bilayer systems using a Fourier method. *Appl Phys Lett* **2000,** 76 (19), 2713-2715.
182. Liu, H. B.; Hamers, R. J. An X-ray photoelectron spectroscopy study of the bonding of unsaturated organic molecules to the Si(001) surface. *Surf Sci* **1998,** 416 (3), 354-362.
183. Wang, Y.; Rafailovich, M.; Sokolov, J.; Gersappe, D.; Araki, T.; Zou, Y.; Kilcoyne, A. D. L.; Ade, H.; Marom, G.; Lustiger, A. Substrate effect on the melting temperature of thin polyethylene films. *Phys Rev Lett* **2006,** 96 (2).
184. Kawai, A.; Kawakami, J.; Sasazaki, H. Surface Energy Change of Si(100) Wafer by Exposing to Air. *J Photopolym Sci Tec* **2008,** 21 (6), 739-740.
185. Sauer, B. B.; Dee, G. T. Surface tension and melt cohesive energy density of polymer melts including high melting and high glass transition polymers. *Macromolecules* **2002,** 35 (18), 7024-7030.
186. Kimani, S. M.; Hardman, S. J.; Hutchings, L. R.; Clarke, N.; Thompson, R. L. Synthesis and surface activity of high and low surface energy multi-end functional polybutadiene additives. *Soft Matter* **2012,** 8 (12), 3487-3496.
187. Kern, W.; Puotinen, D. A. Cleaning Solutions Based on Hydrogen Peroxide for Use in Silicon Semiconductor Technology. *Rca Rev* **1970,** 31 (2), 187-&.
188. Tsui, O. K. C.; Wang, Y. J.; Lee, F. K.; Lam, C. H.; Yang, Z. Equilibrium pathway of spin-coated polymer films. *Macromolecules* **2008,** 41 (4), 1465-1468.
189. Krishnan, S.; Ward, R. J.; Hexemer, A.; Sohn, K. E.; Lee, K. L.; Angert, E. R.; Fischer, D. A.; Kramer, E. J.; Ober, C. K. Surfaces of fluorinated pyridinium block copolymers with enhanced antibacterial activity. *Langmuir* **2006,** 22 (26), 11255-11266.
190. Sun, L.; Akgun, B.; Narayanan, S.; Jiang, Z.; Foster, M. D. Surface Fluctuations of Polymer Brushes Swollen in Good Solvent Vapor. *Macromolecules* **2016,** 49 (19), 7308-7313.
191. Jang, W. S.; Koo, P.; Sykorsky, M.; Narayanan, S.; Sandy, A.; Mochrie, S. G. J. The Static and Dynamic Structure Factor of a Diblock Copolymer Melt via Small-Angle X-ray Scattering and X-ray Photon Correlation Spectroscopy. *Macromolecules* **2013,** 46 (21), 8628-8637.
192. Mochrie, S. G. J. Reptation dynamics of asymmetric diblock copolymer melts via the dynamic random phase approximation. *Macromolecules* **2003,** 36 (13), 5013-5019.
193. Sinturel, C.; Vayer, M.; Morris, M.; Hillmyer, M. A. Solvent Vapor Annealing of Block Polymer Thin Films. *Macromolecules* **2013,** 46 (14), 5399-5415.
194. Kim, S. H.; Misner, M. J.; Xu, T.; Kimura, M.; Russell, T. P. Highly oriented and ordered arrays from block copolymers via solvent evaporation. *Adv Mater* **2004,** 16 (3), 226-+.
195. Bruinsma, R. Slow Spreading of Polymer Melts. *Macromolecules* **1990,** 23 (1), 276-280.
196. Wu, W. L.; Wallace, W. E.; vanZanten, J. H.; Bauer, B. J.; Liu, D. W.; Wong, A. Diffusion of linear polystyrene into crosslinked polystyrene. *Polymer* **1997,** 38 (11), 2583-2594.
197. Asada, M.; Jiang, N.; Sendogdular, L.; Sokolov, J.; Endoh, M. K.; Koga, T.; Fukuto, M.; Yang, L.; Akgun, B.; Dimitriou, M.; Satija, S. K. Melt crystallization/dewetting of ultrathin PEO

films via carbon dioxide annealing: the effects of polymer adsorbed layers. *Soft Matter* **2014,** 10, 6392-6403.
198. Gowd, E. B.; Böhme, M.; Stamm, M., In Situ GISAXS Study on Solvent Vapour Induced Orientation Switching in PS-b-P4VP Block Copolymer Thin Films. In *IOP Conference Series: Materials Science and Engineering*, 2010; Vol. 14, pp 012015-012021.
199. Currie, E. P. K.; Norde, W.; Stuart, M. A. C. Tethered polymer chains: surface chemistry and their impact on colloidal and surface properties. *Adv Colloid Interfac* **2003,** 100, 205-265.
200. Zhu, X. Y.; Jun, Y.; Staarup, D. R.; Major, R. C.; Danielson, S.; Boiadjiev, V.; Gladfelter, W. L.; Bunker, B. C.; Guo, A. Grafting of high-density poly(ethylene glycol) monolayers on Si(111). *Langmuir* **2001,** 17 (25), 7798-7803.
201. Tsuruta, T. On the Role of Water Molecules in the Interface between Biological Systems and Polymers. *J. Biomater. Sci. Polym. Ed.* **2010,** 21, 1831-1848.
202. Morita, S.; Tanaka, M.; Ozaki, Y. Time-Resolved In Situ ATR-IR Observations of the Process of Sorption of Water into a Poly(2-methoxyethyl acrylate) Film. *Langmuir* **2007,** 23, 3750-3761.
203. Tanaka, M.; Mochizuki, A.; Ishii, N.; Motomura, T.; Hatakeyama, T. Study of Blood Compatibility with Poly(2-methoxyethyl acrylate). Relationship between Water Structure and Platelet Compatibility in Poly(2-methoxyethylacrylate-co-2- hydroxyethylmethacrylate). *Biomacromolecules* **2002,** 3, 36-41.
204. Leung, B. O.; Yang, A.; Wu, S. S. H.; Chou, K. C. The Role of Interfacial Water on Protein Adsorption at Cross-Linked Polyethylene Oxide Interfaces. *Langmuir* **2012,** 28, 5724−5728.
205. Zheng, J.; Li, L.; Tsao, H. K.; Sheng, Y. J.; Chen, S.; Jiang, S. Strong Repulsive Forces Between Protein and Oligo (ethylene glycol) Self-Assembled Monolayers: A Molecular Simulation Study. *Biophys. J.* **2005,** 89, 158−166.
206. Nagasawa, D.; Azuma, T.; Noguchi, H.; Uosaki, K.; Takai, M. Role of Interfacial Water in Protein Adsorption onto Polymer Brushes as Studied by SFG Spectroscopy and QCM. *J. Phys. Chem. C* **2015,** 119, 17193-17201.
207. Yamada-Nosaka, A.; Ishikiriyama, K.; Todoki, M.; Tanzawa, H. 1H-NMR studies on water in methacrylate hydrogels. *J. Appl. Polym. Sci.* **1990,** 39, 2443-2452.
208. Hatakeyama, H.; Hatakeyama, T. Interaction between water and hydrophilic polymers. *Thermochim. Acta* **1998,** 308, 3-22.
209. Kishi, A.; Tanaka, M.; Mochizuki, A. Comparative Study on Water Structures in PolyHEMA and PolyMEA by XRD-DSC Simultaneous Measurement. *J. Appl. Polym. Sci.* **2009,** 111, 476-481.
210. Hatakeyama, T.; Tanaka, M.; Kishi, A.; Hatakeyama, H. Comparison of measurement techniques for the identification of bound water restrained by polymers. *Thermochim. Acta* **2012,** 532, 159-163.
211. Tanaka, M.; Mochizuki, A. Clarification of the Blood Compatibility Mechanism by Controlling the Water Structure at the Blood–Poly(meth)acrylate Interface. *J. Biomater. Sci. Polym. Ed.* **2012,** 21, 1849-1863.
212. Koga, T.; Naisheng, J.; Gin, P.; Endoh, M.; Narayanan, S.; Lurio, L.; Sinha, S. K. Impact of an Irreversibly Adsorbed Layer on Local Viscosity of Nanoconfined Polymer Melts. *Phys. Rev. Lett.* **2011,** 107, 225901.

213. Gin, P.; Jiang, N. S.; Liang, C.; Taniguchi, T.; Akgun, B.; Satija, S. K.; Endoh, M. K.; Koga, T. Revealed Architectures of Adsorbed Polymer Chains at Solid-Polymer Melt Interfaces. *Phys. Rev. Lett.* **2012,** 109 (26), 265501 DOI: 10.1103/PhysRevLett.109.265501.
214. Asada, M.; Jiang, N.; Sendogdular, L.; Sokolov, J.; Endoh, M. K.; Koga, T.; M.Fukuto; Yang, L.; Akgun, B.; Dimitriou, M.; Satija, S. K. Melt crystallization/dewetting of ultrathin PEO films via carbon dioxide annealing: the effects of polymer adsorbed layers. *Soft Matter* **2014,** 10, 6392-6403.
215. Jiang, N.; Wang, J.; Di, X.; Cheung, J.; Zeng, W.; Endoh, M. K.; Koga, T.; Satija, S. K. Nanoscale adsorbed structures as a robust approach for tailoring polymer film stability. *Soft Matter* **2016,** 12, 1801-1809.
216. Sen, M.; Jiang, N.; Cheung, J.; Endoh, M. K.; Koge, T.; Kawaguchi, D.; Tanaka, K. Flattening Process of Polymer Chains Irreversibly Adsorbed on a Solid. *ACS Macro Lett.* **2016,** 5 (4), 504-508.
217. Jiang, N.; Shang, J.; Di, X.; Endoh, M. K.; Koga, T. Formation mechanism of high-density, flattened polymer nanolayers adsorbed on planar solids. *Macromolecules* **2014,** 47, 2682-2689.
218. Carrillo, J. M. Y.; Cheng, S. W.; Kumar, R.; Goswami, M.; Sokolov, A. P.; Sumpter, B. G. Untangling the Effects of Chain Rigidity on the Structure and Dynamics of Strongly Adsorbed Polymer Melts. *Macromolecules* **2015,** 48, 4207-4219.
219. Linse, P.; Källrot, N. Polymer Adsorption from Bulk Solution onto Planar Surfaces: Effect of Polymer Flexibility and Surface Attraction in Good Solvent. *Macromolecules* **2010,** 43 (4), 2054-2068 DOI: 10.1021/ma902338m.
220. Jiang, N.; Endoh, M. K.; Koga, T., Structures and Dynamics of Adsorbed Polymer Nanolayers on Planar Solid. In *Non-Equilibrium Phenomena in Confined Soft Matter*, Napolitano, S., Ed. Springer: 2015; pp 129-160.
221. Guiselin, O. Irreversible Adsorption of a Concentrated Polymer Solution. *Europhys. Lett.* **1992,** 17 (3), 225-230 DOI: 10.1209/0295-5075/17/3/007.
222. Wang, Y.; Kozlovskaya, V.; Arcibal, I. G.; Cropek, D. M.; Kharlampiev, E. Highly swellable ultrathin poly(4-vinylpyridine) multilayer hydrogels with pH-triggered surface wettability. *Soft Matter* **2013,** 9 (39), 9420-9429.
223. Burkert, S.; Bittrich, E.; Kuntzsch, M.; Muller, M.; Eichhorn, K. J.; Bellmann, C.; Uhlmann, P.; Stamm, M. Protein Resistance of PNIPAAm Brushes: Application to Switchable Protein Adsorption. *Langmuir* **2010,** 26 (3), 1786-1795.
224. De Gennes, P. G. Scaling concepts in polymer physics. *Cornell University Press, Ithaca, New York* **1979**.
225. Jeon, S. I.; Lee, J. H.; Andrade, J. D.; de Gennes, P. G. Protein-surface interactions in the presence of polyethylene oxide: I. Simplified theory. *J. Colloid Interface Sci.* **1991,** 142, 149-158.
226. Szleifer, I. Polymers and proteins: interactions at interfaces. *Curr. Opin. Solid St. Mater. Sci.* **1997,** 2, 337-344.
227. Szleifer, I. Protein Adsorption on Surfaces with Grafted Polymers. *Biophys. J.* **1997,** 72, 595-612.
228. Harder, P.; Grunze, M.; Dahint, R.; Whitesides, G. M.; Laibinis, P. E. Molecular Conformation in Oligo(ethylene glycol)-Terminated Self-Assembled Monolayers on Gold and Silver Surfaces Determines Their Ability To Resist Protein Adsorption. *J. Phys. Chem. B* **1998,** 102, 426-436.

229. Wang, R. L. C.; Kreuzer, H. J.; Grunze, M. Molecular Conformation and Solvation of Oligo(ethylene glycol)-Terminated Self-Assembled Monolayers and Their Resistance to Protein Adsorption. *J. Phys. Chem. B* **1997,** 101, 9767-9773.
230. Wang, R. L. C.; Kreuzer, H. J.; Grunze, M. The interaction of oligo(ethylene oxide) with water: a quantum mechanical study *Phys. Chem. Chem. Phys.* **2000,** 2, 3613-3622.
231. Pertsin, A. J.; Grunze, M. Computer Simulation of Water near the Surface of Oligo(ethylene glycol)-Terminated Alkanethiol Self-Assembled Monolayers. *Langmuir* **2000,** 16, 8829-8841.
232. Jansen, E. J.; Sladek, R. E.; Bahar, H.; Yaffe, A.; Gijbels, M. J.; Kuijer, R.; Bulstra, S. K.; Guldemond, N. A.; Binderman, I.; Koole, L. H. Hydrophobicity as a design criterion for polymer scaffolds in bone tissue engineering. *Biomaterials* **2005,** 26 (21), 4423-31 DOI: 10.1016/j.biomaterials.2004.11.011.
233. Weibel, D. B.; Whitesides, G. M. Applications of microfluidics in chemical biology. *Curr Opin Chem Biol* **2006,** 10 (6), 584-91 DOI: 10.1016/j.cbpa.2006.10.016.
234. Kartalov, E. P.; Anderson, W. F.; Scherer, A. The analytical approach to polydimethylsiloxane microfluidic technology and its biological applications. *J Nanosci Nanotechnol* **2006,** 6 (8), 2265-77.
235. Wu, M. H.; Huang, S. B.; Lee, G. B. Microfluidic cell culture systems for drug research. *Lab Chip* **2010,** 10 (8), 939-56 DOI: 10.1039/b921695b.
236. Pirmoradi, F. N.; Jackson, J. K.; Burt, H. M.; Chiao, M. A magnetically controlled MEMS device for drug delivery: design, fabrication, and testing. *Lab Chip* **2011,** 11 (18), 3072-80 DOI: 10.1039/c1lc20438f.
237. Kim, J.; Somorjai, G. A. Molecular packing of lysozyme, fibrinogen, and bovine serum albumin on hydrophilic and hydrophobic surfaces studied by infrared-visible sum frequency generation and fluorescence microscopy. *J Am Chem Soc* **2003,** 125 (10), 3150-3158.
238. Zhanga, M.; Desaia, T.; Ferraria, M. Proteins and cells on PEG immobilized silicon surfaces. *Biomaterials* **1988,** 19, 953–960.
239. Wischerhoff, E.; Uhlig, K.; Lankenau, A.; Borner, H. G.; Laschewsky, A.; Duschl, C.; Lutz, J. F. Controlled cell adhesion on PEG-based switchable surfaces. *Angew. Chem. Int. Ed.* **2008,** 47, 5666–5668.
240. An, Y. H.; Friedman, R. J. Concise review of mechanisms of bacterial adhesion to biomaterial surfaces. *J Biomed Mater Res* **1998,** 43 (3), 338-348.
241. Scharfman, A.; Degroote, S.; Beau, J.; Lamblin, G.; Roussel, P.; Mazurier, J. Pseudomonas aeruginosa binds to neoglycoconjugates bearing mucin carbohydrate determinants and predominantly to sialyl-Lewis x conjugates. *Glycobiology* **1999,** 9 (8), 757-764.
242. Cunliffe, D.; Smart, C. A.; Alexander, C.; Vulfson, E. N. Bacterial adhesion at synthetic surfaces. *Appl Environ Microb* **1999,** 65 (11), 4995-5002.